—2—

Superconducting Tunneling Junctions as Phonon Generators and Detectors

W. EISENMENGER

Physikalisches Institut, Universität Stuttgart
Stuttgart, West Germany

I. Introduction

Experiments with acoustical phonons in the frequency range from 10^{10} Hz up to the maximum lattice frequency of about 10^{13} Hz yield information on phonon propagation and scattering, on interactions with impurities and lattice defects, and also on the spectral distribution of phonons emitted in energy conversion and transfer processes. A typical example of the corresponding phonon absorption and emission spectroscopy is the determination of the energy dependence of the phonon scattering cross section of atomic impurities or of the spectral distribution of the phonon emission from thin-film, metallic heat pulse generators (von Gutfeld, 1965). For phonon absorption spectroscopy, coherent acoustic waves can be generated by piezoelectric surface generation (Bömmel and Dransfeld, 1958, 1960) up to the limiting lattice frequency. In recent experiments (Grill and Weis, 1974) phonon pulses in quartz have been generated at 891 GHz using piezoelectric surface excitation by use of a molecular laser. A superconducting bolometer has been used as an energy detector, since wave front distortion with respect to the detector surface at the corresponding wavelength of the order of 10 Å makes coherent detection impossible. This partial coherent technique is well suited for phonon absorption spectroscopy when wide-range tunable far-infrared lasers are available. The most common incoherent method by which spectral information on high-frequency resonant phonon scattering can be obtained is the measurement of low-temperature thermal conductivity. Using heat pulse techniques (von Gutfeld and Nethercot, 1964), i.e., thin-film resistive heaters as generators and superconducting bolometers as detectors, this spectral information can be obtained for all different phonon modes. Phonon radiation of large bandwidth also in the regime of the lattice-limiting frequency is easily obtained with increased heater power (Weis, 1969; Herth and Weis, 1970). Since generators and detectors are fabricated by vacuum deposition, this incoherent technique can be applied to all crystals prepared with clean, optically polished surfaces. It has been demonstrated (Weis, 1972) that the phonon transmission at the boundary between the metallic film and the crystal surface is well described by the

acoustical characteristic impedance data. This indicates that vacuum deposition of generator and detector systems leads to good, reproducible phonon coupling conditions for the crystal sample. As in the case of electromagnetic waves, coherent and incoherent methods in phonon absorption spectroscopy are basically equivalent, if the frequency bandwidth is assumed to agree. In practice, however, the phonon occupation number in coherent techniques is extremely large compared to unity, with the possibility of saturation of direct transitions in two-level systems (compare, e.g., Hunklinger *et al.*, 1972), whereas occupation numbers in incoherent phonon generation have maximum values of the order of unity.

Other techniques for phonon spectroscopy are based on the optical determination of the occupation temperature of magnetically tunable spin systems (Anderson and Sabisky, 1971), further on phonon-induced optical fluorescence (Renk and Deisenhofer, 1971; Renk, 1972), or on changes in microwave absorption induced by phonon transitions (Shiren, 1961). These methods provide tunable detection of incoherent and coherent phonons in the frequency range up to 10^{12} Hz.

The principles of phonon spectroscopy discussed so far do not make use of the detailed quantum mechanical interaction between electrons and phonons in metals or semiconductors. Especially in superconductors, the existence of the energy gap leads to the possibility that phonons can excite quasiparticles in analogy to the intrinsic photoelectric effect. On the other hand, high-energy quasiparticles injected into a superconductor by tunneling are expected to transfer their energy to the lattice in the form of primary phonons with a spectral distribution that strongly deviates from the thermal Planck's law. It is also expected that this primary phonon spectrum depends in a characteristic way on the electron injection energy.

Corresponding to the width of the energy gap in superconductors and the typical operating conditions of tunneling junctions, the primary phonon energies are of the order of milli-electron volts or within the 10^{12}-Hz range. At these energies the phonon mean free path in metals can be estimated by the extrapolation of electronic ultrasonic absorption. Leibowitz (1964a) reported low-temperature normal-state ultrasonic transverse wave attenuation values in tin depending on orientation and polarization of up to $\alpha = 15$ Db/cm at 34 MHz. Assuming a linear frequency dependence of absorption as valid for the electron mean free path exceeding the phonon wavelength (Pippard, 1955, 1960) a mean free phonon path of the order of 1000 Å can be estimated for 5×10^{11} Hz. Therefore, by using phonon generators in the form of thin films, primary phonons can be radiated into single-crystal substrates with moderate or without further interaction and their spectral properties can be analyzed with frequency-selective detectors.

It is the aim of this chapter to review the experimental and theoretical

results obtained by the use of superconducting tunneling junctions (Eisenmenger and Dayem, 1967) as phonon generators and detectors. We first discuss the fundamental processes and their experimental evidence in more qualitative terms in Sections II and III. The quantitative treatment of phonon detection and generation is given in Sections IV and V, while Section VI discusses phonon spectroscopy and other applications.

II. Basic Aspects of Phonon Generation and Detection by Single-Particle Tunneling in Superconductors

A. Single-Particle Tunneling

Phonon detection and phonon generation with superconducting tunneling junctions makes use of single-particle tunneling. Single-particle tunneling is an "elastic" process characterized by the absence of phonon or photon interactions in the tunneling transition. For most phonon experiments the junctions consist of identical superconductors. In the typical I–V characteristic shown in Fig. 1, two tunneling regimes are to be distinguished, which can be discussed in terms of the semiconductor picture (Giaever and Megerle, 1961) of the superconducting density of states according to Figs. 2 and 3. In this representation the tunneling current per energy interval is proportional to the product of the density of occupied states on one side of the barrier times the density of empty states on the other side of the barrier. From this follows that for battery voltages $|V| < 2\Delta/e$ (see Fig. 2), with Δ the superconducting energy gap and e the electron charge, only tunneling of thermally excited quasiparticles is possible. In this voltage range the "thermal" current I_T depends strongly on temperature in proportion to the density of excited quasiparticles N_T. This results in the approximate relation for I_T (cf. Section IV):

$$I_T = \text{const}(V)\sqrt{T}\,e^{-\Delta/kT} \tag{1}$$

for temperatures $T < 0.5T_c$, with T_c the critical temperature.

In most junctions an additional, almost temperature-independent tunneling current at voltages exceeding Δ is observed. This current can be attributed to two-particle tunneling (Wilkins, 1969), A. C. Josephson contributions, and other "leakage" currents.

With battery voltages $eV > 2\Delta$, the tunneling current increases discontinuously and approaches the normal-state asymptotic resistance relation $I = V/R_\infty$. In this voltage range Cooper pairs in the ground state are broken up by the tunneling interaction. Only one of the excited quasiparticles

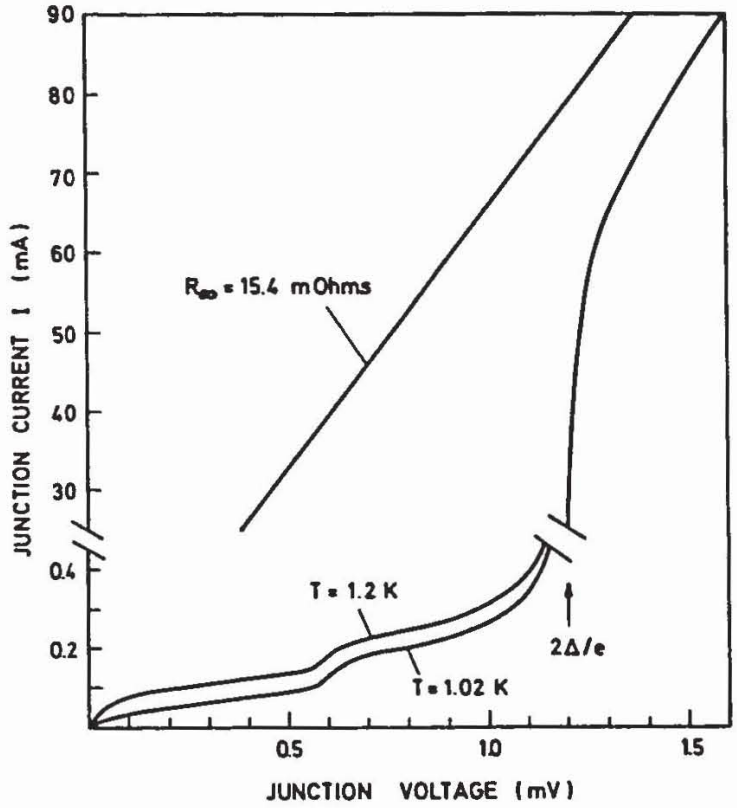

FIG. 1. Current-voltage characteristic of a typical Sn–I–Sn tunneling junction of 1-mm^2 area as used for phonon generation or detection. Current scale is expanded in the thermal tunneling regime of detector operation. The nearly temperature-independent current increase at $eV = \Delta$, $V = 0.6$ mV corresponds to the onset of two-particle tunneling. A magnetic field of about 20 Oe is applied parallel to the junction plane.

crosses the barrier, while the other occupies an excited state of the first film. This description of single-particle tunneling in terms of quasiparticle excitations is energetically equivalent to the semiconductor model, which leads to corresponding hole and electron excitations on both sides of the barrier (Fig. 3).

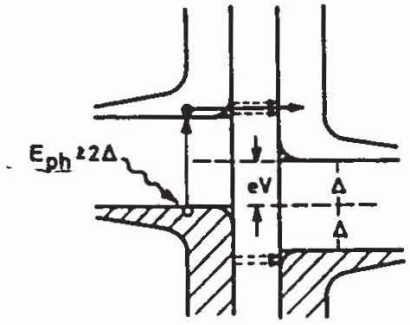

FIG. 2. Phonon detection in the range $0 < eV < 2\Delta$ represented by the energy (vertical) density of states (horizontal) scheme of single-particle tunneling. Phonons with $E_{ph} \geq 2\Delta$ give rise to an increased quasiparticle population by Cooper pair breaking. Phonon detection by hole production on the right side of the tunneling barrier is omitted.

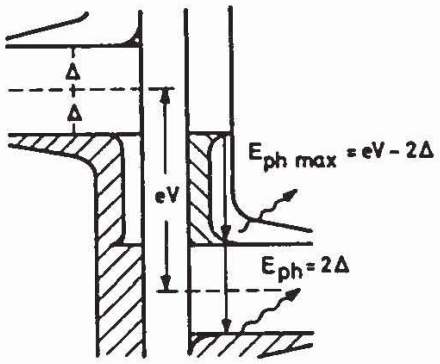

FIG. 3. Phonon generation by quasiparticle relaxation and recombination in the range $eV > 2\Delta$ represented by the energy (vertical) density of states (horizontal) scheme of single-particle tunneling.

B. PHONON DETECTION BY QUASIPARTICLE EXCITATION

As indicated in Fig. 2, quasiparticles can be excited from the superconducting ground state by absorption of phonons with energy $E \geq 2\Delta$ breaking Cooper pairs. Typical values of 2Δ-phonon energies and frequencies for different superconductors are given in Table I.

TABLE I

GAP ENERGY 2Δ, GAP FREQUENCY $f_{2\Delta}$, AND ELECTRONIC DENSITY N_0 OF BLOCH STATES (ONE SPIN AT E_F) FOR Al, Sn, AND Pb[a]

	Al	Sn	Pb
2Δ (meV)	0.3	1.18	2.7
$f_{2\Delta}$ (GHz)	72.5	285.5	653
N_0 ($eV^{-1}\ cm^{-3}$)	1.75×10^{22}	1.42×10^{22}	2.22×10^{22}

[a] N_0 has been obtained directly from electronic specific heat data reported by Sheahen (1966; cf. also Kittel, 1967).

The increase in quasiparticle population by 2Δ-phonon absorption results in a current or voltage change if the junction is biased at $0 < eV < 2\Delta$ in the thermal tunneling current regime. It is also possible to use the current or voltage signal at a bias of $eV = 2\Delta$ (Adkins, 1973) resulting from the small reduction of the energy gap with increased quasiparticle population. This phonon detection mechanism is analogous to the intrinsic photoelectric effect in semiconductors. In fact, Burstein *et al.* (1961) proposed quasiparticle excitation via photon absorption for infrared detection.

Efficient phonon detection with superconducting tunneling junctions requires that the film thickness exceeds the phonon mean free path for

Cooper pair breaking. For phonons with energy $E = 2\Delta$, the mean free path in superconductors at $T = 0$ is reduced in comparison to the normal state value by a factor 1 : 1.57 (Tewordt, 1962a; Bobetic, 1964). As estimated before, the mean free phonon path in normal conducting tin amounts to about 1000 Å. This leads to the conclusion that superconducting tunneling junctions with typical total film thickness values ranging from 1000 to 3000 Å are well suited for quantitative phonon detection.

Whereas the pair-breaking detection mechanism has the critical onset energy $E_{ph} = 2\Delta$, a weak phonon absorption contribution at $E_{ph} < 2\Delta$ by scattering of excited quasiparticles is also possible. This process, as known from ultrasonic absorption in superconductors, is strongly temperature dependent and results in superconducting to normal-state absorption ratios $\alpha_S : \alpha_N < 0.05$ for temperatures $T < 0.5T_c$. The entire theoretical frequency dependence of $\alpha_S : \alpha_N$ for longitudinal phonons (Bobetic, 1964) is shown in Fig. 4, revealing the jump in absorption by the onset of pair breaking at

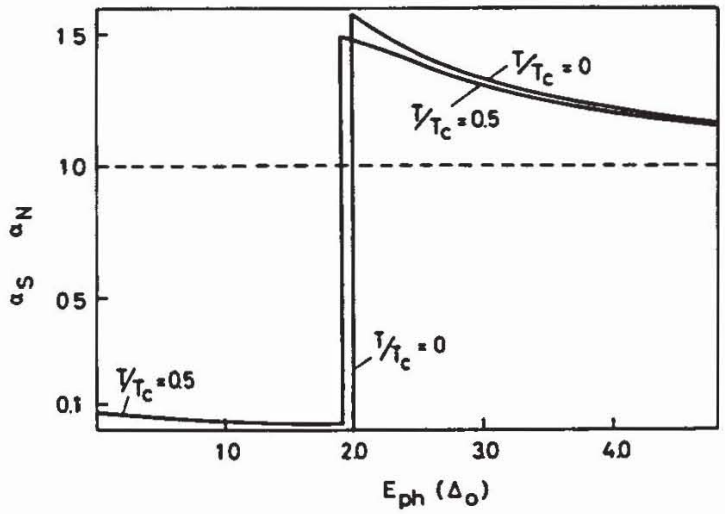

FIG. 4. Energy dependence of phonon absorption in a superconductor $\alpha_S : \alpha_N$ compared to the normal state. Δ_0 is the energy gap in the zero temperature limit and T_c the critical temperature. The steplike absorption increase at $E_{ph} = 2\Delta$ corresponds to the breaking of Cooper pairs (Bobetic, 1964).

$E_{ph} = 2\Delta$ for different temperatures. The detection rate for phonons with energy below 2Δ will be discussed in more detail in connection with calculations of the absolute detector sensitivity in Section IV.

C. Phonon Generation by Quasiparticle Recombination

Quasiparticles injected by tunneling or excited by 2Δ-phonon absorption recombine to form Cooper pairs resulting in the emission of phonons with energy 2Δ. The inverse time constant of recombination or the recombination rate $1/\tau_{eff}$ is directly proportional to the number of quasiparticles

N_T. Under the condition of a small disturbance of quasiparticle population from thermal equilibrium, the recombination lifetime τ_{eff} has the temperature dependence (cf. Section IV)

$$\tau_{eff} = \text{const } T^{-1/2} e^{\Delta/kT} \tag{2}$$

τ_{eff} is a multiple of the intrinsic recombination time τ_R since phonons emitted in recombination are reabsorbed and reemitted (Rothwarf and Taylor, 1967; Eisenmenger, 1969) until they leave the superconducting film by transmission across the boundary into the substrate. Typical time constants for recombination depending on temperature range from 10^{-8} to 10^{-6} sec. Using a tunneling junction as phonon generator, the number of recombination phonons $\dot{n}_{rec}$ emitted per unit time depends on the "generator" tunneling current I_G according to the relation

$$\dot{n}_{rec} = I_G/e \tag{3}$$

Note: $\dot{n}_{rec}$ does not contain contributions resulting from reabsorption of *relaxation* phonons with $E_{ph} > 2\Delta$ in the generator (cf. Section III,C).

Equation (3) holds for tunneling junctions with identical superconductors. It is further required that the tunneling current contribution by excited quasiparticles, double-particle tunneling, metal bridges, etc., is small compared to the pair-breaking single-particle current. Since with a battery voltage of 2Δ each tunneling electron gives rise to the emission of one 2Δ-phonon, the energy conversion rate according to Eq. (3) corresponds to 100%. Estimates of the recombination rate under 2Δ-photon emission (Burstein *et al.*, 1961) resulted in negligible contributions, because the density of radiation states entering the transition rate for recombination is much higher for phonons than for photons.

D. Phonon Generation by Quasiparticle Relaxation

In single-particle tunneling, battery voltages exceeding $2\Delta/e$ result in quasiparticles being injected above the upper edge of the energy gap, as indicated in Fig. 3. The energy supplied under this condition exceeds the pairbreaking energy 2Δ. Both quasiparticles share the excess energy $eV - 2\Delta$, which can be interpreted as kinetic energy. The energy distribution of the quasiparticles ranges continuously from Δ to $eV - \Delta$. This result, i.e., the continuous distribution of the excess energy obtained from energy conservation, is already contained in Fig. 3. Quasiparticles are created in "electron" and "hole" energy states continuously, ranging from Δ to $eV - \Delta$.

Deexcitation of quasiparticles with excess energy higher than a small fraction of Δ mainly occurs by relaxation transitions predominantly to the

gap edge as a consequence of the singularity in the density of superconducting states. The corresponding decay time constants are of the order of 10^{-10} to 10^{-8} sec (Miller and Dayem, 1967) and depend on the quasiparticle excess energy. Also, in relaxation transitions the quasiparticle energy is converted to phonon radiation, whereas photon contributions are again negligibly small by the same arguments as in recombination. Phonons emitted in relaxation cover a continuous energy range extending from zero frequency to the maximum excess energy $eV - 2\Delta$. In rough approximation, this spectrum can be assumed to be of rectangular shape. The number of relaxation phonons is twice as high as the number of recombination phonons, as both quasiparticles undergo a relaxation transition before recombination takes place. Since relaxation phonon radiation bears a resemblance to continuous X-ray radiation, the name "phonon bremsstrahlung" has also been used by Kinder (1972a). The most remarkable feature of the relaxation spectrum is its tunability of the upper spectral edge at $E_{ph} = eV - 2\Delta$ simply by changing the battery voltage. This property makes it possible to give experimental evidence for the phonon processes discussed so far and provides phonon spectroscopy by electronic modulation techniques.

III. Basic Experiments

A. Experimental Techniques

1. *Sample and Junction Preparation*

In phonon propagation experiments (Eisenmenger and Dayem, 1967) the generator and detector junctions are fabricated by vacuum deposition on the two opposing, optically scratch-free polished surfaces of the substrate single crystal. As indicated in Fig. 5 it is not necessary to use the cross-strip configuration for the films but instead a rectangular shape with a square overlap zone, as tunneling area is of advantage if high generator currents are used. As in most solid state work the substrate crystals

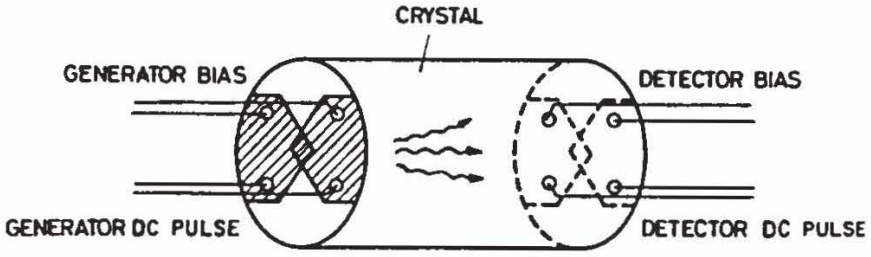

FIG. 5. Sample configuration for phonon generation and detection experiments with superconducting tunneling junctions. Typical crystal dimensions range from 3 to 10 mm in length, and about 10 mm in diameter.

preferably should not contain unknown impurities. In addition, impurity clusters or crystal defects in the form of clusters are to be avoided. In optically transparent crystals this can be easily checked by laser light scattering. There should be no visible light scattering from a 4-mW He–Ne laser light beam passing through the bulk of the crystal. Meanwhile successful phonon experiments have been performed with a large variety of different pure and doped crystals such as sapphire, Si, Ge, KBr, and NaF, crystals that have been also used in heat pulse experiments. Sample dimensions are of the order of 1 cm in diameter and thickness. If time of flight separation is not important, a reduction of the sample thickness and thereby of the generator detector distance increases the signal to noise ratio.

The samples are often mounted in a crystal holder that is also used during junction fabrication. The electric connections to the junction are preferably made by four indium pressure contacts.

In preparing tunneling junctions as phonon generators and detectors, the general prescriptions (Giaever, 1969; see also Solymar, 1972) can be used. Vacuum requirements for film deposition of 10^{-6} to 10^{-5} Torr are sufficient. For film thickness control during evaporation, a quartz crystal resonance monitor may be used. Typical asymptotic tunneling resistances R_∞ ranging from 10^{-3} to 10^{-1} Ω/mm^2 can be chosen depending on voltage requirements at the critical current by which the junction becomes normal conducting. In order to obtain high critical currents, fast evaporation avoiding granular film structure appears advantageous. As pointed out by Giaever (1969) the ease in junction preparation for the often used superconductors decreases in the sequence Al, Sn, Pb.

In preparing Al junctions with film thicknesses ranging from 1000 to 2000 Å the first Al layer can be evaporated in a few seconds. After oxidation by exposing the film to dry, pure oxygen at 10 to 100 Torr for several minutes the second film can be deposited. Aluminum junctions with enhanced energy gap and granular film structure can be prepared by evaporation under oxygen atmosphere in the pressure range of 10^{-5} Torr (Abeles *et al.*, 1966).

For Sn films (width 1 mm, thickness 2000 Å) fast evaporation with a rate of about 200 Å/sec is also required for high critical film currents of the order of 2 A. The oxide barrier of Sn films is usually formed by glow discharge in oxygen at pressures of 0.05 to 0.5 Torr. It appears necessary that the luminous part of the discharge does not reach the sample. This can be accomplished by a relatively high oxygen pressure of 0.3 to 0.5 Torr (Kinder, 1973a), by an increased distance to about 20 cm between sample and discharge electrodes, or by screening with a metal grid. The oxide growth can be observed by the quartz resonance monitor. After a few min-

utes oxidation, the growth rate saturates by passivity. It is expected that pinholes and weak spots of the barrier are closed in growth saturation.

For the reduction of leakage currents it has been recommended (Kinder, 1973a) that the Sn film be exposed to pure oxygen immediately after evaporation. Also fast vacuum deposition of the Sn films under oxygen pressure of 10^{-5} Torr (Forkel and Trumpp, 1975) improved the junction quality, possibly by increasing the density of oxidation nuclei, by higher film smoothness, or by preventing surface contamination with other residual gases. The junction quality can be defined by the ratio of the maximal tunneling current at the 2Δ-edge and the leakage current below $V \leq 2\Delta$. For "good" junctions this "2Δ current ratio" ranges from 200 to 1500. As will be discussed in Section IV,F, high 2Δ current ratios are important for the signal to noise ratio attainable in phonon detection.

Whereas Al and Sn junctions can be produced with a success ratio of about 90% the situation is more difficult with lead. With careful control of the substrate temperature (Rolcke, 1973) at about 40°C during evaporation and oxidation in pure oxygen under atmospheric pressure the number of good quality junctions can be higher than 50%, depending on the substrate material. One of the problems to be avoided during oxidation is growth of whiskers, which form metallic bridges penetrating the oxide barrier (Rolcke, 1973). Improved results have been obtained with Pb–In and Pb–Bi alloy junctions (Campbell *et al.*, 1966; Kinder and Dietsche, 1974) showing the additional advantages of a much sharper energy gap compared to pure lead junctions. In general, the purity of the metals used for evaporation is of less importance. A very important condition in the preparation of all junctions is that the substrate must be free from dust particles in the tunneling overlap area, for otherwise the junction will exhibit a short circuit.

2. *Electronic Measuring System and Temperature Control*

Phonon experiments with Sn and Pb and to some extent also with Al junctions can be performed in the temperature range 1 to 4°K, using a ^{4}He glass cryostate together with an efficient pumping system. For most measurements the sample can be in direct contact with liquid ^{4}He. Only for the absolute determination of the phonon signal amplitude and the detector time constant (Trumpp *et al.*, 1972b) must the sample be kept under vacuum conditions, because phonon radiation into the ^{4}He bath exceeds radiation into the crystal substrate. An electronic feedback system may serve for temperature control together with a carbon resistor thermometer and a resistive heater. Since the sensitivity of the tunneling junction as phonon detector strongly depends on the average number of excited quasiparticles, or the corresponding occupation temperature, the average tunneling current or

voltage can be used instead of the bath temperature for stabilizing the occupation temperature. This is especially useful in modulation experiments (Kinder, 1972a) with high generator power levels, where the detector quasiparticle occupation temperature exceeds the temperature of the ^{4}He bath (compare with Section IV,A).

Phonon experiments can be performed under pulsed or dc conditions. In pulse measurements (Fig. 6) pulse transformers serve for matching the

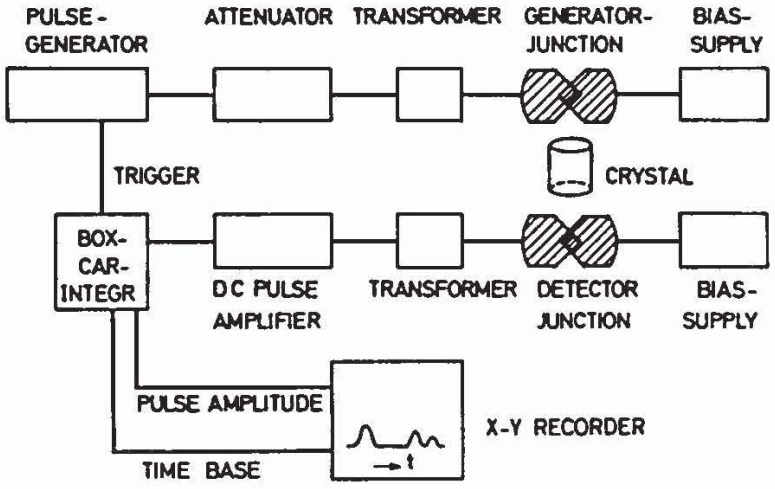

FIG. 6. Electronic pulse measurement system. In order to record the pulse amplitude for the longitudinal or transverse phonon signal as a function of temperature or generator current, the time position of the box-car gate is held fixed. The same operation mode is used in taking the derivatives of the detector signal versus generator bias current.

mostly low ohmic generator junctions to the pulse generator output impedance, as well as the detector to the low-noise pulse amplifier input impedance of in general 50 Ω. If the pulse transformers are not located close to the sample, a connecting strip line with characteristic impedance ranging from 2 to 5 Ω may be used. For short electronic rise times of the order of 0.1 μsec low-inductance connections to the junction and transformer are required. If generator and detector impedances are close to 50 Ω (Forkel, 1974b) the use of twisted wires without pulse transformers is also sufficient in pulse experiments. For each junction the usual four probe measurements of the I–V characteristic under dc or pulsed conditions should be possible. In detector operation a constant dc bias current from a high ohmic source is fed to the junction, resulting in a bias voltage of about $1.2\Delta/e$. A phonon signal incident on the junction increases the number of quasiparticles. The corresponding almost parallel shift of the tunneling characteristic to higher currents reduces the voltage at constant current bias. Thus, the phonon signal results in a corresponding voltage drop.

In phonon experiments the pulse signal amplitude can be recorded as a function of time or of the generator pulse current or voltage by use of the

sampling technique. The results are directly displayed on the x-y recorder. The derivative of the pulse signal with respect to the generator current di_s/di_G, being important in phonon spectroscopy, is obtained using modulation techniques.

If the generator pulse current amplitude carries a small but constant sinusoidal amplitude modulation, the resulting modulation amplitude of the detector signal corresponds to di_s/di_G, the derivative of the detector signal with respect to the generator current. Instead of using a pulse generator with amplitude modulation, constant current pulses can also be applied to the generator junction, additionally superimposing a small-amplitude sine current. The basically nonlinear operation of the generator leads to the equivalence of this method with the direct modulation of the generator pulse. The method is simple and has the advantage that the inductive "feed-through" signal can be completely suppressed. A third modulation scheme is provided by applying a variable dc current to the junction instead of a pulse current and superposing small current pulses of constant amplitude. The detector pulse signal amplitude is now directly proportional to the derivative di_s/di_G. This method, which is also simple, may show the disadvantage of high power dissipation in the helium bath at increased dc current levels accompanied by a temperature increase. If pulse detection is not required, conventional sine modulation and lock-in technique can be applied (Forkel *et al.*, 1973).

In all measurements, improvement of the signal to noise ratio by boxcar integration or lock-in technique may be applied if necessary. Detector impedance matching by use of pulse transformers also improves the signal to noise ratio. A more efficient means of detector impedance matching consists

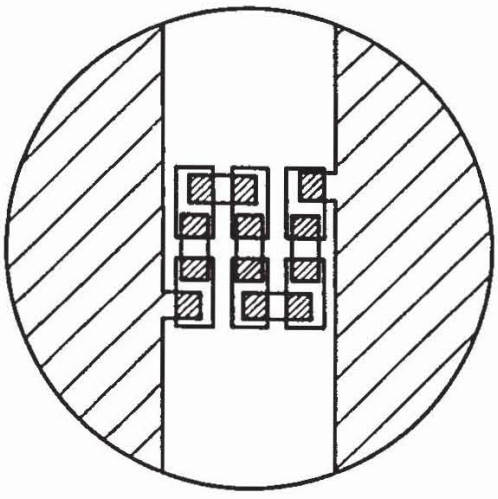

FIG. 7. Tunneling detector with a number of junctions connected in series for impedance matching to the pulse amplifier without pulse transformer. The densely hatched squares are the tunneling areas. The total effective area is of the order of 1 mm^2. The widely hatched parts of the film are for pressure contacting (Forkel and Eisenmenger, 1976).

in dividing the 1-mm^2 junction into a sufficiently large number of small area junctions, which are connected in series, by use of suitable evaporation masks. Such a "multijunction" (Forkel and Eisenmenger, 1976) is shown in Fig. 7. With this type of detector it is possible to obtain a dynamical resistance equal to or exceeding 50 Ω combined with a high tunneling probability, which is necessary for sensitive detection.

Since large dc Josephson currents result from high tunneling probability, the detector must be operated in a parallel magnetic field of about 20 Oe in order to suppress switching from the biasing point to the zero resistance state. It is also advisable that the junctions be oriented parallel to the earth magnetic field in order to avoid magnetic flux trapped in the films when the bath temperature is lowered across T_c.

B. Time of Flight Measurements

In pulse experiments generator pulses from 0.2 to 5 μsec in duration with repetition frequencies up to 10 kHz are used. Time displays of the detector signal, as shown in Figs. 8–10, clearly reveal the different phonon modes and energy propagation velocities known from ultrasonic data. In Fig. 8, a Pb–I–Pb junction has been used as phonon generator and a Sn–I–Sn junction as phonon detector (Eisenmenger, 1969). *A*-axis propagation in Al_2O_3 involves one longitudinal, one fast transverse, and one slow transverse mode. An additional signal can be attributed to diffuse scattering of the strong fast transverse signal from the unpolished cylindrical sidewall of the crystal. The amplitude difference between the fast and slow transverse mode is in accord with phonon focusing (Taylor *et al.*, 1971).

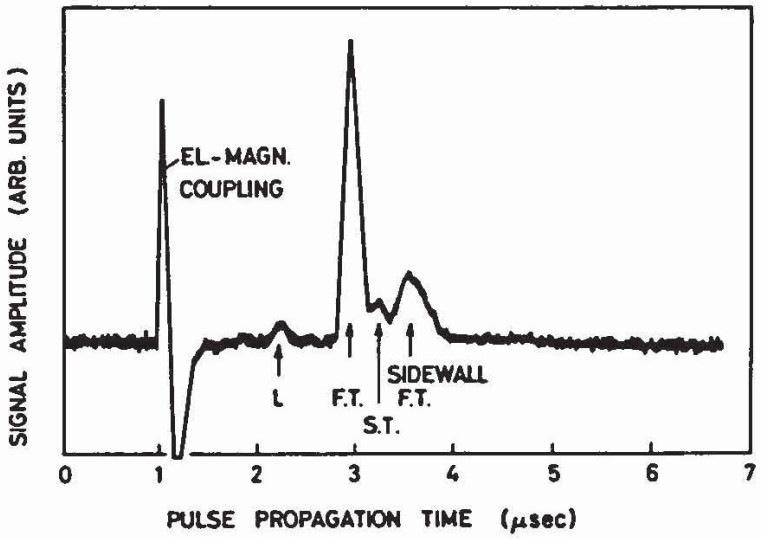

Fig. 8. Phonon pulse signals obtained with a Pb–I–Pb generator and a Sn–I–Sn detector on Al_2O_3 in *A*-direction. Crystal length, 12 mm; *L*, longitudinal phonons; F.T., fast transverse phonons; S.T., slow transverse phonons; temperature, 2°K (Eisenmenger, 1969).

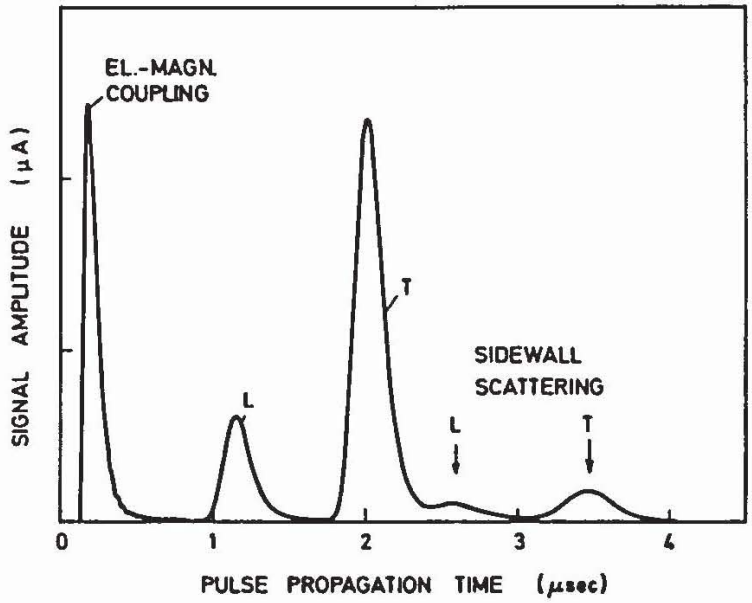

FIG. 9. Phonon pulse signals obtained with a Sn-I-Sn generator and detector on Si in [111] direction. Crystal length 9.15 mm. L = longitudinal phonons. Temperature is 1.45°K (Trumpp, 1971).

Since diffuse sidewall scattering implies omnidirectional phonon radiation from the optically plane generator, it can be concluded that phonons are produced incoherently.

The results with other junctions and substrates, e.g., Si, are similar to those of Figs. 9 and 10 (Trumpp, 1971). Temperature has a pronounced influence on the signal amplitude as well as on the signal decay time. In

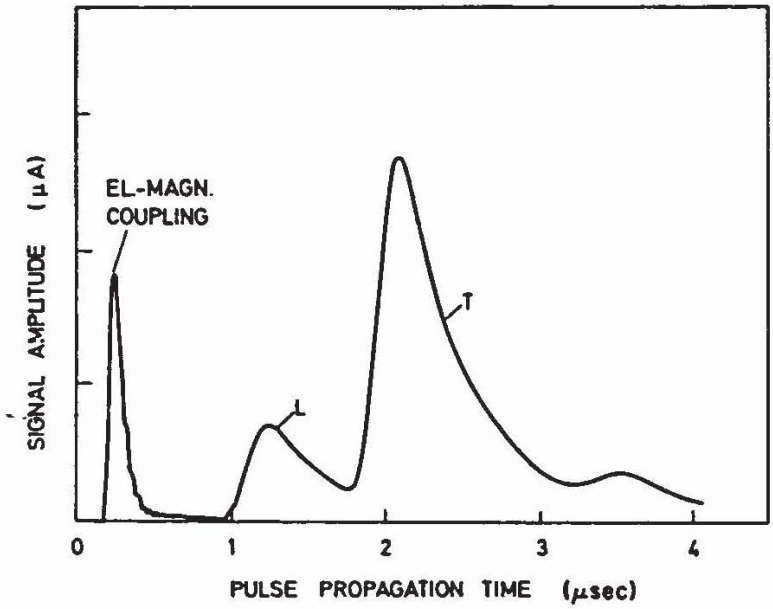

FIG. 10. Phonon pulse signals with the same sample as in Fig. 9 but at $T = 1.02$°K (Trumpp, 1971).

Fig. 10, at $T = 1.02°K$ the signal decay time is significantly longer than in Fig. 9 at $T = 1.45°K$. Since there is no possibility for a temperature dependence of the electronic components the influence of temperature can only be attributed to properties of the superconducting junction, such as the effective recombination time τ_{eff}.

C. Signal Dependence on Generator Voltage

Whereas pulse experiments so far clearly reveal the phonon nature of the signals detected, frequency information can be obtained by the measurement of the dependence of the detector signal amplitude as a function of generator current and voltage. With identical junctions for generation and detection, i.e., $\Delta_D = \Delta_G = \Delta$, only generator phonons with energy E_{ph} equal or exceeding the detector threshold 2Δ, i.e., $E_{ph} \geq 2\Delta$, contribute to the signal. From this it follows that for generator voltages with $2\Delta < eV < 4\Delta$ the signal should increase in proportion to the generator current I_G as given by Eq. (3). Within this voltage range only recombination phonons radiated from the generator can contribute to the signal. Relaxation phonons have the maximum energy $eV - 2\Delta$ and they can only contribute to the signal if the battery energy exceeds the value $eV = 4\Delta$. At this voltage the onset of the relaxation phonon contribution leads to a sudden increase in the slope

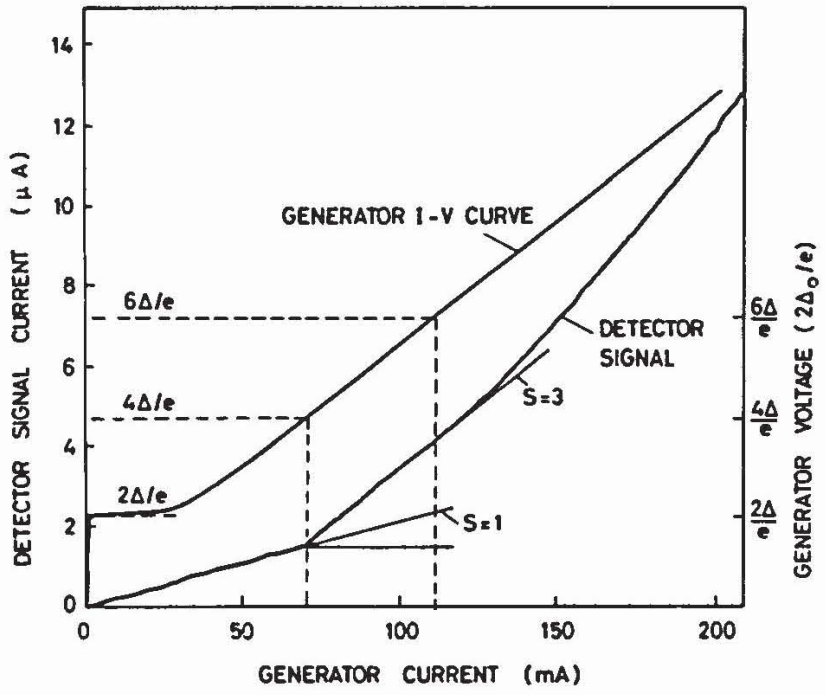

Fig. 11. Detector signal as a function of the generator current and voltage with Sn-I-Sn generator and detector. Sample as in Fig. 9, with $T = 1.01°K$. The generator I-V curve is introduced for comparison with the characteristic generator voltages $4\Delta/e$ and $6\Delta/e$. $S = 1$ and $S = 3$ are the gradients below and above $V_G = 4\Delta/e$. The theoretical gradient ratio amounts to 3.1 [Trumpp (1971); compare also Eisenmenger and Dayem (1967) and Kinder *et al.* (1970)].

di_s/di_G of the detector signal–generator current dependence. The experimental result shown in Fig. 11 is in accord with this discussion (Eisenmenger and Dayem, 1967; Kinder *et al.*, 1970; Trumpp, 1971) and the main qualitative spectral features of the phonon emission processes in the generator are verified. In comparing the generator current–signal dependence of Fig. 11 with the generator I–V characteristic introduced as obtained from pulse measurements, a beginning change of slope at $eV = 6\Delta$ is also observed. This is more clearly revealed by a measurement of the signal derivative with respect to generator current, di_s/di_G, as shown in Fig. 12, using the modula-

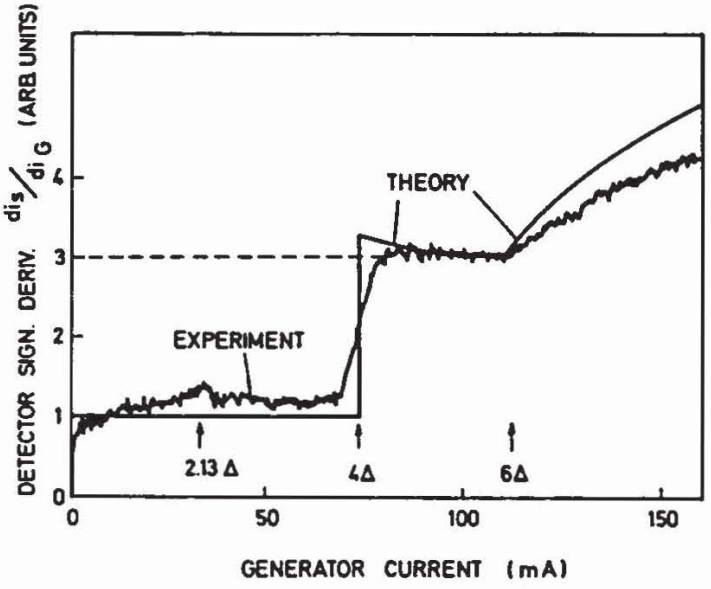

FIG. 12. Derivative di_s/di_G of the detector signal with respect to the generator current as a function of the generator current. Sn-I-Sn generator and detector. Sample as in Fig. 9, with $T = 1.03$°K. The theoretical result is introduced for comparison. The finite slope at the onset of the relaxation phonon contribution at $V_G = 4\Delta/e$ is mainly determined by the modulation width in taking the derivative. The increase at $V_G = 6\Delta/e$ is caused by additional 2Δ phonons resulting from energy splitting of 4Δ relaxation phonons by reabsorption. The structure at $V_G = 2.13\Delta$ is caused by the limited voltage dependence of the maximum recombination phonon energy. See Figs. 19 and 21. [Trumpp (1971); compare also Eisenmenger and Dayem (1967) and Kinder *et al.* (1970)].

tion techniques described before. The change in slope at 6Δ can be attributed to relaxation phonon reabsorption and pair breaking within the generator (Kinder *et al.*, 1970). Relaxation phonons of energy $E_{ph} > 2\Delta$ can be reabsorbed by breaking Cooper pairs, as illustrated in Fig. 13, thereby exciting quasiparticles with excess energy E_Q above the Fermi level in the range $\Delta < E_Q < E_{ph} - \Delta$. By the relaxation of these quasiparticles, secondary phonons of maximum energy $E_{ph} - 2\Delta$ are reemitted. Since $E_{ph\,max} = eV - 2\Delta$, the secondary phonon energy exceeds the 2Δ-detection threshold at $eV = 6\Delta$, the total probability of this process increasing in

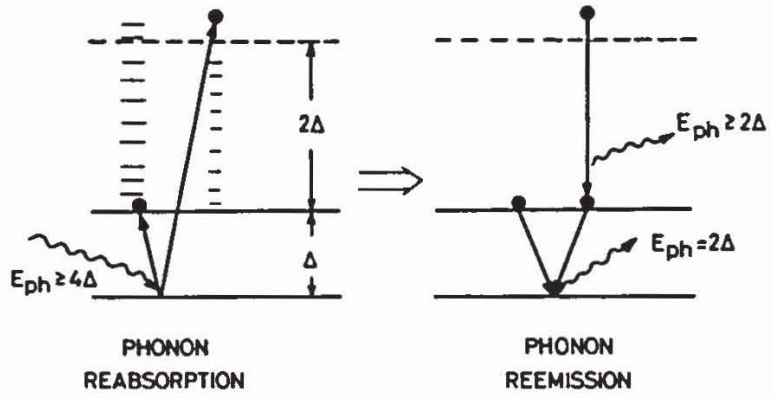

FIG. 13. Creation of additional 2Δ phonons by reabsorption of 4Δ relaxation phonons via Cooper pair breaking and succeeding relaxation of quasiparticles with maximum excess energy. This process contributes to the detector signal at $V_G > 6\Delta$ for equal energy gap of the generator and detector, as observed in Figs. 11 and 12.

proportion to the excess energy $eV - 6\Delta$. The onset of the relaxation phonon contribution at $eV = 4\Delta$ and the slope increase at 6Δ have been treated quantitatively by Kinder *et al.* (1970) (cf. Section V,B,1). The result is introduced in Fig. 12 showing good agreement with experiment. The strong evidence for reabsorption of primary relaxation phonons with energy larger than 2Δ has been confirmed by other experiments (Eisenmenger, 1967a,b; Narayanamurti and Dynes, 1971; Kinder, 1973a) but especially in connection with recombination lifetime measurements to be discussed in Sections III,D and IV,C. For Sn we estimated a normal-state phonon mean free path of the order of 1000 Å for phonons with energy $E_p = 2\Delta_{Sn}$. This value is further reduced by a factor 1 : 1.57 in the superconductor in agreement with a more direct estimate from experiment (Narayanamurti and Dynes, 1971). Sn–I–Sn phonon generators with total film thickness of typically 3000 Å are, therefore, not expected to emit relaxation phonons with energy higher than 2Δ. Since generator and detector in the measurements of Fig. 12 have the same energy gap, the corresponding discussion of the 4Δ step and the change in slope at 6Δ is not affected by the reabsorption of phonons already in the generator. In this experiment, reabsorption in the generator and reabsorption in the detector are equivalent.

Recombination and relaxation phonon radiation as well as the detector frequency dependence are confirmed by the measurements shown in Figs. 11 and 12. The characteristic behavior at $eV = 4\Delta$ in measurements as in Fig. 11 or 12 is an important general frequency criterion in phonon experiments with superconducting tunneling junctions, giving evidence that phonon propagation and detection is mediated by 2Δ-phonons and not by heat.

D. Signal Dependence on Temperature

Measurements of the exponential decay time constant of the signals in Figs. 9 and 10 as a function of temperature can be well described by the temperature law of Eq. (2), as shown in Fig. 14. The observed detector time

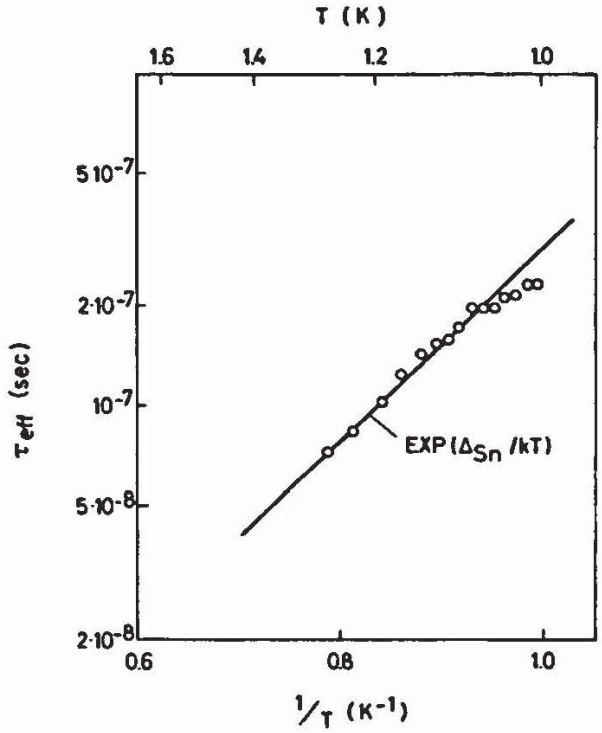

FIG. 14. Effective recombination time τ_{eff} directly observed as exponential pulse decay time constant of the detector as a function of temperature. Compare Figs. 9 and 10. Sn–I–Sn detector on Al_2O_3 substrate in contact with liquid ^{4}He. Total detector thickness 2000 Å (Eisenmenger, 1969).

constant thus agrees with τ_{eff}, the effective recombination lifetime of quasiparticles. Reabsorption and reemission of 2Δ-phonons increase τ_{eff} in comparison to τ_R by a temperature-independent factor. This ratio, however, depends very strongly on the phonon escape probability, as can be demonstrated by τ_{eff} measurements shown in Fig. 15, with different junction thickness and boundary conditions (Eisenmenger, 1967a; Gray *et al.*, 1969; Eisenmenger *et al.*, 1975). Phonon reabsorption, therefore, is also confirmed by τ_{eff} measurements using phonon pulses.

If identical junctions for phonon generation and detection are used in τ_{eff} measurements, the generator phonon pulse must be short compared to τ_{eff}. In general, this condition is satisfied in pulse experiments by current overinjection in the generator (cf. Sections IV,B and V,B,1).

Finally, measurements of the influence of temperature on the signal

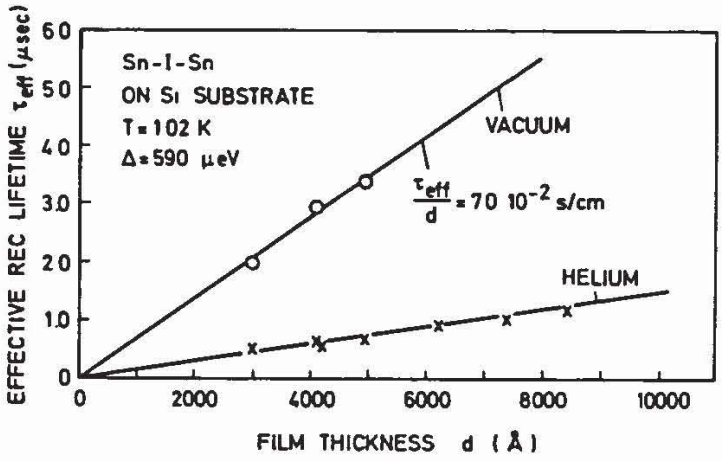

FIG. 15. Effective recombination time τ_{eff} of Sn–I–Sn detectors on (111) Si substrate for different film thickness values under vacuum conditions and in contact with liquid ^{4}He (T = 1.02°K). The theoretical film thickness dependence under vacuum conditions results in $\tau_{eff}/d = 6.8 \times 10^{-2}$ sec/cm (Eisenmenger *et al.*, 1975).

amplitude in the range $T = 1$ to 2°K with constant generator pulse current and with pulse duration long compared to τ_{eff} show the same temperature dependence as τ_{eff} (Eisenmenger, 1969). As the detector sensitivity is directly proportional to τ_{eff} (cf. Section IV), it follows that the number of phonons arriving from the generator does not depend on temperature. This is consistent with the temperature independence of spontaneous phonon generation by recombination and relaxation for temperatures $T < 0.5T_c$, where thermal phonon occupation numbers at the energy of 2Δ are very small compared to unity.

IV. Quantitative Phonon Detection Model

Experimental evidence shows pair breaking by 2Δ-phonon absorption to be the main detection process. Contributions of other detection mechanisms, e.g., phonon-assisted tunneling or ac Josephson effect (Dayem *et al.*, 1971; Kleinman, 1963; Cohen *et al.*, 1970; Jacobsen, 1974), if present, are comparatively small. Also, absorption of phonons with energy less than 2Δ by excited quasiparticles can be mostly neglected. An estimate of this influence will be given in Section 4.5.

A. Measurement of the Detector Signal

Generator phonons absorbed in the detector by pair breaking give rise to an increase of the quasiparticle density by δN compared to the thermal quasiparticle density N_T. The total resulting quasiparticle density corresponds to an occupation temperature exceeding the bath temperature. As a consequence of the quasiparticle density increase the detector I–V character-

istic (Fig. 16a) in the thermal tunneling regime is shifted to higher currents described by the short-circuit signal current $i_S(V, T, \delta N)$. This quantity is therefore more directly related to the phonon intensity than the open-circuit voltage change at constant bias current, as can be also seen from the discussion in Section IV,B. [If the gap energy reduction (Adkins, 1973) is used as signal source at a bias voltage of $eV = 2\Delta$, a similar discussion may be based on the close relation between the open circuit voltage and the quasiparticle density.]

Under pulsed conditions i_S is measured indirectly by the voltage signal V_S across the load resistance R_L in Fig. 16b, representing, e.g., the low ohmic terminal of the pulse transformer at the preamplifier input. In practice, R_L is ac-coupled to the junction by a capacitor providing a low-frequency cutoff

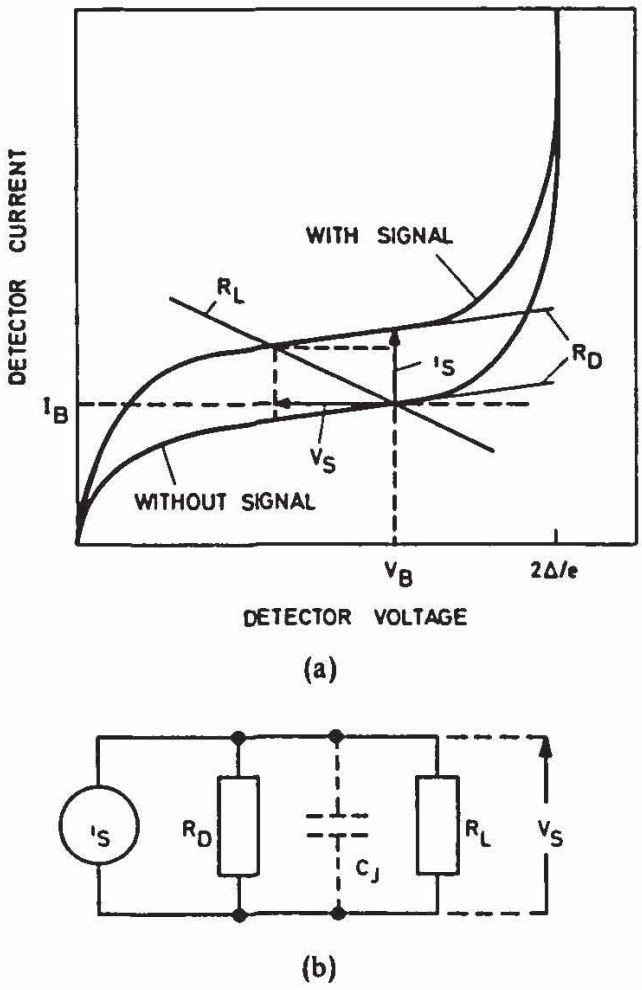

FIG. 16. (a) Load line consideration for the detector signal. i_s, constant-voltage current signal; R_L, load line corresponding to the load resistance R_L; R_D, characteristic corresponding to the dynamical junction resistance R_D; I_B, detector bias current; V_B, detector bias voltage without signal; V_S, signal voltage. (b) Small-signal equivalent circuit of the detector with load. i_S, R_D, R_L, V_S as-in Fig. 16a. C_J, junction capacitance.

with sufficiently long time constant. The variable bias current I_B is supplied from a high ohmic dc source and the bias voltage V_B can be adjusted to the center of the most linear portion of the I–V curve. Small-signal analysis or inspection of Fig. 16 leads to a linear relation between V_S and i_S:

$$i_S = -V_S\left(\frac{1}{R_D} + \frac{1}{R_L}\right) \tag{4}$$

where $R_D = (\partial V/\partial I)_{T,V_B}$ is the dynamic junction resistance at the biasing point. At larger signal amplitudes the nonlinearities of the I–V characteristic forbid the application of Eq. (4) and only computer-aided evaluation with respect to i_S using the full I–V curve or direct calibration by simulated i_S signals is possible. In modulation measurements, as for taking the signal-generator current derivative, eventually a large steady-state generator bias current causes a finite shift of the detector I–V curve and the voltage biasing point. This can be avoided by a feedback control of the bias current in order to stabilize V_B. Changes in R_D and the sensitivity of i_S with respect to δN are still present. In order to prevent these changes, the biasing point V_B and the current I_B can also be stabilized (Kinder, 1972a) by controlling the ^{4}He bath temperature. This corresponds to a stabilization of the average quasiparticle occupation temperature in the detector, i.e., with increasing average signal amplitude, the bath temperature must decrease. Of course, the time constant of the feedback control system must be sufficiently long so that the modulation of the signal i_S is not affected.

In pulse detection the junction time constant at low temperatures is determined by τ_{eff}, the effective quasiparticle recombination lifetime [Eq. (2)]. With increasing temperature, τ_{eff} may become smaller than the electronic detector time constant

$$\tau_e = C_J[R_D R_L/(R_D + R_L)] \tag{5}$$

where C_J is the junction capacitance. Typically τ_e is smaller or equal to 10^{-8} sec, with R_D and R_L of the order of 1 Ω and $C_J \approx 10^{-8}$ F for junctions with $R_\square \approx 10^{-3}$ Ω. τ_e or the $C_J R_D$ product decreases with decreasing thickness of the tunneling barrier since $C_J \propto d^{-1}$ and $R_D \propto R_\square \propto \exp(2\kappa w)$ with κ the "imaginary" electron wavenumber in the insulating barrier of the width w (Kane, 1969). In most applications the electronic time constant can be neglected. Very low dynamic resistances and short electronic time constants are possible by the gap edge detection mode (Adkins, 1973). This operation mode also improves the detector sensitivity of high ohmic junctions.

B. Analysis of the Detector Sensitivity

In the limit of incident small-intensity 2Δ-phonon radiation, the increase of the quasiparticle steady-state density δN in the detector can be described by the simple relation (Eisenmenger, 1969)

$$\delta N = \tau_{\text{eff}} I_{\text{Q}} \tag{6}$$

with $I_{\text{Q}} = 2\dot{n}_{\text{ph}}/V$ the quasiparticle excitation rate per unit time and volume. $\dot{n}_{\text{ph}}$ is the total number of 2Δ-phonons absorbed per unit time in the junction volume V, each phonon creating two quasiparticles. If phonons of much higher energy than 2Δ are detected, the relation between I_{Q} and $\dot{n}_{\text{ph}}$ becomes frequency dependent, as will be discussed in Section IV,D. τ_{eff} is the effective time constant directly obtained from the detector signal decay in pulse measurements as described in Section III,D. Before extending relation (6) to the more general situation of finite phonon radiation intensity and higher energies than 2Δ, the relation between δN and the short-circuit signal current i_{S} will be discussed using the theoretical results of tunneling between identical superconductors (Giaever and Megerle, 1961; see also Meservey and Schwartz, 1969).

In the semiconductor scheme (Giaever and Megerle, 1961) the tunneling current integral for two identical superconductors can be written

$$I_{\text{SS}} = \frac{1}{eR_{\infty}} \int_{-\infty}^{+\infty} dE \frac{E(E+eV)[f(E) - f(E+eV)]}{\{(E^2-\Delta^2)[(E+eV)^2-\Delta^2]\}^{1/2}} \tag{7}$$

where e is the electron charge, R_{∞} the normal conductor tunneling resistance, and $f(E), f(E+eV)$ the Fermi functions at E and $E+eV$, respectively. The expressions $E/(E^2-\Delta^2)^{1/2}$ and $(E+eV)/[(E+eV)^2-\Delta^2]^{1/2}$ describe the superconductor density of state functions.

In the thermal tunneling range, i.e., $0 < eV < 2\Delta$, the only contributions to the integral (see Fig. 2) are from thermally excited electronlike quasiparticles at and above $E = \Delta$ and "holes" at $E = -\Delta$, where the integrand in the density of states function $E/(E^2-\Delta^2)^{1/2}$ has singularities. The other slowly varying density of states function $(E+eV)/[(E+eV)^2-\Delta^2]^{1/2}$ can be replaced by its value at the singularity $E = \pm\Delta$. With $kT \ll eV$ and correspondingly $|f(eV+\Delta)| \ll 1$, we obtain from Eq. (7) an approximate expression for the thermal quasiparticle current I_{SST}:

$$I_{\text{SST}} = \frac{1}{eR_{\infty}} \frac{(eV+\Delta)}{[(eV+\Delta)^2-\Delta^2]^{1/2}} 2 \int_{\Delta}^{\infty} \frac{E}{(E^2-\Delta^2)^{1/2}} f(E)\, dE \tag{8}$$

The integral corresponds to $N_{\text{T}}/4N_0$, N_{T} being the total density of thermally excited quasiparticles and N_0 the density of electron states for one spin. The

factor of 4 in front of N_0 takes account of electron and holelike excitations and both spin states contributing to N_T.

Replacing the integral by $N_T/4N_0$ the total thermal tunneling current can be expressed by

$$I_{SST} = \frac{1}{2eR_\infty}\frac{N_T}{N_0}\frac{(eV+\Delta)}{[(eV+\Delta)^2-\Delta^2]^{1/2}} \tag{9}$$

The more general but also complicated expression can be found in the article of Meservey and Schwartz (1969). For N_T, the approximate integration valid for $T < 0.5T_c$ results in

$$N_T = 2N_0[2\pi\Delta(T)kT]^{1/2}e^{-\Delta(T)/kT} \tag{10}$$

where $\Delta(T)$ can be replaced by $\Delta(0)$ for $T \ll 0.5T_c$. N_T is consistent with the BCS specific heat contribution of both "electron" and "holelike" excitations with energy at low temperatures. Since Eq. (9) describes the tunneling current for a thermal quasiparticle distribution of width $\delta E \approx kT$ and $0 < \delta E < eV < 2\Delta$, the approximation used in Eq. (8) can be also applied to nonthermally distributed quasiparticle excitations as long as their distribution width is small compared to eV. Such nonthermal distributions of excitations above the energy gap Δ may occur in detection of phonons of energy $E \gtrsim 2\Delta$ or if 2Δ-phonons in a narrow band $\delta E < kT$ are being absorbed. Under these conditions the thermal quasiparticle density N_T can be replaced by a generalized density N and it is possible to define an occupation temperature T^* by Eq. (10) setting $N = N_{T*}$. For most experimental situations Eq. (9) in this generalized interpretation provides a sufficiently accurate description, being also applicable if quasiparticles are primarily excited to a higher energy than Δ, since these quasiparticles decay within a very short relaxation time to the gap edge. Moreover, deviations from the thermal quasiparticle distribution can be checked experimentally by comparing the thermal I–V characteristic at different temperatures with the shifted I–V characteristic under 2Δ-phonon radiation. In using Sn junctions as phonon generators and detectors agreement between the influence of a temperature increase and 2Δ-phonon radiation was found within experimental error limits (Eisenmenger, 1967b). Absolute calibration of the detector is therefore possible by using Eq. (9) in the form

$$i_S = \frac{(eV+\Delta)}{2eR_\infty N_0[(eV+\Delta)^2-\Delta^2]^{1/2}}\,\delta N \tag{11}$$

where the quantities in front of δN express the total tunneling probability. Often nonideal properties of the tunneling junction make it difficult to determine R_∞. Instead, the experimental value of the thermal tunneling current

I_{SST} at the biasing point V provides a more reliable calibration. Dividing Eq. (11) by Eq. (9) results in the simple and plausible relation

$$i_S = \delta N(I_{SST}/N_T) \tag{12}$$

I_{SST} is obtained from the experimental thermal tunneling current by subtracting the leakage current. The latter can be determined graphically by plotting the measured current as a function of $\sqrt{T}e^{-\Delta/kT}$ and extrapolating to $T = 0$. N_T has to be calculated according to Eq. (10) by the use of N_0, as derived from electronic specific heat measurements (Kittel, 1967; Sheahen, 1966). N_0 data for Al, Sn, and Pb are found in Table I.

A further calibration method makes use of a measurement of the derivative of the thermal tunneling current $(dI_{SST}/dT)_{V=\text{const}}$ with respect to a change in bath temperature at the biasing point. Taking the derivation of Eqs. (9) and (10) with $\Delta(T) = \Delta(0) = \Delta$ we obtain from Eq. (11)

$$i_S = \left(\frac{dI_{SST}}{dT}\right)_V \frac{T}{N_T} \frac{1}{[\frac{1}{2} + (\Delta/kT)]} \delta N \tag{13}$$

Any one of Eqs. (11), (12), and (13) together with Eq. (6) makes it possible to determine the absolute number of 2Δ-phonons $\dot{n}_{ph}$ absorbed in the detector per unit time. As is directly evident from Eq. (11) the calibration terms on the right-hand side of Eqs. (11)–(13) in the limits of our approximation do not depend on temperature but only on voltage. Therefore, calibration at one temperature is sufficient, if the bias voltage is not changed.

In generalizing Eq. (6) the relation between δN and $\dot{n}_{ph}$ at finite phonon intensities can be calculated by using rate equations for quasiparticles and phonons. Following Rothwarf and Taylor (1967) these equations are

$$\dot{N} = I_Q + \beta N_\omega - RN^2 \tag{14}$$

$$\dot{N}_\omega = \frac{RN^2}{2} - \beta\frac{N_\omega}{2} - (N_\omega - N_{\omega T})\tau_\gamma^{-1} \tag{15}$$

where N is the quasiparticle density, I_Q the quasiparticle injection rate per unit volume, e.g., by 2Δ-phonon absorption, β the rate constant for quasiparticle generation by phonon reabsorption, R the rate constant for quasiparticle recombination, N_ω the density of 2Δ-phonons, $N_{\omega T}$ the thermal equilibrium density of 2Δ-phonons, and τ_γ the phonon escape rate into the substrate or other phonon losses.

Under equilibrium conditions $\dot{N} = 0$ and $\dot{N}_\omega = 0$, combining Eqs. (14) and (25) results in

$$I_Q = 2(N_\omega - N_{\omega T})\tau_\gamma^{-1} \tag{16}$$

i.e., the rate of quasiparticle injection by phonon absorption from incident

radiation is in equilibrium with twice the number of phonons emitted from or decaying within the junction. Quasiparticle losses, e.g., by diffusion out of the tunneling area can be assumed small and are not contained in Eqs. (14) and (15). In thermal equilibrium the detailed balance between phonons and quasiparticles is obtained with

$$\beta N_{\omega T} = R N_T^2 \tag{17}$$

Equations (16) and (17) inserted in (14) result in

$$N^2 = N_T^2 + I_Q 2\tau_{eff} N_T \tag{18}$$

with

$$\tau_{eff} = \frac{1}{2RN_T}\left(1 + \frac{\beta\tau_\gamma}{2}\right) \tag{18a}$$

and

$$\tau_R = 1/2RN_T \tag{18b}$$

the intrinsic recombination time. Equation (18) reduces to Eq. (6) if $\delta N \ll N_T$ in $N = \delta N + N_T$.

The range of weak phonon intensities, with $\delta N \ll N_T$ and δN depending linearly on I_Q or on the phonon intensity, is called linear limit of phonon detection. At high intensities with N or $\delta N > N_T$, a "square root limit" dependence on I_Q and $\dot{n}_{ph}$ is obtained in Eq. (18) (Dayem *et al.*, 1971). Experimentally both ranges can be easily distinguished from the measured ratio of i_S and I_{SST} as indicated by Eq. (12). For absolute measurements it is convenient but not necessary to avoid the "square root" or "overinjection" range. For the absolute determination of $\dot{n}_{ph}$ in the overinjection range $I_Q = 2\dot{n}_{ph}$ is calculated from Eq. (18) by inserting $N = \delta N + N_T$. δN and τ_{eff} are obtained from the experiment. Note: τ_{eff} must be measured using the detector pulse decay with small phonon intensities.

C. Detector Time Constant and 2Δ-Phonon Reabsorption

As can be seen from Eqs. (6) and (11) only τ_{eff} can give rise to a significant temperature dependence of 2Δ-phonon detection. Rothwarf and Taylor (1967) presented the first calculation of τ_{eff} as given in Eq. (18a). The factor $(1 + \frac{1}{2}\beta\tau_\gamma)$ describes the lifetime enhancement by repeated phonon emission and reabsorption or phonon trapping, β being the rate constant for 2Δ-phonon absorption by pair breaking and τ_γ the time constant for phonon escape or bulk decay. Both are independent of temperature in the range $T < 0.5T_c$. Only τ_R, the intrinsic recombination lifetime, is temperature dependent as follows from Eq. (18b) together with Eq. (10):

$$\tau_R = (2R)^{-1}(2\pi\Delta kT)^{-1/2} e^{\Delta/kT} \tag{19}$$

In all steady-state or pulse measurements of τ_{eff} the temperature dependence of Eq. (19) has been found (compare Fig. 14). Deviations at low temperatures can be attributed to magnetic frozen flux or to overinjection. For the calculation of the trapping factor $(1 + \frac{1}{2}\beta\tau_\gamma)$ and the influence of the film thickness, acoustical models have been used (Trumpp *et al.*, 1972b; Long, 1973a; Eisenmenger *et al.*, 1975). Experimentally the most important thickness range $d > \Lambda_w$ (where d is the total film thickness and Λ_w the 2Δ-phonon reabsorption mean free path) shows a linear increase of $\tau_{eff}(d)$ (see Fig. 15). For this range and pure surface phonon escape, τ_{eff} can be expressed by (Eisenmenger *et al.*, 1975):

$$\tau_{eff} = d\frac{N_T}{N_{\omega T}}\left(\frac{1}{c_t^3} + \frac{1}{2c_l^3}\right)\left(\frac{\overline{T}_t}{c_t^2} + \frac{1\overline{T}_l}{2c_l^2}\right)^{-1} \tag{20}$$

with

$$\overline{T}_{t,l} = \int_0^{\pi/2} d\varphi T_{t,l}(\varphi)\sin 2\varphi$$

as the average phonon transmissions and $T_{l,t}(\varphi)$ the angle-dependent longitudinal and transverse phonon transmission factors at the superconductor–substrate boundary as calculated by Little (1959) and Weis (1972). N_T and $N_{\omega T}$ are the quasiparticle and 2Δ-phonon densities at thermal equilibrium, c_t and c_l the transverse and longitudinal sound velocities in the film. Measurements in vacuum (see Fig. 15) with Sn–I–Sn detectors on silicon substrates show good agreement with calculation. The experimental slope was $\tau_{eff}/d = 7.0 \times 10^{-2}(\text{sec}\cdot\text{cm}^{-1})$, while the calculated τ_{eff}/d relation resulted in $\tau_{eff}/d = 6.8 \times 10^{-2}(\text{sec}\cdot\text{cm}^{-1})$ both at $\Delta = 590\ \mu\text{eV}$ and $T = 1.02°\text{K}$. Corresponding results were reported for Al detectors on Al_2O_3 substrates (Long, 1973a).

Inserting the detailed balance relation Eq. (17) in Eq. (20), it can be verified that the same temperature dependence is obtained as in Eq. (19). The proportionality between τ_{eff} and d for $d > \Lambda_w$ in the case of pure surface phonon escape can be explained as follows: τ_{eff} is determined by the ratio of the total number of quasiparticle excitations in units of 2Δ in the film divided by the phonon escape rate. This ratio is proportional to the volume to surface ratio of the-junction, which is equal to d. In the case of dominant volume losses, in contrast the surface or the thickness d has no influence on τ_{eff}. Therefore, with phonon surface escape and small volume losses a linear $\tau_{eff}(d)$ dependence is expected. Only at larger thickness values will τ_{eff} saturate and become independent of d.

From the experimental observation of a linear thickness dependence of τ_{eff} two conclusions can be drawn:

(i) The 2Δ-phonon mean free path is smaller than the lowest film thickness value d for which τ_{eff} still obeys the linear thickness dependence

law. From the measurement in Fig. 15 on Sn films, this results in $\Lambda_w < 2000$ Å in agreement with the estimate $\Lambda_w \lesssim 700$ Å of Narayanamurti and Dynes (1971) and the estimate from extrapolating ultrasonic absorption resulting in $\Lambda_w < 1000$ Å. The above conclusion is based on the theoretical result (Eisenmenger *et al.*, 1975) that $\tau_{eff}(d)/\tau_R$ in the limit of small d ($d \lesssim \Lambda_w$) approaches a thickness independent trapping factor ≥ 1. This limiting trapping factor depends on the angle of total phonon reflection at the film–substrate boundary resulting in a beginning deviation from the linear $\tau_{eff}(d)$ law at $d \sim \Lambda_w$.

(ii) With increasing film thickness up to $d = 5000$ Å no deviation of the linear relation between τ_{eff} and d has been observed. This indicates that bulk loss processes of 2Δ-phonons or other energy-decay processes within the film volume are negligibly small. Therefore, energy decay only takes place by phonon emission into the substrate or the helium bath. The result bears special importance for 2Δ-phonon generation since it can be concluded that all 2Δ phonons produced in recombination are finally emitted under vacuum conditions into the substrate even with high phonon trapping rates in the superconducting junction. For a Sn junction of $d = 3000$ Å thickness on silicon substrates a phonon trapping factor of 145 has been calculated (Eisenmenger *et al.*, 1975).

For efficient phonon detection the detector thickness d would be equal or larger than the 2Δ-phonon reabsorption mean free path. Under this condition τ_{eff} for typical phonon detectors can be calculated from Eq. (20). Results for the more important superconductors and substrates are given in Table II for vacuum conditions together with average phonon transmission rates and acoustical data. Contact to liquid ^{4}He reduces τ_{eff} by a factor ranging from 3 to 5. It has been suggested that τ_{eff} also weakly depends on the energy distribution of the excited quasiparticles although with different energy dependence (Dayem and Wiegand, 1972; Long and Adkins, 1973). Careful measurements should provide an answer to this question.

For the absolute determination of phonon intensities it is most reliable and convenient to determine τ_{eff} directly from the temperature-dependent pulse decay time of the detector.

D. Boundary Condition, Film Thickness, and Frequency Influence on the Number of Detected Phonons

In most experiments phonons are detected under normal incidence at the substrate–detector boundary. The corresponding vertical transmission factors $T_\perp$ calculated from the acoustical characteristic impedances of the substrate and junction are also listed in Table II. In most situations the transmission $T_\perp$ ranges from 0.9 to 1.

TABLE II

ACOUSTICAL DATA AND τ_{eff}/d AT $\Delta = 4kT^a$

	Al	Sn	Pb
ρ (g cm^{-3})	2.72	7.3	11.8
c_l (cm sec^{-1})	6.4×10^5	3.32×10^5	2.35×10^5
c_t (cm sec^{-1})	3.1×10^5	1.67×10^5	1.03×10^5
$T_{\perp l}$ on Al_2O_3	0.81	0.92	0.95
$T_{\perp t}$ on Al_2O_3	0.75	0.89	0.91
$T_{\perp l}$ on Si	0.99	1	0.99
$T_{\perp t}$ on Si	0.97	1	0.99
$\bar{T}_l$ on Al_2O_3	0.3	0.084	0.043
$\bar{T}_t$ on Al_2O_3	0.17	0.068	0.026
$\bar{T}_l$ on Si	0.45	0.126	0.063
$\bar{T}_t$ on Si	0.35	0.103	0.037
τ_{eff}/d (sec cm^{-1}) on Al_2O_3	5.3×10^{-2}	4.4×10^{-3}	1.3×10^{-3}
τ_{eff}/d (sec cm^{-1}) on Si	2.8×10^{-2}	2.9×10^{-3}	0.88×10^{-3}

[a] Compare Eq. (20) for superconducting films of Al, Sn, and Pb on Al_2O_3 and Si substrates. The acoustical data for Al_2O_3 are $\rho = 4.0$ g cm^{-3}, $c_l = 11.0 \times 10^5$ cm sec^{-1}, $c_t = 6.04 \times 10^5$ cm sec^{-1} both in c-direction. The data for Si are $\rho = 2.35$ g cm^{-3}, $c_l = 9.35 \times 10^5$ cm sec^{-1}, $c_t = 5.2 \times 10^5$ cm sec^{-1} both in [111] direction. For the evaluation of $\bar{T}$ in the case of Al the results of Little (1959) have been used. The values of $\bar{T}$ for Sn and Pb are approximated by $T(\varphi) = T_\perp$ for $\varphi < \varphi_{max}$ and $T(\varphi) = 0$ for $\varphi > \varphi_{max}$ [cf. Eq. (20)]. τ_{eff}/d has been calculated using the data for Δ and N_0 of Table I.

The acoustical treatment is justified in the frequency range of superconducting tunneling junctions by the good agreement between experiment and τ_{eff} calculations as discussed in Section IV,C. Corresponding evidence for the validity of the acoustic mismatch model was obtained in the heater experiments of Weis (1972).

The number of absorbed 2Δ-phonons $\dot{n}_{ph}$ depends on the mean free path Λ_w and the film thickness d. By taking account of multiple noninterfering reflections within the film we obtain under vacuum conditions at the free film surface

$$\dot{n}_{ph} = \frac{I_{ph\,2\Delta}}{2\Delta} F T_\perp \frac{(1 - e^{-2d/\Lambda_w})}{1 - (1 - T_\perp)e^{-2d/\Lambda_w}} \tag{21}$$

where $I_{ph\,2\Delta}$ is the incident phonon intensity within the substrate in front of the detector with area F. With $d = \Lambda_w$ and $T_\perp = 0.9$ we find from Eq. (21)

that 79% of the incident phonons are contributing to pair breaking. For Sn-detectors with typical thicknesses of 2000 to 3000 Å and $\Lambda_w \leq 1000$ Å the number of detected 2Δ-phonons $\dot{n}_{ph}$ is determined by $T_\perp$ alone, since phonon absorption in the detector reaches at least 98%. For Pb junctions the situation is similar. Films of Pb and Sn with $d < 2000$ Å are difficult to prepare at room temperature. Pure Al films instead have been obtained at room temperature evaporation with minimum d values of 100 Å. With Λ_w between 1000 and 2000 Å for 2Δ-phonons as estimated from quasiparticle recombination lifetime (Eisenmenger *et al.*, 1975) the thickness dependence in Eq. (21) is expected to be significant. The measurement of the influence of d on the number of detected phonons, in principle, provides a method for determining Λ_w.

So far, the discussion has been limited to phonons of the energy 2Δ. Including the influence of frequency, two aspects are important. First, Λ_w and α_S, the constant of absorption in the superconducting state, are functions of the frequency ω in the form $\alpha_S(\omega) = f(\omega)\alpha_n(\omega)$ with $\Lambda_w = (2\alpha_S)^{-1}$. The function $f(\omega)$ has been calculated by Tewordt (1962a) and Bobetic (1964), as shown in Fig. 4, within the framework of the BCS theory for longitudinal phonons. The results for $f(\omega)$ are also expected to be applicable to transverse waves. With respect to the attenuation $\alpha_n(\omega)$, only estimates both for longitudinal and transverse phonons are possible. For normal processes in the electron–phonon interaction α_n increases linearly with frequency if $ql > 1$ (Morse, 1959; Pippard, 1960), where q is the phonon wave number and l the electronic mean free path. This proportionality to ω has been used for determining Λ_w for 2Δ-phonons by the extrapolation of experimental ultrasonic absorption data. In view of the neglect of Umklapp processes and phonon collision drag (Yokota *et al.*, 1966; Clairborne and Morse, 1964; Leibowitz, 1964a,b) the order of magnitude agreement with experimental data is satisfactory. Λ_w values for longitudinal and transverse phonons are of the same order of magnitude, i.e., ~1000 Å in the 500-GHz frequency range as follows from the high detection rate for both polarizations in superconducting tunneling junctions.

More accurately calculated data of Λ_w for Pb, Sn, and Al than obtained by the extrapolation of ultrasonic absorption are presently not available. Observation of a frequency dependence of Λ_w is possible again by using Al-detector junctions with small thickness d, i.e., in the range $d < \Lambda_w$. Experimental indication of Λ_w for transverse phonons decreasing with frequency in thin granular Al detectors was found by Kinder (1972b).

A second influence of frequency on phonon detection arises from the

possibility that a phonon with multiples of energy 2Δ can excite more than two quasiparticles. This can be expressed by a multiplicator function or counting rate $m(E_{ph})$ to be introduced in I_Q in Eq. (6):

$$I_Q = (2\dot{n}_{ph}/V)m(E_{ph}) \tag{22}$$

The form of this function (see Fig. 17) can be discussed in analogy to the influence of phonon reabsorption and reemission at battery voltages of $eV = 6\Delta$ (compare Figs. 12 and 13).

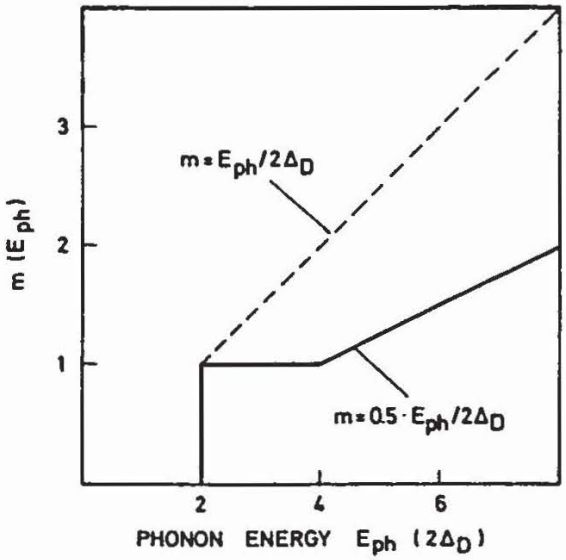

FIG. 17. Detector phonon counting rate m as a function of phonon energy E_{ph}. $m = 1$ corresponds to the excitation of two quasiparticles by Cooper pair breaking in the energy range $2\Delta < E_{ph} < 4\Delta$. For higher energies the counting rate is expected to increase as $m = 0.5E_{ph}/2\Delta$ by additional 2Δ-phonons produced by quasiparticle relaxation in the detector as indicated in Fig. 13. The dashed line corresponds to a counting rate increasing in proportion to energy with $m = 1$ at $E_{ph} = 2\Delta$ (Forkel 1973).

For phonon energies E_{ph} below 2Δ the function $m(E_{ph})$ is zero. The unit step at $E_{ph} = 2\Delta$ continues to $E_{ph} = 4\Delta$ followed by an almost linear increase with energy. In the phonon range $2\Delta < E_{ph} < 4\Delta$ quasiparticles are excited by pair breaking in a continuous energy range from Δ to $E_{ph} - \Delta$. During relaxation these quasiparticles emit phonons in the continuous band $E_{ph} - 2\Delta$. Incident phonon energies exceeding $E_{ph} = 4\Delta$ produce an almost linear increase of the number of relaxation phonons now additionally exciting quasiparticles by reabsorption. Thus only in the energy range $2\Delta < E_{ph} < 4\Delta$ is the detector acting as a frequency-independent phonon counter. At energies above $E_{ph} = 4\Delta$ the number of quasiparticles or the

detector current depends linearly on energy. These energy-detecting properties have been verified in experiments with Al tunneling junctions as high-frequency phonon generators and Sn junctions as detectors (Forkel *et al.*, 1973) (to be discussed in Sections V,D and VI,C). Quasiparticle generation in proportion to energy has also been assumed in recombination lifetime measurements by use of optical excitation (Parker and Williams, 1972; Rothwarf *et al.*, 1974). Since the thermal energy of the superconducting film at $T \approx 0.5T_c$ is represented by quasiparticle excitations whereas lattice contributions can be neglected, it has been noted that a high fraction of up to 0.8 of the entire optical energy absorbed by the metal film will be converted to quasiparticle excitations. This would correspond to almost complete splitting of incident quanta, either photons or phonons, into units of 2Δ. The corresponding multiplicator function $m(E) = E/2\Delta$ for $E \geq 2\Delta$ has been introduced in Fig. 17 as a dashed line. The model of quantitative energy splitting does not account for quasiparticle relaxation with phonon emission below $E_{ph} = 2\Delta$, as would be expected in repeated phonon reabsorption and relaxation, and also does not describe the $m = 1$ energy range of phonon-counting properties. The use of a multiplicator function $m(E) = 1$ for $2\Delta < E_{ph} < 4\Delta$ and $m(E) = 0.5E/2\Delta$ for $E > 4\Delta$ in Fig. 17, describing phonon counting between 2Δ and 4Δ and energy detection beginning with energy 4Δ, therefore appears more realistic. As compared to a complete energy conversion of high-energy quanta to quasiparticle excitations, in this model about 50% of the total energy will be converted to phonons, with energies below 2Δ emitted in relaxation. These phonons are not reabsorbed and can directly escape from the film into the substrate. Consequently, their contribution to the thermal energy is not delivered to quasiparticle excitations, which efficiently trap phonons of energy 2Δ within the film. Typical time constants for low-energy phonon escape are of the order of 10^{-9} to 10^{-8} sec as obtained in heat pulse experiments (von Gutfeld, 1965), whereas time constants τ_{eff} for quasiparticle recombination and 2Δ-phonon trapping are of the order 10^{-7} to 10^{-6} sec (cf. Fig. 14) (Eisenmenger, 1969). A quantitative treatment of the $m(E)$ function on the basis of the decay rate expressions given in Section V taking account of multiple decay steps would be useful.

E. Detector Sensitivity for Low-Energy Phonons

In the BCS calculation of phonon absorption, phonons with energy less than 2Δ are attenuated by excited quasiparticles being scattered into states of higher energy. This absorption is strongly temperature dependent and reaches about 5% of $\alpha_s(2\Delta)$ for $T = 0.5T_c$. As an upper limit for the entire frequency range $0 < E_{ph} < 2\Delta$ the BCS expression for low-frequency ultra-

sonic attenuation can be used (compare Fig. 3):

$$\alpha_S = 2\alpha_n(e^{\Delta(T)/kT} + 1)^{-1} \tag{23}$$

With $\Delta/kT \sim 6.5$ as a typical operation condition for Sn detectors we obtain $\alpha_S = 3 \times 10^{-3}\alpha_n$. With Λ_w of the order of 1000 Å, this results in $\alpha_n \sim 5 \times 10^4$ cm^{-1}. For a detector film thickness of about 3000 Å the fraction of low-energy absorption therefore amounts to about 1% of the incident power. This energy is contained in the quasiparticle energy exceeding $E = \Delta$ and does not result in an additional tunneling signal since the number of quasiparticles has not been changed. Within time constants of 10^{-9} to 10^{-8} sec quasiparticle relaxation and the corresponding emission of low-energy phonons with $E_{ph} < 2\Delta$ again leads to a fast escape of this energy into the substrate. The ratio of the time constants for this low-energy phonon absorption and reemission process of about 10^{-8} sec and of the effective recombination time of 10^{-6} sec is of the order of 10^{-2}. Referring to equal amounts of absorbed power in the detector the stationary energy density for low-energy phonons and excitations, therefore, will be smaller by a factor 10^{-2} than the energy density in the case of quasiparticle excitations by 2Δ-phonon absorption. Since the transfer of energy from the low-energy phonon system to the quasiparticle population cannot be larger than this ratio it follows that for the Sn detector discussed the signal contribution of low-energy phonons being absorbed at a ratio of 1% is smaller by at least a factor of 10^{-4} than the 2Δ-phonon sensitivity. In heat pulse experiments (Frick *et al.*, 1975) it has been found that the low-energy part of the emitted spectrum is not detected by Sn junctions. Also low-energy phonon radiation from Al-tunneling generators (Welte *et al.*, 1972a,b; Forkel *et al.*, 1973) is not detected by Sn junctions. At higher temperatures $T > 0.5T_c$, increased phonon absorption can result in finite low energy phonon signal contributions as has been found with Al detectors (Welte, 1973, Forkel, 1975a).

F. Numerical Example for the Detector Signal–Noise Limits and Practical Considerations

For most applications it is convenient to discuss the detector properties in terms of noise equivalent power for a bandwidth of 1 Hz or the corresponding integration constant of 0.25 sec. Since the phonon detector is at liquid helium temperature the input noise of the electronic amplifier at room temperature will be the dominant noise source. We are not discussing the possibility of low-noise preamplification where the Nyquist or the shot noise (Forkel and Eisenmenger, 1976) of the detector determines the signal power

limit. In the frequency range from dc to several megahertz the input noise of available electronic amplifiers is close to the Nyquist noise at room temperature of about $(\overline{V^2})^{1/2} = 1.3 \times 10^{-10}$ V (Hz Ω)$^{-1/2}$. With a dynamical junction resistance $R_D = 1\ \Omega$ matched to the amplifier, the corresponding short-circuit equivalent noise current i_{SN} amounts to 1.3×10^{-10} A for a 1-Hz bandwidth. Using Eq. (11) with $R_\infty = 10^{-3}\ \Omega$, $N_0 = 1.4 \times 10^{22}$ eV^{-1} cm^{-3} for Sn, and a biasing voltage $eV = \Delta$, the necessary increase of the quasiparticle population in the detector is obtained with $\delta N = 3 \times 10^9$ cm^{-3}.

The number of phonons absorbed per unit time giving rise to this quasiparticle population amounts to $\dot{n}_{ph} = 1.2 \times 10^9$ sec^{-1} as calculated from Eq. (6) with $\tau_{eff} = 0.5 \times 10^{-6}$ sec and the tunneling junction volume $V = 0.1 \times 0.1 \times 4.10^{-5}$ cm^3. From this, the 2Δ-phonon noise equivalent power for $2\Delta_{Sn} = 1.2$ meV gives $P_N = 2.3 \times 10^{-13}$ W at a 1-Hz bandwidth. This is comparable to the signal detection capabilities of the best far infrared detectors. The corresponding signal–noise resolution has been reached in phonon experiments using lock-in techniques (Forkel, 1973). For pulse detection in the 1-μsec range the bandwidth is increased by a factor of 10^6 and the noise equivalent power amounts to $P_N = 2.3 \times 10^{-10}$ W. Providing a factor of 10 for better amplitude resolution and a maximum factor of 10^6 for possible generator–detector propagation losses, a generator signal power of 10^{-3} W is sufficient for single-pulse detection. Using boxcar integration this power can be again significantly reduced.

In phonon detection with junctions of large "2Δ current ratio" (cf. Section III,A,1) or of "high quality" a good signal to noise ratio is also observed. This can be easily understood in generalizing the foregoing discussion. Under perfectly matched conditions, i.e., $R_L = R_D$ (dynamic resistance equal to load resistance), the signal power supplied to the preamplifier input amounts to $P_S = 0.25 i_S^2 R_D$, whereas the equivalent noise power of the amplifier input is given by $P_N = 4kT^*\Delta\nu$ (T^* is the effective noise temperature and $\Delta\nu$ the bandwidth) not dependent on the detector. The ratio of the signal to noise current or voltage is $I_S : I_N = V_S : V_N = (P_S : P_N)^{1/2}$, and we obtain $V_S : V_N \propto i_S (R_D)^{1/2}$. Using Eq. (11) this results in

$$V_S : V_N \propto \delta N (R_D)^{1/2} : R_\infty = \delta N (R_D/R_\infty)^{1/2} (1/R_\infty)^{1/2}.$$

Since the "2Δ current ratio" can be approximated by $R_D : R_\infty$, the improved signal to noise ratio for good quality junctions is correctly described. In addition, it is important that the junction be "low ohmic" as expressed by the factor $1/(R_\infty)^{1/2}$. Similarly for high ohmic termination, $R_L > R_D$, it is found that

$$V_S : V_N \propto \delta N (1/R_L)^{1/2} (R_D/R_\infty)$$

and for low ohmic termination, $R_L < R_D$, the signal to noise ratio is determined by

$$V_S : V_N \propto \delta N(R_L)^{1/2}(1/R_\infty)$$

High or low ohmic termination in general is inferior to matched conditions with respect to the signal to noise ratio. These considerations are independent of the special matching techniques used, e.g., electrical transforming or dividing the junction into smaller elements operating in series (see Fig. 7).

V. Phonon Emission Spectra

A. General Relation for Quasiparticle–Phonon Interaction

Phonon emission in recombination and relaxation transitions of excited quasiparticles in superconductors can be treated within the framework of the BCS theory. The primary phonon spectrum is obtained from the normalized decay probability of a quasiparticle with energy E under the emission of a phonon with energy Ω. Normalization refers to a total decay probability of unity. Convolution integration of the normalized decay probability with the quasiparticle injection distribution as used in the tunneling integral (Giaever and Megerle, 1961) results in the total primary phonon spectrum. Secondary and other spectra arise from further decay steps if allowed.

In general, primary phonons undergo further electron–phonon interactions within the superconducting film before escaping into the substrate. Phonon emission into the substrate, therefore, also depends on reabsorption and reemission processes within the film and on the boundary conditions at the film–substrate interface. As a limiting situation one can expect that primary phonons are emitted into the substrate with little further interaction if the film thickness is small compared to the phonon reabsorption mean free path and also that contributions of secondary decay steps are negligibly small. A complete treatment of the spectrum in general being involved, different approximations have been used depending on the special situation. The bases of calculation are the following BCS transition probabilities describing quasiparticle decay and excitation [see, for example, Dayem and Wiegand (1972), Long and Adkins (1973)]. The same equations have also been obtained by Tewordt (1962a,b). The differential transition probabilities $d\Gamma$ are

(i) Relaxation transition of a quasiparticle injected at the energy E to the energy E' in the interval $dE' = d\Omega$ under the emission of one phonon with energy $E_{ph} = \Omega$:

$$d\Gamma_{E\to E',\Omega} = C\, d\Omega\Omega^2[1 + g(\Omega)]N_S(E')[1 - f(E')][1 - (\Delta^2/EE')] \quad (24)$$

where E and $E' = E - \Omega$ range from the maximum injection energy E_{max} to the minimum energy of quasiparticles at the gap edge, $E_{max} = eV - \Delta$ in tunneling between identical superconductors. C is a constant describing the electron–phonon interaction for one phonon mode under the assumption of isotropic conditions [cf. Tewordt (1962a,b), Dayem and Wiegand (1972), Long and Adkins (1973)]. In the factor Ω^2 one Ω describes the frequency dependence of the square of the electron–phonon matrix element while the second factor Ω represents the effective phonon density of states resulting from momentum conservation. Within the limits of the BCS model, these Ω-proportionalities are only applicable to longitudinal phonons and normal processes with electron mean free paths exceeding the phonon wavelength. An extension of the Ω proportionality in the electron–phonon interaction and in the phonon density of states also to transverse waves and Umklapp processes appears possible for the case of Al (Long and Adkins, 1973). The linear Ω-dependence of the phonon density of states can be applied as long as the radius of curvature of the Fermi surface is large compared to the phonon wavenumber q. The factor $1 + g(\Omega)$ describes spontaneous and stimulated phonon emission with $g(\Omega) = (e^{\Omega/kT} - 1)^{-1}$, the Bose factor. $N_S(E') = N_0 E'(E'^2 - \Delta^2)^{-1/2}$ is the BCS density of states, which multiplied by $[1 - f(E')]$ corresponds to the density of unoccupied final states, $f(E') = (e^{E'/kT} + 1)^{-1}$ being the Fermi factor. N_0 is the normal density of states at the Fermi level. The last term in Eq. (24) is the BCS coherence factor approaching zero for $E \to \Delta$ and $\Omega \to 0$, significant for destructive interference. The coherence factor applies equally well for transverse and longitudinal waves.

(ii) Recombination transition of a quasiparticle injected at E with quasiparticles at the energy E' in the interval $dE' = d\Omega$ under the emission of a phonon of energy $E_{ph} = \Omega$. With $\Omega = E + E'$ and $E \geq \Delta$ as $E' \geq \Delta$ the differential probability is given by

$$d\Gamma_{E,\,E' \to \Omega} = C\, d\Omega \Omega^2 [1 + g(\Omega)] N_S(E') f(E') [1 + (\Delta^2/EE')] \qquad (25)$$

The terms of Eq. (25) are defined as the corresponding expressions in Eq. (24). In contrast to relaxation the differential probability for recombination is proportional to the density of occupied partner states $N_S(E')f(E')$. For the lowest energies $E = E' = \Delta$, the coherence factor $[1 + (\Delta^2/EE')]$ is now constructive and has its maximum value.

(iii) Quasiparticle excitation from energy E to E' by the absorption of one phonon with energy $\Omega = E' - E$ is described by the differential probability

$$d\Gamma_{\Omega,\,E \to E'} = C\, d\Omega \Omega^2 g(\Omega) N_S(E') [1 - f(E')] [1 - (\Delta^2/EE')] \qquad (26)$$

Nonthermal phonon distributions can be entered by their actual occupation

numbers instead of $g(\Omega)$. From the differential probability the differential number of transitions $d\dot{N}$ per unit time and volume can be obtained by multiplying Eq. (26) with the density of occupied initial quasiparticle states:

$$d\dot{N}_{\Omega, E\to E'} = d\Gamma_{\Omega, E\to E'} N_S(E) f(E)$$
$$= C\, d\Omega\Omega^2 g(\Omega) N_S(E) f(E) N_S(E')[1 - f(E')][1 - (\Delta^2/EE')] \quad (27)$$

Equation (27) describes the absorption of low-energy phonons by excited quasiparticles.

Phonon detection via pair breaking is given by the formally similar expression:

$$d\dot{N}_{\Omega\to E, E'} = C\, d\Omega\Omega^2 g(\Omega) N_S(E)[1 - f(E)] N_S(E')[1 - f(E')][1 + (\Delta^2/EE')] \quad (28)$$

Pair breaking processes are only possible if the final states E, E' are empty and $\Omega \geq 2\Delta$ since $E, E' \geq \Delta$. The coherence factor is maximal for $E = E' = \Delta$ in contrast to the coherence factor in Eq. (27). Therefore, phonon absorption by thermally excited quasiparticles is further reduced by destructive interference of probability amplitudes, whereas pair breaking is enhanced by constructive interference. Equations (24)–(28) or corresponding relations have been used by different authors for the treatment of the spectral properties of phonon generation and detection.

So far, in these calculations little information is available on the absolute interaction strength between electrons and phonons as expressed by the constant C in Eqs. (24)–(28). Even the relative transition rates with respect to longitudinal and transverse phonons can only be estimated. This is mainly due to the complicated anisotropic deformation potential of real metals but also to influences of Umklapp processes modifying the phase space of allowed transitions and additional unknown interaction contributions. By comparison with the BCS transition probability (cf. Dayem and Wiegand, 1972) it is easily found that the constant C depends as $C \propto (D/c^2)^2$ on the deformation potential $D = \frac{2}{3}E_F$ and the sound velocity c. $D = \frac{2}{3}E_F$ applies for the free electron gas approximation with a spherical Fermi surface, resulting only in longitudinal phonon interactions. We can tentatively extend this model to transverse phonon interaction by normal processes at asymmetric regions of the Fermi surface assuming an average effective transverse deformation potential $\bar{D}_t$ in real metals of about the same strength as the average longitudinal deformation potential $\bar{D}_l$. This would result in longitudinal transition rates in proportion to c_l^{-4} and transverse phonon rates in proportion to $2c_t^{-4}$. The factor of 2 results from the degeneracy of transverse modes. With $c_l \sim 2c_t$ the transition probability, e.g., in relaxation Eq. (24), is higher by a factor of 32 for transverse phonon emis-

sion than for longitudinal phonon emission. This rough estimate is at least qualitatively in agreement with the experimental experience that transverse phonon generation often exceeds longitudinal phonon contributions.

In recombination phonon generation with strong phonon trapping, a quasithermal equilibrium between quasiparticle excitations and longitudinal and transverse 2Δ-phonons is established (cf. Section V). The phonon radiation intensities result from the phonon densities of state $\propto c_l^{-3}$ and $\propto 2c_t^{-3}$ by multiplication with the sound velocities in proportion to c_l^{-2} and $2c_t^{-2}$ for longitudinal and transverse phonons, respectively, i.e., a different result than for relaxation with equal values of the average effective deformation potentials $\bar{D}_t$ and $\bar{D}_l$. The experimental comparison of longitudinal and transverse pulse amplitudes between recombination phonon generation at $\Omega = 2\Delta_G$ with strong phonon trapping, and relaxation phonon emission without trapping in the range $\Omega < 2\Delta_G$ in principle opens a possibility for obtaining information on the ratio of $\bar{D}_l$ and $\bar{D}_t$ (cf. also Long, 1972). This comparison can be applied to the experimental results of Kinder (1971), indicating $\bar{D}_t \approx 0.5\bar{D}_l$ for Sn junctions as phonon generators (cf. Section VI,B). This result can be compared with phonon mean free path determinations in superconducting Al films (Long, 1972) with values of $\Lambda_t \approx 3400$ Å and $\Lambda_l \approx 1600$ Å at $\Omega = 2\Delta_{Al}$. Expressing Λ_w for both phonon modes with the help of Eq. (28) and the density of phonon states we obtain $\bar{D}_t \approx 0.3\bar{D}_l$ from the Λ_w data of Long. The comparatively weaker transverse wave interaction in Al as compared to Sn may be attributed to the simpler Fermi surface of Al.

B. Recombination Phonons

1. *General Conditions*

According to Eq. (3) it is assumed that the number of primary recombination 2Δ-phonons $\dot{n}_{ph\,G}$ produced in the generator per unit time, is equal to the number of tunneling single quasiparticles, i.e., $\dot{n}_{ph\,G} = \dot{n}_{rec} = I_G/e$. This assumption is justified since the thermal tunneling current, the double particle tunneling current, the ac Josephson induced dc currents, as well as other "leakage" currents are generally small compared to the pair-breaking single-particle current. Only with extremely low ohmic junctions $R < 10^{-3}\,\Omega$ (area 1 mm^2) do thermally excited quasiparticles or additionally populated quasiparticles excited by reabsorption of generator 2Δ-phonons as well as double particle tunneling, etc., contribute to an increasing but still small fraction of the tunneling current. For this fraction of the tunneling current one must expect that Eq. (3) is violated. At generator voltages $eV > 2\Delta$ thermally excited quasiparticles are injected at the energy $E_Q > 3\Delta$ above the Fermi level. In relaxation to the gap edge $E'_Q = \Delta$,

only a small fraction of energy is emitted in the form of 2Δ-phonons, the larger part being phonons of less energy than 2Δ. Recombination in this case does not contribute to phonon generation since the quasiparticles have already been thermally excited before tunneling by 2Δ-phonon absorption via pair breaking. Also in the thermal tunneling regime at $|eV| < 2\Delta$ no 2Δ-phonon generation is possible in single-particle tunneling since the energy of the relaxation phonons is smaller than 2Δ. This is to be contrasted with experiments performed by Kinder (1971), who observed 2Δ-phonon generation at $|eV| < 2\Delta$ by applying a parallel magnetic field to a low ohmic generator junction. In the range of enhanced dc tunneling currents resulting from strong Josephson ac oscillations in the barrier, photon–phonon energy up-conversion was demonstrated by the correlation between the detected changes of the 2Δ-phonon signal amplitude at characteristic subharmonic generator voltages $eV = 2\Delta/n$ ($n = 2, 3, 4, \ldots$). Dayem (1972) measured excess currents in low ohmic detector junctions at $\Delta < eV < 2\Delta$, which he attributed to 2Δ-phonon generation in the detector produced by ac Josephson currents. Finally, also double-particle tunneling (Wilkins, 1969) is expected to contribute to 2Δ-phonon generation in the voltage range $\Delta < eV < 2\Delta$. Generally, low ohmic detector junctions under vacuum conditions show an increase of quasiparticle population compared to thermal equilibrium if biased. This can be experimentally checked by the change in the I–V characteristic when the junction is brought in direct contact with liquid helium or by a measurement of the thermal tunneling current at constant voltage as a function of temperature and by comparing with Eq. (9). This "heating" influence is partly due to the above processes being related to the "leakage" currents dominating at lower temperatures. Since all these current contributions in good junctions are small, i.e., $< 1\%$, compared to the generator current at $eV \geq 2\Delta$ they are not further discussed with respect to phonon generation.

In phonon generation by recombination the steep tunneling current increase at $eV = 2\Delta$ leads to quasiparticle excitations with $E_Q = \Delta$. As long as the thermal quasiparticle population is only weakly disturbed, the quasiparticles recombine within τ_{eff}. From Eq. (6) the quasiparticle current $I_{Q\,max}$ for the onset of overinjection is obtained by setting $\delta N = N_T$. This results in $I_{Q\,max} = N_T(\tau_{eff})^{-1}$. Since $I_{Q\,max} V_D = 2I_G e^{-1}$ with I_G the tunneling current, e the electron charge, and V_D the tunneling junction volume, we can calculate the corresponding generator current limit for a typical Sn junction. Using $V_D = 0.1 \times 0.1 \times 4 \times 10^{-5}$ cm^3, $\tau_{eff} = 0.5 \times 10^{-6}$ sec, $N_T = 3 \times 10^{16}$ cm^{-3}, as obtained from Eq. (10), with $\Delta = 0.58$ meV, $T = 1.0$°K, and $N_0 = 1.4 \times 10^{22}$ eV^{-1} cm^{-3}, the overinjection current limit results with $I_G = 2 \times 10^{-3}$ A. For Al at the same $T : T_c$ ratio, the overinjection current limit of the generator is reduced at least by one order of magnitude. Phonon experi-

ments with sufficient signal amplitude under the condition of a small disturbance of the thermal equilibrium in the generator can be performed preferably if generator and detector are in close phonon contact, separated only by a 1000 Å SiO layer (Long and Adkins, 1973).

2. *Recombination Phonon Emission in the Thermal Equilibrium Limit*

Injected quasiparticles at tunneling voltages close to $eV = 2\Delta$ recombine predominantly with thermally excited quasiparticles at the gap edge. Even at small excess voltages $|eV - 2\Delta| < kT$, the primary recombination phonon emission occurs at an average energy $E_{ph} = 2\Delta + \delta E$, with δE the phonon bandwidth of order kT. Long (1973a) noticed that recombination transitions according to Eq. (25) with strong phonon trapping can be shown to result in a Bose or Planck spectrum high-energy tail of the form

$$S(\omega)\, d\omega \propto \omega^2 e^{-\omega/kT}$$

with a sharp cutoff below $\hbar\omega = 2\Delta$. Also for wider energy distributions of injected quasiparticles, recombination phonon emission at 2Δ with a bandwidth of kT is to be expected for small disturbances of the thermal quasiparticle distribution and strong phonon trapping. Experimental evidence for the energy width kT of recombination phonons in this limit has been given by Long (1973b). Aluminum junctions for phonon generation and detection have been evaporated on top of each other with a separating thin SiO layer. The energy gaps of the two junctions were different. Using the junction with larger gap as generator all recombination phonons contributed to detection, and the temperature dependence of the signal amplitude at constant generator current could be accurately described by the temperature dependence of the detector time constant. In reverse operation with $\Delta_G < \Delta_D$ (with Δ_G the energy gap of the generator and Δ_D the energy gap of the detector) the signal amplitude was reduced, and only the high-energy thermal tail of recombination phonons above $2\Delta_D$ contributed to a detector signal. The temperature dependence of the signal amplitude in this case deviated from the temperature dependence of the detector time constant, thus confirming the variation of the spectral bandwidth $\delta E \approx kT$ of the generator phonons.

A more detailed calculation of the recombination phonon spectrum as a function of the generator voltage has been performed by Dayem and Wiegand (1972) for the case of finite phonon escape. Taking account of all processes described by Eqs. (24)–(28), i.e., in addition to recombination also the contribution of relaxation, quasiparticle excitation, and pair breaking, Dayem introduced detailed balance relations for 40 equally spaced energy levels in the quasiparticle energy range from $E = \Delta$ to $E = 3\Delta$. For each level the rate of quasiparticle injection according to the tunneling integral Eq. (7)

was set in balance to the rate of relaxation to all other levels, to the rate of further excitations by phonon absorption, to the rate of recombination with other quasiparticles, and to the rate of quasiparticle injection by relaxation from other levels or by pair excitation. The corresponding phonon balance equations contained a phonon escape parameter describing the influence of phonon trapping. Since the phonon lifetime for escape into the substrate (without taking account of reabsorption) was approached by $\tau = d(c^{-1})$ (with d the total junction thickness and c the sound velocity) corresponding to perfect boundary transmission, phonon trapping is not very strong in this model. The numerical solutions of the rate equations limited to the case of a weak disturbance of the thermal quasiparticle population were obtained for the BCS density of states distribution and also for the experimental density of states as determined from a typical tunneling characteristic. The resulting spectrum for quasiparticle injection by tunneling only into the first level at the energy $E = \Delta$ is shown in Fig. 18. The finite width of the 2Δ-phonon line

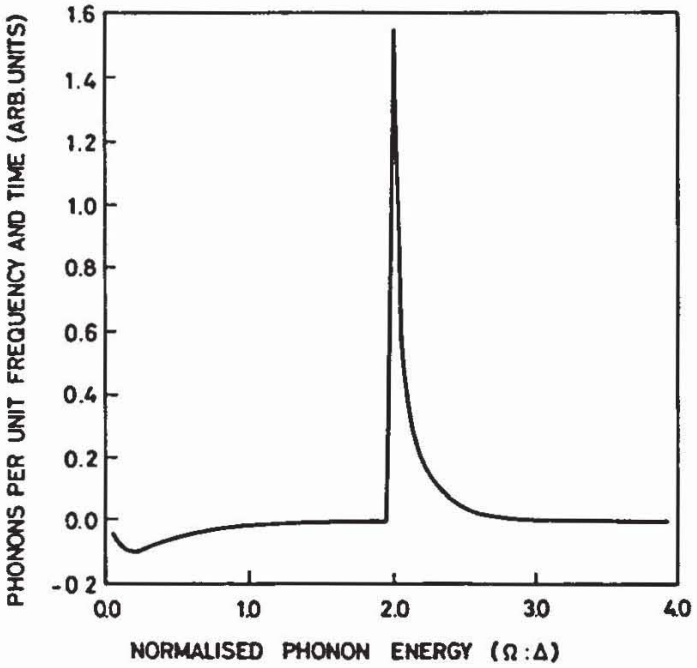

FIG. 18. Calculated generator phonon spectrum for the generator voltage $V_G = 2.0\Delta/e$, at $kT = 0.159\Delta$. The spectrum shows recombination phonons with a steep onset at the energy $\Omega = 2\Delta$ and a spectral width corresponding to kT (Dayem and Wiegand, 1972).

results from the recombination of injected quasiparticles at $E = \Delta$ with thermally excited quasiparticles of higher energy. Inelastic scattering of the injected quasiparticles at $E = \Delta$ to higher levels is indicated by the negative phonon emission rate in the range $0 < \Omega/\Delta < 1$, Ω being the phonon energy. With increasing battery voltage the maximum quasiparticle energy $E = eV - \Delta$ becomes higher than the thermal excitation width kT. The

primary phonon spectrum, therefore, contains strong energy contributions from the recombination of injected quasiparticles with maximum energy $eV - \Delta$ and thermal quasiparticles at $E = \Delta$. This result is shown in Fig. 19 for the maximum injection energy $E = 1.25\Delta$. The recombination spectrum for the BCS case contains an additional maximum at $\Omega = 2.25\Delta$. This maximum results from the high injection rate at $E = eV - \Delta$, reflecting the density of states singularity in the fully occupied states (cf. Fig. 3). The total

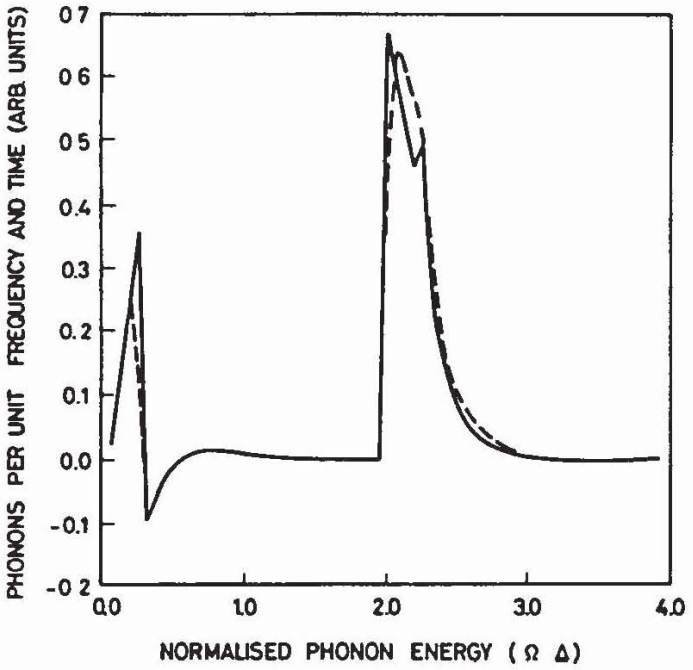

FIG. 19. Calculated generator phonon spectrum for $V_G = 2.25\Delta/e$ at $kT = 0.159\Delta$. The spectral width of the recombination phonons is increased by the excess energy of 0.25Δ. At low energies the relaxation spectrum with the maximum energy $\Omega = eV_G - 2\Delta_G = 0.25\Delta$ starts to develop. The solid line corresponds to the BCS density of states; the dashed line has been calculated for an experimental density of states distribution (Dayem and Wiegand, 1972).

width of the recombination spectrum being larger than 0.25Δ indicates the influence of the recombination of quasiparticles injected at $E = 1.25\Delta$ with thermally excited quasiparticles in the range $E = \Delta + kT$. The low-energy part of the phonon spectrum in Fig. 19 extending to the energy of 0.25Δ reveals the increasing contribution of relaxation now competing with recombination. The decay rate Γ for relaxation increases roughly according to $\Gamma \propto N_0(E - \Delta)^3$ for quasiparticles injected at $E \gg \Delta$, as results from integrating Eq. (24) over all final states. For injection energies $\Delta < E < 2\Delta$ the variation of the transition rate with energy is even faster, since at E close to Δ the relaxation transitions are further suppressed by strong destructive interference. This is indicated by the coherence factor approaching zero. The recombination rate dependence on the energy of the injected quasiparticle follows from Eq. (25). The integration with respect to all final states can be

limited to $E' \approx \Delta$, since only these states are thermally occupied. The transition rate for recombination results with $\Gamma \propto N_T(E + \Delta)^3/E$ (Long and Adkins, 1973). The number of thermally excited quasiparticles N_T is obtained from the integration of $N_S(E')f(E')\,dE'$ in Eq. (25), the other terms of the integral remaining almost constant in the range of thermal quasiparticle population. At $E = \Delta$ the recombination rate in contrast to relaxation has the finite value $N_T 8\Delta^2$. The recombination rate increases with E^2 in the limit of high injection energies, i.e., with roughly a factor of E less than the relaxation rate. With increasing E, therefore, quasiparticle decay occurs first by relaxation and then by succeeding recombination. This results in a limit of the increase of the spectral width of recombination phonons, as can be seen in Fig. 20, where the maximum injection energy amounts to $E = 3\Delta$.

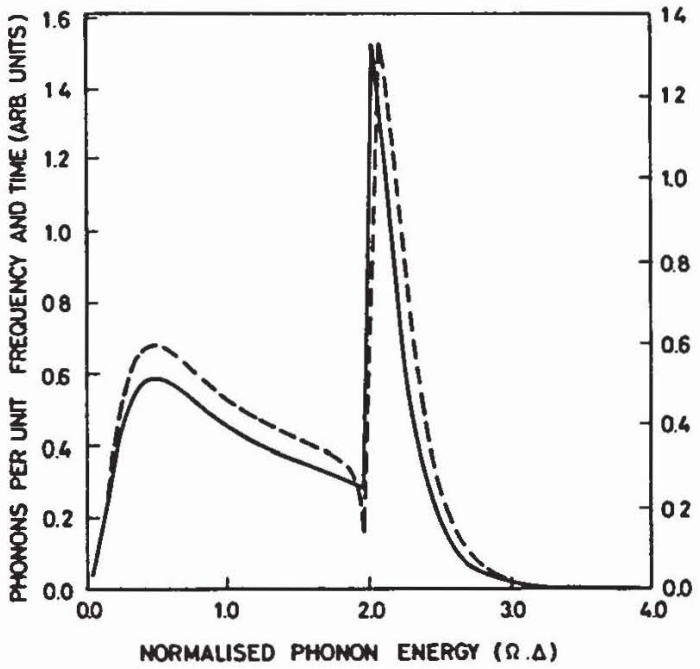

FIG. 20. Calculated generator phonon spectrum for the generator voltage $V_G = 4\Delta/e$ and $kT = 0.159\Delta$. The width of the recombination phonon spectrum is reduced by relaxation dominating at increased quasiparticle energies and reaches a limit of 0.2Δ. The continuous relaxation spectrum at this voltage has the maximum energy of 2Δ with a steplike cutoff. This is clearly revealed by the experimental density of states distribution (dashed line). The solid line represents the BCS density of states model (Dayem and Wiegand, 1972).

The bandwidth of the recombination peak is even reduced as compared to Fig. 19. Also the satellite maximum at $\Omega = 2.25\Delta$ has disappeared. A remaining small contribution of recombination phonons expected up to $\Omega = 4\Delta$ is not found, since phonon reabsorption strongly increases for $\Omega > 2\Delta$. Figure 20 also shows the spectrum of relaxation phonons now extending to the maximum energy $\Omega = 2\Delta$. For the "experimental" case of the density of states the calculation clearly indicates this upper frequency

edge. The absence of a singularity at the upper end of the relaxation spectrum (Dayem *et al.*, 1971) is in accord with Eq. (24), taking account of all relaxation transitions from E to E' in the continuous energy range $\Delta < E' < E$. The corresponding result has been obtained in the calculation of Kinder *et al.* (1970) (cf. Section V,C,1).

The variation of the spectral width of the recombination phonons with generator voltage is shown in Fig. 21. The BCS density of states distribution

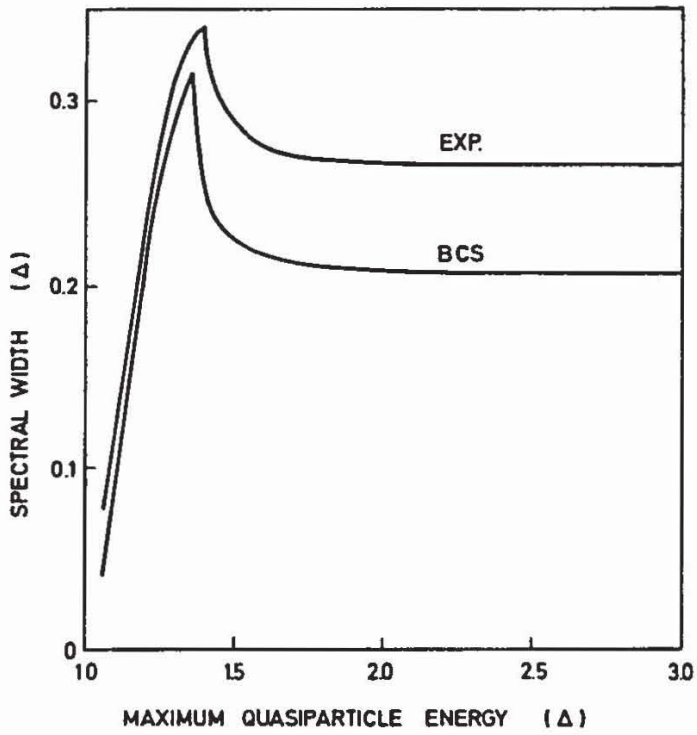

FIG. 21. Spectral width of recombination phonons as a function of the maximum energy of injected quasiparticles. The two curves refer to the BCS and experimental density of states distribution (Dayem and Wiegand, 1972).

reveals a stronger variation than the model using the experimental density of states function.

The calculations of Dayem and Wiegand (1972) were also performed in order to describe the experimental observation of a nonlinearity (Eisenmenger and Dayem, 1967; Kinder *et al.*, 1970; Dayem and Wiegand, 1972) in the increase of the detector signal i_S with generator current i_G between $eV = 2.1\Delta$ and $eV = 2.4\Delta$ (compare also Fig. 12). With a detailed balance model for the detector similar to the model of the generator Dayem and Wiegand obtained computed i_S (i_G) functions showing the nonlinearity in the correct order of magnitude of their measurement. It should be noted that these experiments were not performed under the condition of a small disturbance from the thermal equilibrium. With generator currents at $eV \approx 2.4\Delta$ of the order of 20 to 100 mA the overinjection limit of 1 mA for 1-mm^2

junctions has been exceeded, as discussed at the beginning of this section. In order to interpret the nonlinearity, which can be described by a positive deviation of up to 10% in the voltage range $2\Delta < eV < 2.5\Delta$ with a maximum at $eV = 2.4\Delta$, Dayem conjectured a limited increase with frequency of the detector sensitivity, resulting from a corresponding increase in τ_{eff}. Figure 21 shows a maximum at $eV = 2.4\Delta$ in the bandwidth of recombination phonons as a function of the generator voltage. A corresponding maximum in τ_{eff} and the deviation from nonlinearity in the i_S (i_G) function therefore can be explained if τ_{eff} becomes larger with frequency. Since this contradicts the recombination rate depending on quasiparticle excitation energy E, as $N_T[(E + \Delta)/E]^3$ questions were raised (Dayem, 1972). Therefore, the careful direct measurement of $\tau_{eff}(E)$ by pulse methods appears worthwhile. A straightforward explanation of a detector sensitivity increase with phonon energy is provided by the finite sharpness of the energy gap leading to a steep but finite width of the slope at the 2Δ-detector threshold (about 2% of 2Δ). Slight differences between the generator and detector energy gap in connection with this property lead to a nonlinearity in the i_S (i_G) dependence, as discussed in Section V,B,3.

The important result of Dayem's calculation is the voltage-dependent finite width of the recombination spectrum if reabsorption is not very large. It is to be expected that the maximum width 0.3Δ (cf. Fig. 21) also depends on the phonon escape properties of the film and substrate. At very high phonon trapping rates the maximum recombination bandwidth is expected to reduce to the thermal bandwidth corresponding to Long's (1973a) results.

3. *Recombination Spectrum at High Generator Currents*

Generally in phonon pulse experiments with superconducting junctions, tunneling currents exceeding the limiting value for weak disturbances of quasiparticles from thermal equilibrium are used. In these experiments generator and detector are separated by a substrate of several millimeters thickness. The generator currents are in the range from 10 mA to several amperes, leading to overinjection in the generator. Experimental evidence for overinjection can be obtained by the measurement of phonon escape times in recombination. At low injection current the phonon escape time is equal to τ_{eff}. Beginning with overinjection the escape time is drastically reduced in accordance with a shorter effective recombination time. Kinder (1973a) observed anomalously long escape times for recombination phonons generated with injection currents in the milliampere range at $eV = 2\Delta_{Sn}$ in low ohmic Sn generators. The abrupt decrease in escape time with currents exceeding about 10 mA is consistent with the overinjection limit estimated in Section V,B,1. Therefore, the escape time at low injection currents can be attributed to τ_{eff}. Since overinjection increases the density of

quasiparticles in excess of the thermal population, an increased occupation temperature T^* (compare Section IV,B) can also be defined. Depending on the strength of phonon trapping, not only the total density of quasiparticles but also the quasiparticle distribution will reach a quasithermal equilibrium described by T^*. In addition, the high population of quasiparticles leads to a reduction of the energy gap. If phonon trapping is not strong enough for establishing a quasithermal equilibrium of excitations, the recombination phonon spectrum is well approximated by the primary decay processes (Welte, 1974). With generator voltages $eV > 2\Delta_G$ recombination takes place between quasiparticles injected with singularities at $E_1 = eV - \Delta_G$ and $E_2 = \Delta_G$ (cf. Fig. 3). The population at $E_2 = \Delta_G$ being larger than at E_1 even with comparatively small thermal quasiparticle population, the resulting recombination phonon spectrum has the width $eV - 2\Delta_G = \delta E$, i.e., with the leading edge at $2\Delta_G$, the trailing edge has the energy eV. This spectrum is similar to the low injection spectrum shown in Fig. 19, but since the population of quasiparticles at the level $eV - \Delta_G$ can be relatively high, recombination of quasiparticles within this level is also possible, leading to a high-frequency contribution at $2\Delta + 2\delta E$. When the generator voltage eV exceeds the value 2.5Δ the onset of relaxation continuously reduces the high-frequency part of the recombination spectrum, thus leading again to a smaller effective spectral width. A very significant difference compared to the low injection case is the reduction of the energy gap with increasing injection. These spectral properties have been verified by Welte (1974) in experiments with low ohmic Al junctions of identical energy gap (at zero current). As shown in Fig. 22, the differential detector signal amplitude (di_S/di_G) begins with a very sharp maximum at zero (higher resolution indicates 0.5 mA) current. This maximum can be attributed to the abrupt reduction of the generator energy gap beginning with quasiparticle overinjection in the low ohmic generator and a corresponding reduction of the phonon energy of $2\Delta_G$ below the detector threshold $2\Delta_D$. As a consequence of the finite sharpness of the detector energy gap, the phonon absorption and also the detector sensitivity for 2Δ-phonons depend continuously on frequency from zero to its maximum value in a small but finite energy range of about 1% of 2Δ. A small generator gap reduction $\Delta'_G < \Delta_D$ by overinjection thus leads to signal decrease. With higher currents the generator voltage is first limited to $2\Delta'_G$ until the upper 2Δ-current region of the I–V curve is reached and the voltage begins to rise again with increasing current. At this point, A in Fig. 22, the upper edge of the recombination phonon spectrum with $E_{ph} = eV$ also begins to move to higher frequencies with a corresponding rise in the differential detector signal amplitude. This continues until the generator voltage reaches the value $eV = 2\Delta_D$, B in Fig. 22. Recombination phonons at the upper spectral edge are now detected with the maximum

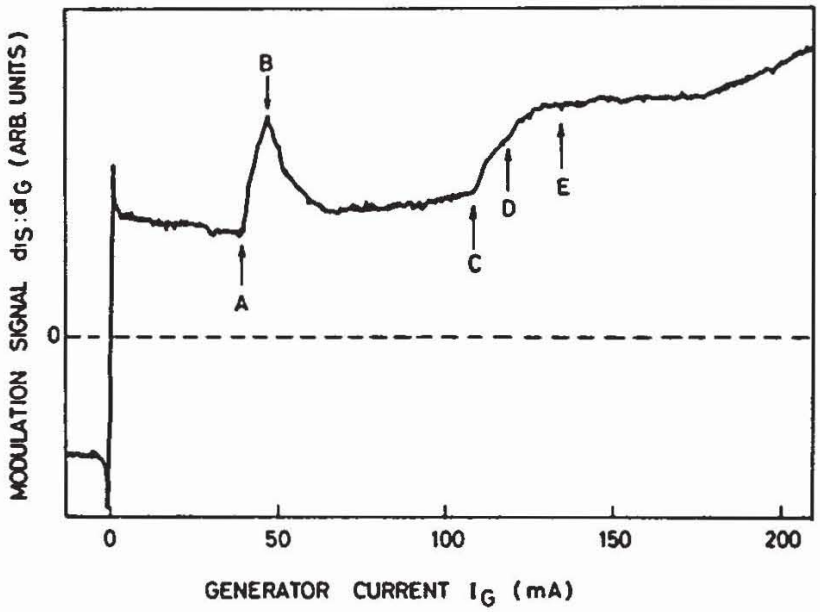

FIG. 22. Detector signal derivative di_S/di_G for a low ohmic Al–I–Al generator as a function of the generator current. The energy gap of the Al–I–Al detector is equal to the energy gap Δ_{0G} of the generator at zero generator current. $\Delta_G = \Delta_D$, $I_G = 0$, $T = 0.45°K$. (A) Onset of increasing energy of the generator recombination phonons at $eV_G \geq \Delta'_G$ with $\Delta'_G < \Delta_{0G}$ resulting from overinjection in the generator. (B) $eV_G = 2\Delta_D$ with the maximum energy of recombination phonons equal to $2\Delta_D$. (C) $eV_G = 4\Delta'_G$. (D) $eV_G = 2\Delta'_G + 2\Delta_D$. (E) $eV_G = 4\Delta_D$. For further discussion see text (Welte, 1974).

attainable sensitivity. The decreasing differential signal amplitude at generator voltages higher than $eV = 2\Delta_D$ is caused by the influence of competing relaxation transitions. The structure at points C and D can be also explained in terms of the gap reduction: Point D corresponds to the voltage $eV = 2\Delta'_G + 2\Delta_D$, where relaxation phonons of $E_{ph} = 2\Delta_D$, which are directly escaping the generator, produce a step in the signal response. At point C the generator voltage is $4\Delta'_G$ with the onset of the reabsorption of relaxation phonons in the generator. This increases the total rate of recombination phonons leading to the step at C. At point E with $eV = 4\Delta_D$ no structure is expected, in agreement with experiment.

In order to verify these spectral properties an experiment with a high ohmic generator and detector was also performed, the detector being prepared with a slightly enhanced energy gap. The observed similar structures (Welte, 1974) supported the interpretation of the results in Fig. 22.

In general, measurements with identical generator and detector show the nonlinearity in the i_S (i_G) relation at $eV \sim 2.2\Delta$ or the corresponding maximum in (di_S/di_G) to increase in relative height as the tunneling resistance R_∞ is reduced. This is in accord with the description of the result in Fig. 22. Since the reduction of the generator energy gap is larger for low ohmic junctions, the total change in the detector response determining the

height of the maximum at $eV \sim 2.2\Delta$ increases with higher tunneling currents. These generator and detector properties in the nonthermal equilibrium regime are also of significance in the experiments with higher ohmic junctions. In measurements with high ohmic generators and detectors with slightly different gaps nonlinearities at $\sim 2.2\Delta$ are observed for $2\Delta_D > 2\Delta_G$. These nonlinearities are absent for $2\Delta_D < 2\Delta_G$, i.e., interchanging generator and detector (Welte, 1974; Bindel, 1973).

The spectrum of emitted recombination phonons discussed so far rests on the finite escape probability of primary phonons. For strong reabsorption and trapping the final recombination phonon spectrum reaches a quasithermal distribution and width as discussed before. Long and Adkins (1973) were able to describe their experimental results in Al-generator and detector junctions of equal and different energy gaps also in terms of such a quasithermal population of quasiparticles for low ohmic generator junctions. Their experimental arrangement uses generator and detector junctions evaporated with a separating SiO layer of about 1000 Å on one side of a sapphire crystal. Generator and detector are in close contact and phonon escape into the substrate is only possible within a small angle limited by total reflection. Since the measurements were performed under vacuum conditions, phonons are trapped within the generator–detector system to a much higher degree than in phonon pulse propagation experiments with a finite generator–detector distance and sample contact to liquid ^{3}He or ^{4}He, as used by Dayem and Wiegand (1972) and Welte (1974). The observations of a quasithermal recombination spectrum in the experiments of Long and Adkins is therefore well in accord with the expected behavior at large trapping factors.

4. *Phonon Fluorescence in Superconductors*

Using quasiparticle excitation in superconducting films by intense phonon radiation from resistive heaters, Narayanamurti and Dynes (1971) and Dynes and Narayanamurti (1972) observed intense phonon fluorescence at the energy of 2Δ. In these experiments the high-energy tail of the thermal phonon spectrum of the heater is strongly absorbed via pair breaking. Frequency down-conversion by relaxation and repeated reabsorption and reemission of recombination radiation leads to a finite band of 2Δ-phonons emitted by the superconducting film. Calculations of the spectral shape (Dayem and Wiegand, 1972; Dynes and Narayanamurti, 1972) show a result similar to recombination radiation from tunneling generators (cf. Fig. 20) at high generator voltage. The maximum power emitted in phonon fluorescence depends on the quasiparticle population in the superconducting film. Power limitations result from the reduction of the energy gap with increased quasiparticle and 2Δ-phonon occupation temperature, as is also observed in the recombination radiation from tunneling generators.

C. Relaxation Spectrum

1. *Relaxation Spectrum for* $T = 0$

A first calculation of the relaxation spectrum using the spontaneous theoretical decay rates given by Tewordt (1962a) was performed by Kinder *et al.* (1970),[1] for the condition $T = 0$, taking account of primary decay phonons. The spectrum was obtained by a numerical evaluation of the convolution integral between the quasiparticle injection distribution as used in the tunneling integral Eq. (7) and a normalized relaxation probability derived from Eq. (24). The total decay probability of a quasiparticle injected at the level E being unity for sufficient long times, this condition has been used to determine the normalization factor for Eq. (24). The result of this calculation is presented in Fig. 23, showing a discontinuous high-frequency

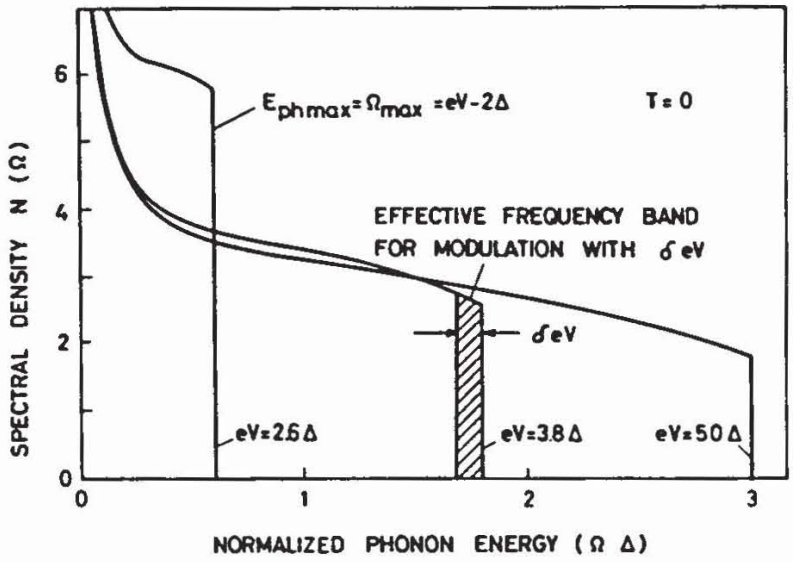

FIG. 23. Calculated relaxation spectrum for $T = 0$. Modulation results in a small effective phonon bandwidth (cf. Section VI,B) (Kinder *et al.*, 1970).

cutoff at the phonon energy $eV - 2\Delta_G$. A singularity in the phonon spectrum at this energy as obtained from a simple two-level model (Dayem *et al.*, 1971; Dynes and Narayanamurti, 1972) is not found. This follows from the continuous distribution of the final states in the transitions of Eq. (24). The singularity at zero frequency is not obtained in calculations at finite temperature, taking account of recombination (cf. Sections V,B,2 and V,C,2). The relaxation spectrum of Fig. 23 has been used to calculate the differential detector signal $(di_S/d\bar{i}_G)$ as a function of the generator current in Fig. 12. It has been assumed that all recombination phonons and all relaxation phonons with $E_{ph} \geq 2\Delta$ are detected. The theoretical result has been fitted to

[1] For details of the calculation, see Kinder (1973a).

the experiment at about $eV = 5\Delta$. The agreement between measurement and theory especially at the onset of the relaxation phonon step at $eV = 4\Delta$ is satisfactory. The finite width of the 4Δ-structure can be related to the finite gap resolution and to the experimental modulation amplitude. The absolute value of the step at 4Δ is smaller than calculated. Theory and experiment do not show a singularity at $eV = 4\Delta$ as would be expected from a possible singularity at the upper edge of the relaxation spectrum (Dayem *et al.*, 1971). In some measurements (Dynes and Narayanamurti, 1973; Dayem *et al.*, 1971) pronounced maxima at $eV = 4\Delta$ in the di_S/di_G function have been reported. It is possible that these experimental results can be described if relaxation transitions stimulated by highly populated 2Δ-phonons in low ohmic generators or at low temperatures are taken into account. Further processes not contained in the BCS approximation may be discussed. For example, the decay of a quasiparticle of energy $E_Q = 3\Delta$ to the gap edge via direct pair breaking (Pokrovskii, 1961) would lead to a 4Δ singularity in the di_S/di_G curve. In contrast to this prediction, calculations of Tewordt (1962a) with respect to the electron–electron interaction leading to direct pair breaking indicate that these processes have a transition probability about two orders of magnitude smaller than the relaxation rate under phonon emission. Since other experiments on the spectral phonon distribution, described in Sections V,C,2 and VI,B, also confirm that the relaxation spectrum does not contain a singularity at $eV - 2\Delta$, the reported observations of a 4Δ maximum may result from 2Δ-phonon stimulated relaxation processes in the generator, or from lifetime (or overinjection) effects in the generator and in the detector.

The relaxation spectrum calculations for $T = 0$ were extended (Kinder *et al.*, 1970) to include first-step phonon reabsorption and succeeding relaxation by use of the transition probability for pair breaking by phonon absorption [Eq. (28)]. The result of the numerical solution of the corresponding convolution integrals is introduced in Fig. 12, showing qualitative agreement with the experimental change of slope in the di_S/di_G curve at $eV = 6\Delta_G$. Therefore, further strong evidence for the reabsorption of 2Δ-phonons is provided in addition to the result that the effective number of secondary 2Δ-phonons increases in proportion to the phonon energy of primary phonons with energy larger than 4Δ (cf. Section IV,D).

The experimental ratio of the signal amplitudes above and below the 4Δ step in most measurements was found to be smaller than the theoretical value of 3.1. In the direct signal amplitude i_S (i_G) as a function of the generator current, this corresponds to a smaller gradient ratio than expected. The "gradient ratio deficit" has been discussed in detail by Long and Adkins (1973). They assume that injected quasiparticles colliding with the tunneling barrier many times before relaxation takes place can be inelastically

scattered in the tunneling barrier and therefore lost for detection to a finite percentage. This explanation can be applied to Al junctions with elastic scattering 10^4 times faster than relaxation decay. For Pb and Sn junctions elastic scattering times are only one order of magnitude smaller than relaxation times. Therefore, inelastic barrier scattering is not expected to account for the deviation of the 4Δ step amplitude in Sn and Pb junctions. Experimentally it has been observed (Eisenmenger *et al.*, 1969) that low ohmic junctions exhibit a stronger gradient deficit or smaller 4Δ step. Since direct recombination is competing with relaxation, the increase in quasiparticle population at $E_Q = \Delta$, found in low ohmic generators as a consequence of overinjection, significantly contributes to the observed deviation from theory. For typical Sn junctions of 1 mm^2 and generator currents of 200 mA the quasiparticle population increases by about a factor of 10 compared to the thermal population at 1°K as follows from Eq. (18).

From the approximate rates for recombination and relaxation (cf. Section V,B,2) one obtains the ratio

$$\frac{\Gamma_{rec}}{\Gamma_{rel}} \approx \frac{N_T}{N_0} \frac{1}{E} \frac{(E+\Delta)^3}{(E-\Delta)^3} \tag{29}$$

With $E = 3\Delta$ and the N_T/N_0 value [cf. Eq. (10)] for Sn at 1°K increased by a factor of 10, Eq. (29) yields a 10% contribution of direct recombination compared to relaxation. The experimental gradient deficits for junctions with corresponding generator current at 4Δ are in accord with this estimate.

Calculations in the low generator current limit of the gradient change of the i_S (i_G) dependence at the onset of relaxation phonon detection were also performed by Long and Adkins (1973) for differing energy gaps of the detector and the generator. In addition, the influence of temperature on the rate of relaxation to recombination transitions was evaluated by these authors. Increasing temperature reduces the 4Δ step. Equal rates for recombination and relaxation of quasiparticles at $E = 3\Delta$ are reached at the temperature $T = \Delta/2k$.

2. *Relaxation Spectrum for* $T > 0$

At finite temperatures the primary phonon relaxation spectrum contains additional spectral contributions resulting from temperature-dependent processes, as shown in Fig. 24. Besides the already discussed contributions from recombination A and relaxation B, now direct recombination C and relaxation D of thermally excited quasiparticles injected by tunneling will result in additional phonon radiation centered at the energy eV. Also the recombination transition E of thermally injected quasiparticles with thermally excited quasiparticles (Forkel, 1973) weakly contributes to

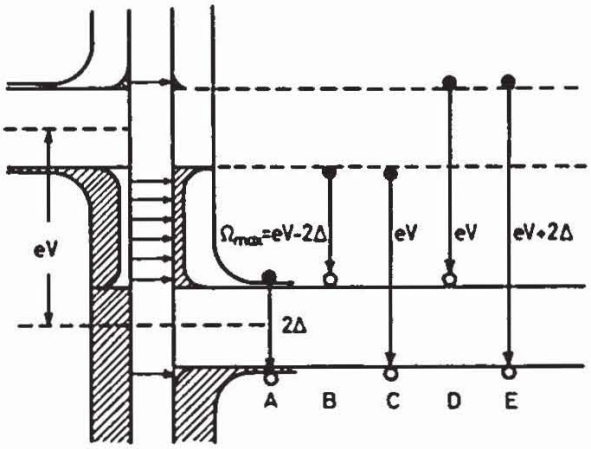

FIG. 24. Quasiparticle transitions at finite temperatures and characteristic phonon energies of the generator spectrum. (A) Recombination of quasiparticles at the gap edge. (B) Relaxation of quasiparticles injected from highly occupied states to the gap edge. (C) Direct recombination of quasiparticles injected from highly occupied states with quasiparticles at the gap edge. (D) Relaxation of quasiparticles injected from thermally occupied states to the gap edge. (E) Recombination of quasiparticles injected from thermally occupied states with quasiparticles at the gap edge.

the spectrum. The total primary phonon spectrum at finite temperature was calculated by Welte *et al.* (1972b) (see also Forkel *et al.*, 1973).

Using the transition probability relations Eqs. (24) and (25), numerical convolution integration with the quasiparticle injection distribution resulted in the phonon spectra for different generator voltages shown in Fig. 25. The calculation reproduces the qualitative expectation of a thermally induced phonon peak at $E_p = \Omega = eV$, with the sharp relaxation phonon cutoff at

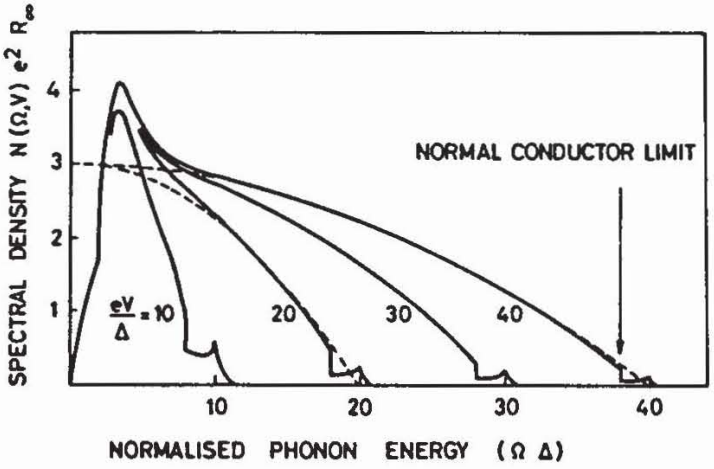

FIG. 25. Calculated generator spectrum at finite temperature ($T = \Delta : 1.6^{\circ}$K) for primary decay processes with different generator voltages. The contribution of secondary processes as recombination of quasiparticles after relaxation is not contained. The dashed curves are normal conductor relaxation spectra for $T = 0$. The spectral density $N(\Omega, V)e^2R_\square$ is defined according to Eq. (30) (Welte *et al.*, 1972b; Forkel *et al.*, 1973).

$\Omega = eV - 2\Delta_G$ still the most characteristic spectral property. The low-frequency singularity for $T = 0$, as found in Fig. 23, is not present because recombination is the faster decay process at low injection levels. Since only first-step processes are used in the calculation for Fig. 25 the recombination spectrum of quasiparticles having first undergone a relaxation transition is not contained. For comparison, the relaxation transition Eq. (24) has been used to calculate the phonon spectrum for zero temperature and vanishing energy gap, i.e., the case of a normal conductor at $T = 0$. The convolution integrals of tunneling injection Eq. (7) and relaxation Eq. (24) can be easily solved and the phonon spectrum $N(\Omega)$ is expressed by

$$N(\Omega)\, d\Omega = 6(2e^2 R_\alpha)^{-1}[1 - \Omega^2(eV)^{-2}]\, d\Omega \tag{30}$$

where $N(\Omega)\, d\Omega$ is the total number of phonons emitted in the interval $d\Omega$. This normal conductor spectrum is introduced as dashed lines in Fig. 25, indicating that for high generator voltages the superconductor spectrum is well approximated by the normal conductor spectrum. It is further to be noted that about 75% of the total relaxation phonon energy is emitted in the first relaxation step. The contributions of secondary and other steps are adding to the lower-energy portion of the spectrum and can be neglected for high-frequency applications (Forkel, 1973).

D. Escape Conditions for Relaxation Phonons

Relaxation phonons of energy below $2\Delta_G$ can easily escape from the generator since phonon mean free path values of the order of 10^4 to 10^5 Å are expected in clean and homogeneous superconducting films (cf. Section IV,E). Convincing evidence for this high escape probability has been given by the experiments of Kinder (1972a), demonstrating the possibility of tunable phonon absorption spectroscopy. The upper frequency limit of this method is caused by $2\Delta_G$ phonon reabsorption in the generator.

In order to observe the primary decay spectrum of relaxation phonons also at energies above $2\Delta_G$, reabsorption can be reduced by small film thickness values of the generator junction. Electrical film homogeneity requirements set a lower thickness limit of about 200 Å for Al and 2000 Å for Sn and Pb films. Especially for Sn and Pb generators, phonon mean free path values for $E_{ph} > 2\Delta$ are smaller than these lower film thickness limits. In Al junctions, the phonon mean free path can instead be larger than the film thickness. From this it is to be expected that primary relaxation phonons of energy above $2\Delta_G$ escape more easily from Al generators than from Pb or Sn junctions.

In order to calculate the primary phonon escape rate especially for

$E_{ph} > 2\Delta_G$, a simple model taking account of diffusive motion of injected quasiparticles during relaxation decay can be used.

In the WKB approximation of tunneling, the k-vectors of injected quasiparticles are confined to a small cone vertical to the oxide barrier. By momentum conservation the relaxation decay by normal processes in the meV energy range is only possible with phonon emission at right angles. Thus, tunneling electrons moving perpendicular to the barrier emit phonons in directions parallel to the substrate boundary and the probability for primary phonon escape becomes very small. For nonspherical energy surfaces oblique electron injection is also possible, and phonons can be emitted in directions more perpendicular to the barrier. Umklapp processes in relaxation or tunneling have a similar result. More isotropic primary phonon emission follows from elastic quasiparticle scattering, which we discuss now. Relaxation times τ_{rel} of the order of 10^{-10} to 10^{-8} sec (Miller and Dayem, 1967) are long compared to elastic scattering times τ_{el} of 10^{-13} sec as estimated from the Fermi velocity and the elastic scattering mean free path of about 1000 Å. Elastic scattering being the dominant scattering process at low temperatures, the mean free path can be obtained from residual resistance measurements. Multiple elastic scattering in times short compared to the relaxation time leads to quasiparticle diffusion with finite lifetime. The stationary distribution of quasiparticles that have not decayed and are at their original injection energy E can be obtained by solving the one-dimensional diffusion equation for the geometry of Fig. 26:

$$\left(\frac{\partial}{\partial t} - D \cdot \nabla^2\right) N_E(x) = -\frac{N_E(x) - N_{T,E}}{\tau_{rel,E}} \tag{31}$$

where $D = \frac{1}{3} l_{el} V_F$ is the diffusion constant with l_{el} the elastic quasiparticle

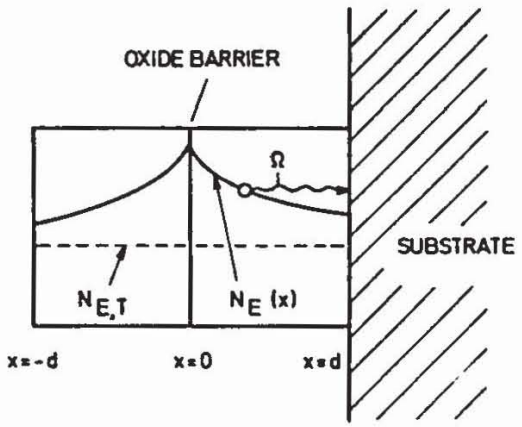

FIG. 26. Model of high energy relaxation phonon escape from the generator junction enhanced by excited quasiparticle diffusion. $N_E(x)$ is the stationary density distribution by diffusion of quasiparticles with injection energy E, $N_{F,T}$ the thermal density of quasiparticles with energy E, and Ω the phonon emission by quasiparticle relaxation.

mean free path and V_F the Fermi velocity. $N_E(x)$ is the density of quasiparticles of energy E at the position x, $N_{T,E}$ the thermal density of quasiparticles at E, assumed to be negligibly small (cf. Fig. 26), and $\tau_{rel,E}$ the relaxation lifetime of quasiparticles at energy E. The diffusion Eq. (31) is applicable if $\tau_{el} \ll \tau_{rel}$, i.e., $l_{el} \ll \tau_{rel} V_F$. Equation (31) can be solved for the boundary condition $\mathbf{j}(x = 0) = I(E)$ and $\mathbf{j}(x = d; -d) = 0$, with the diffusion current density $\mathbf{j} = -D\nabla N_E$. $I(E)$ is the quasiparticle injection current density at E The solution for the film in contact with the substrate is given by

$$N_E(x) = I(E)\frac{L}{D}e^{-x/L}\frac{1 + e^{-2(d-x)/L}}{1 - e^{-2d/L}} \tag{32}$$

where $L = [\frac{1}{3}l_{el} V_F \tau_{rel}(E)]^{1/2}$ is the diffusion length. In the limit $d \gg L$ the quasiparticle density $N_E(x)$ varies in proportion to $e^{-x/L}$ as long as $x < d$. The solution for the film not in contact with the substrate is analogous to Eq. (32).

Relaxation of quasiparticles at x leads to isotropic phonon emission in proportion to $N_E(x)$. Relaxation phonons of energy $E_{ph} = \Omega$ propagating in the x-direction, i.e., normal to the substrate, have a probability $\exp[-(d - x)/\Lambda_\Omega]$ for arriving at the substrate boundary, $(d - x)$ being the distance of propagation. The limitation to phonon propagation in the x-direction is justified for experiments in which the distance between generator and detector is large compared to the lateral junction dimensions. Λ_Ω is the mean free path for phonon reabsorption. For calculating the phonon intensity arriving at the substrate boundary the complicated convolution integration over the phonon emission rates depending on $N_E(x)$, the relaxation probability Eq. (24), and the phonon reabsorption function $e^{-(x-d)/\Lambda_\Omega}$ has to be performed with respect to all injection energies E and distance values x at constant frequency Ω. The result of this integration is described by the current of phonons $\dot{n}_{GD}(\Omega)\, d\Omega$ in the frequency interval $d\Omega$ arriving at the detector of area F_D:

$$\dot{n}_{GD}(\Omega)\, d\Omega = \frac{F_D c_G^2}{4\pi r^2 c_S^2} T_{GS}\, f_{ph}\, T_{SD}\, N(\Omega) G(\Omega)\, d\Omega \tag{33}$$

where F_D is the detector area, r the distance from generator to detector, c_G the generator sound velocity, and c_S the substrate sound velocity. The ratio of sound velocities describes acoustical refraction at the generator–substrate boundary. T_{GS} and T_{SD} are the normal incidence phonon transmission factors at the generator–substrate and the substrate–detector boundaries. The factor f_{ph} describes phonon focusing in the substrate (Taylor *et al.*, 1971), attenuation being neglected. $N(\Omega)$ is the total number of primary relaxation phonons emitted per unit time and frequency by all decaying quasiparticles

as obtained in the calculation of the relaxation phonon spectrum (Section V,C). Phonon reflection at the "free" boundary of the generator not in contact with the substrate is not taken into account in Eq. (33). This is justified for liquid helium contact with more than 60% of phonons escaping across the generator–helium boundary (Trumpp *et al.*, 1972b). $G(\Omega)$ is the frequency-dependent factor describing the total influence of quasiparticle diffusion and phonon reabsorption in the generator as obtained from the convolution integration discussed before. The experimentally important limiting cases and the corresponding $G(\Omega)$ can be discussed as follows (see also Welte *et al.*, 1972a,b; Forkel, 1973).

For a large phonon mean free path $\Lambda_\Omega \gg d$ and arbitrary diffusion length L the calculation results in $G(\Omega) = 1$, in agreement with negligible phonon reabsorption. With $L \ll d$ and $\Lambda_\Omega < d$ phonons are generated in the small region L close to the barrier and are strongly reabsorbed in propagating the full distance d to the substrate. In this limit $G(\Omega)$ can be approximated by $G(\Omega) = e^{-d/\Lambda_\Omega}$. For $L \gg d$ and $\Lambda_\Omega \ll d$, quasiparticles are homogeneously distributed in the film by diffusion, but only phonons generated in a region of width Λ_Ω close to the substrate contribute to the phonon current $\dot{n}_{GD}(\Omega)$. From the geometrical ratio $\Lambda_\Omega : 2d$ of the contributing quasiparticles, it follows that $G(\Omega) = \Lambda_\Omega/2d$. These simple limiting situations apply to a number of experimental conditions. In the intermediate range of L and Λ_Ω comparable to d, numerical evaluation of the convolution integral is required.

As a general rule, for high relaxation phonon escape the necessary condition $L + \Lambda_\Omega \geq d$ must obviously be fulfilled.

Experimentally, relaxation phonons in the energy range $\Omega = eV - 2\Delta_G < 2\Delta_G$ fulfill the condition $\Lambda_\Omega \gg d$ for generator films of the order of 1000 Å thickness. With l_{el} of the order of 1000 Å and τ_{rel} of the order of 10^{-10} sec the ratio $\tau_{rel} V_F : l_{el} \approx 10^3$ indicates the validity of the diffusion model. The emission of primary phonons of $\Omega \leq 2\Delta_G$ is not influenced by reabsorption, i.e., $G(\Omega) = 1$. This property was successfully used by Kinder (1972a) in his method of phonon absorption spectroscopy (cf. Section VI,B). With Sn–I–Sn generators and Al–I–Al detectors, Kinder demonstrated the direct escape of relaxation phonons with $\Omega < 2\Delta_G$ from the Sn generator. Efficient relaxation phonon escape in the range $\Omega < 2\Delta_G$ was also found with Pb–I–Pb generators using Sn–I–Sn junctions as detectors (Eisenmenger, 1967a) and with Pb : Bi alloy generators (Kinder and Dietsche, 1974). The onset of reabsorption of relaxation phonons at $\Omega = eV - 2\Delta_G \geq 2\Delta_G$ was demonstrated by an additional time delay in phonon escape (Kinder, 1973a).

The emission of relaxation phonons with energy exceeding the generator gap could not be observed in these experiments, with Sn or Pb junctions

as phonon generators. This indicates that for Sn and Pb the phonon reabsorption mean free path Λ and also the diffusion length L of quasiparticles with high excitation energy are smaller than 1000 Å.

In experiments on the emission rate of relaxation phonons with energy exceeding the generator gap, Welte *et al.* (1972a,b) and Forkel *et al.* (1973) used Al–I–Al generators and Sn–I–Sn detectors on Al_2O_3 and Si substrates. Since the detector energy gap is about four times as large as the generator gap, recombination phonons from the generator cannot be observed. Only relaxation phonons of energy $\Omega = eV - 2\Delta_G \geq 2\Delta_D > 2\Delta_G$ are expected to result in a detector signal. The experimental result with Al generator and Sn detector on a Si substrate is shown in Fig. 27, with the signal derivative di_S/di_G plotted as function of the generator voltage V. The signal maximum at $eV = 2\Delta_D$ and the step at $eV = 2\Delta_D + 2\Delta_G$ in Fig. 27 result from the corresponding structures in the phonon spectrum of Fig. 25 at $\Omega = eV$ and $\Omega = eV - 2\Delta_G$, respectively. The "thermal" maximum at $\Omega = eV$ has been verified as strongly temperature dependent. These results provide evidence for the emission of primary relaxation phonons with $\Omega > 2\Delta_G$ from Al generators. The finite low-frequency contributions for $\Omega = eV < 2\Delta_D$ can be attributed to the thermal energy distribution of quasiparticles. In recent

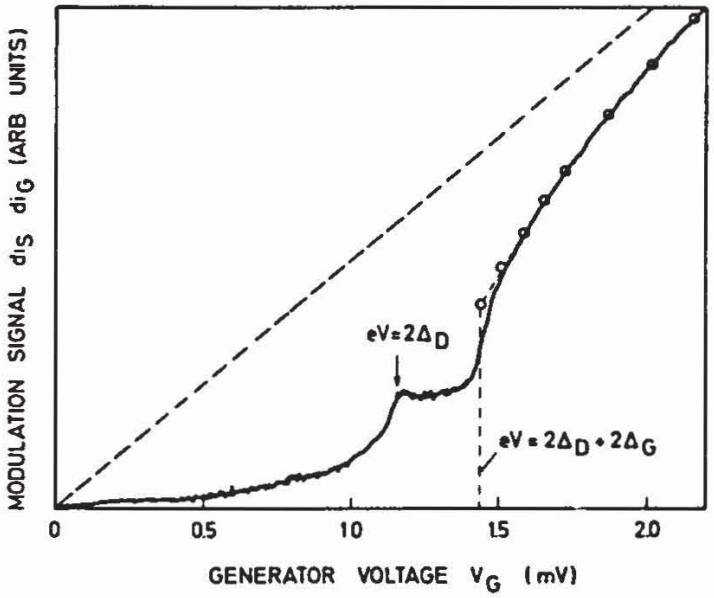

FIG. 27. Detector signal derivative di_S/di_G as a function of generator voltage with Al–I–Al generator, Sn–I–Sn detector, and undoped Si crystal as substrate. $T = 0.985°K$. High-frequency phonon emission is verified by the signal structure at $eV = 2\Delta_D$ and the steep onset of the main relaxation phonon contribution at $eV = 2\Delta_D + 2\Delta_G$. Circles and dashed-dotted lines indicate the result of an approximate calculation using the normal conductor spectrum with a cutoff at $\Omega = eV_G - 2\Delta_G$. The dashed line corresponds to the asymptotic behavior at high phonon energies with a detector response in proportion to phonon energy (Forkel, 1973; see also Welte *et al.*, 1972a,b).

experiments (Forkel, 1975b) evidence for the direct recombination of quasiparticles injected from thermal excitations above the energy gap (process E in Fig. 24) has also been found in the form of a small signal maximum at $eV = 2\Delta_D - 2\Delta_G$ corresponding to $\Omega = 2\Delta_G + eV$. The similarity in shape of the signal amplitude dependence on the generator voltage in Fig. 27 and of the calculated spectrum in Fig. 25 with reversed frequency scale can be qualitatively understood from the frequency-selective properties of the detector and the modulation technique used.

In low ohmic junctions, e.g., $R_\infty < 10$ mΩ, an additional contribution at $\Omega = eV$ from increased quasiparticle population by current overinjection is observed.

The dashed-dotted line in Fig. 27 was obtained by a calculation (Forkel, 1973) using the spectrum of Fig. 25 in the normal conductor approximation but with a cutoff at $\Omega = eV - 2\Delta_G$. The detection was approximated by a linear dependence on energy above the threshold $2\Delta_D$. Measurement and calculation were amplitude fitted at the highest generator voltage.

The experimental results can be further discussed as follows:

Applying the criterion for quasiparticle diffusion and relaxation to Al films we find with $l_{el} \approx 1000$ Å and $\tau_{rel} \approx 10^9$ sec (Miller and Dayem, 1967) that $\tau_{rel} V_F : l_{el} \approx 10^4$, indicating the diffusion model to be appropriate. The phonon reabsorption mean free path is of the order of 2000 Å for $\Omega \approx 2\Delta_G$ (Long, 1973b). The diffusion length follows from Eq. (32) with $L \approx 60{,}000$ Å, i.e., large compared to the film thickness. Quasiparticles therefore are homogeneously distributed within the film before relaxation takes place. Since Λ in the generator is of the order of the film thickness d, we expect $G(\Omega)$ to depend on Λ and d approximately as $G(\Omega) = 0.5\Lambda d^{-1}$, or even to approach the limiting value $G(\Omega) = 1$. With $\Lambda_w < d$ in the Sn detector ($\Lambda_w \leq 700$ Å, $d = 3000$ Å; cf. Section IV,D) and $G(\Omega) = 1$ in the Al generator the calculated signal dependence in proportion to energy as introduced in Fig. 27 is only expected for phonon energies $\Omega > 4\Delta_D$. The good agreement between measurement and calculation in Fig. 27, where a linear energy dependence of the detector response for $2\Delta_D < \Omega < 4\Delta_D$ has also been assumed, is not fully understood. A more realistic comparison requires the use of the relaxation spectrum in its unapproximated form. Measurements in a wider frequency range with oxygen-doped Si substrates (Fig. 33) again show proportionality of the signal derivative with phonon energy for frequencies $\Omega > 4\Delta_D$ but with a larger constant of proportionality than in the range $2\Delta_D < \Omega < 4\Delta_D$. In this measurement qualitative evidence for the onset of reabsorption in the detector is found by a weak structure at $\Omega = 4\Delta_D = eV - 2\Delta_G$.

Absolute measurements of the signal intensity (Welte *et al.*, 1972a,b; Forkel, 1973) indicated that the experimental phonon intensity amounts to about 30% of the calculated value. The absolute number of detected phonons was obtained from the signal amplitude by detector calibration (cf. Section IV). The number of phonons reaching the detector has been calculated from Eq. (33), i.e., assuming phonon attenuation within the crystal to be small (cf. Section VI,E).

With respect to the frequency dependence of the phonon mean free path for reabsorption, only estimated values can be used in Eq. (33); the same situation holds for $\tau_{rel}(E)$ for which better than order of magnitude data are not available. Although more reliable experimental data on the frequency dependence of Λ and τ_{rel} are required for a detailed comparison between experiment and theory all decay processes predicted within the BCS transitions are experimentally verified in their essential spectral properties. In addition, order of magnitude agreement is obtained for the absolute signal amplitudes. The voltage dependence of the upper phonon frequency edge of the relaxation spectrum has been successfully used for phonon absorption spectroscopy (cf. Sections VI,B and VI,C).

VI. Applications

The ease of preparing tunneling junctions as phonon generators and detectors with good acoustical contact to the substrate crystal and the possibility of obtaining frequency information by voltage or current measurements have stimulated various applications in studies of phonon generation and propagation.

A. Phonon Spectroscopy with Recombination Phonons

Recombination phonons are confined to a small frequency band either of width equal to kT or of width up to 20% of 2Δ, depending on the battery voltage and the degree of phonon trapping (cf. Section V,B). The first experiment intended to measure this bandwidth directly was performed by Dynes *et al.* (1971) using the tunability of the level splitting of the ground state donor levels of Sb in Ge by mechanical stress. Figure 28a shows the sample orientation and the phonon propagation direction with Sn–I–Sn generator and detector and the direction of the applied stress. Figure 28b reveals the hydrogenlike donor ground state level splitting as a function of stress. The stress values corresponding to $2\Delta_{Sn}$ fast transverse- and longitudinal-phonon transitions, respectively, are indicated by arrows. Slow transverse mode coupling is not expected. The detector signal in Fig. 28c as a function of stress shows maximum absorption for the fast transverse wave transition at a level

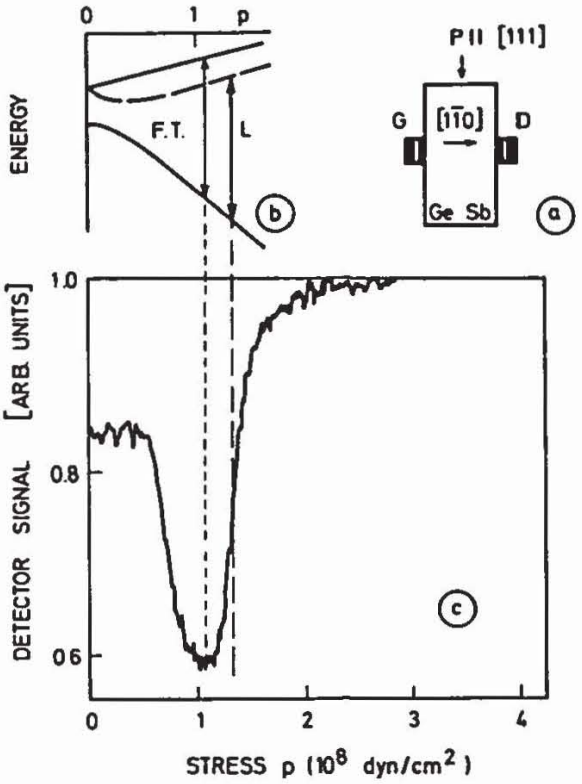

FIG. 28. 2Δ-phonon absorption by stress tuning of phonon resonant scattering in Ge : Sb. (a) Sample configuration; G, Sn–I–Sn generator; D, Sn–I–Sn detector; stress and phonon propagation direction are indicated by arrows. (b) Energy level splitting of the electronic ground state of Sb in Ge as a function of stress. The allowed fast transverse and longitudinal phonon transitions at the energy difference $2\Delta_{Sn}$ are indicated by arrows. (c) Detector signal as a function of stress, average of fast transverse and longitudinal phonons. The predominance of transverse phonons is demonstrated by the signal minimum at the stress value for the fast transverse transition (Dynes *et al.*, 1971).

spacing of $2\Delta_{Sn}$. Since the relative contribution of longitudinal waves is comparatively small, the position of the signal minimum shows good agreement with the calculated value for transverse phonon transitions. In time-resolved pulse measurements the stress value for the maximum absorption of longitudinal waves has also been verified. This method of absorption line tuning in principle corresponds to emission spectroscopy. Linewidth resolution was not better than 20% as a consequence of lifetime broadening and stress inhomogeneity. Therefore, an influence of the generator voltage on the experimental linewidth has not been observed. Similar measurements of the signal as a function of applied stress in Ge : Sb have been performed by using the 2Δ-phonon fluorescence of Sn and $Pb_{0.5}$: $TL_{0.5}$ films (Dynes and Narayanamurti, 1972). The superconducting film was in direct contact with the substrate. Quasiparticles were excited by a heat pulse generator on top of the superconducting film with an insulating SiO layer in between. The fluorescence radiation spectrum was analyzed by stress tuning of the Sb

levels and found to be very similar to recombination radiation in tunneling junctions. In additional experiments magnetic tuning of the energy gap under the condition of film thickness $d < \lambda$ (λ is the London penetration depth) has been analyzed. In Sn films the magnetic field dependence of the recombination frequency was verified in accordance with theory. Gap reductions were achieved in the order of 40%, and in using $Al_2O_3 : V^{3+}$ as substrate the groundstate splitting of the V^{3+} ion could also be observed as phonon absorption maximum (Narayanamurti and Dynes, 1971; Dynes and Narayanamurti, 1972). Magnetically tuning can, in principle, also be applied to tunneling junctions as phonon generators and detectors. With respect to the upper phonon power limit radiated from fluorescence—or tunneling generators—basically no difference is expected. For both generators the power and correspondingly the radiation temperature at 2Δ is linked to the quasiparticle occupation temperature. In increasing the occupation temperature of quasiparticles the energy gap will finally be closed. For the use of the fluorescence generator a high phonon escape rate into the substrate or helium bath appears to be important. If multiple phonon interactions in the heater–superconductor system take place with or without little phonon escape, the superconductor quasiparticle and lattice temperature comes into equilibrium with the heater temperature, and the phonon radiation into the substrate may approach a Planck distribution.

Another direct method for investigating the 2Δ recombination radiation was used by observing phonon resonances (Blackford, 1972) in adsorbed ^{4}He films. In these experiments a sandwich of three Al films separated by tunneling barriers was prepared. One barrier has been used for quasiparticle injection (generator), the other barrier for probing the density of quasiparticles (detector). In condensing liquid ^{4}He on top of the sample and measuring the ^{4}He film thickness via vapor pressure, phonon interferences were found as indicated by thickness-dependent minima of the steady-state population of quasiparticles. The fact that these minima were analogous to the observations of Anderson and Sabisky (1971) verified the phonon gap frequency $2\Delta_{Al} h^{-1} = 80$ GHz $= f$ from the film resonance condition $d = n\lambda + \frac{1}{4}\lambda$ with $\lambda = c_{He}/f$. The reduction in quasiparticle population arises from the maximum phonon dissipation under resonance conditions. The strength of the observed minima indicates that the Kapitza resistance anomaly at least partly rests upon an increased phonon transition rate and not only on strong dissipation processes localized in the surface region.

Phonon spectroscopy with recombination phonons, especially with magnetic tuning, is limited to a frequency resolution of about 10 to 20% of 2Δ. Higher resolution of at least one order of magnitude has been obtained in relaxation phonon or "Bremsstrahlung" spectroscopy, as we discuss next.

B. Phonon Spectroscopy with Relaxation Phonons in the Energy Range $2\Delta_D < \Omega < 2\Delta_G$

As shown in Fig. 23 the relaxation phonon spectrum at the maximum frequency $\Omega = eV - 2\Delta_G$ has the shape of a step function. This property can be used for voltage-tunable absorption spectroscopy as demonstrated by Kinder (1972a). A small change δV in the generator voltage V results in the differential phonon radiation confined to the narrow frequency band of $e\,\delta V\,h^{-1}$. The change δV can easily be produced by the superposition of a small sinusoidal or pulse voltage (current) on the generator dc bias. The detector signal modulation or differential pulse signal then corresponds to the response with respect to the frequency band $e\,\delta V\,h^{-1}$. This modulation technique corresponds to the experimental method of taking the first derivative di_S/di_G of the detector signal with respect to the generator current as described in Section III. The result of phonon pulse absorption measurements using this technique is shown in Fig. 29 for an Al_2O_3 substrate doped

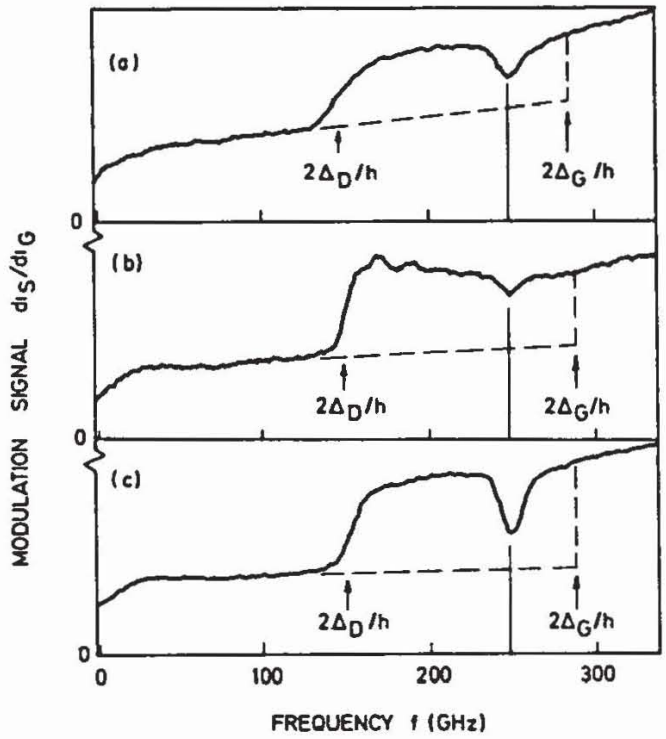

FIG. 29. Phonon-resonant scattering in $Al_2O_3 : V^{3+}$ observed by voltage tuning of the differential relaxation (phonon bremsstrahlung) spectrum. Sn–I–Sn generator and Al–I–Al detector with enhanced energy gap. Time of flight separation of phonon polarization. $T = 1.02$–1.05 K. The frequency range for phonon spectroscopy extends from $2\Delta_D/h$ to $2\Delta_G/h$. The V^{3+} absorption maximum is found at 248 GHz. (a) Fast transverse phonon absorption in a direction. (b) Longitudinal phonon absorption in c direction. The V^{3+} transition is forbidden by selection rules but crystal inhomogeneities might account for the observed absorption. Above $2\Delta_D/h$ oscillating structure in the modulation signal results from phonon interference (thickness resonance) in the Al detector film. (c) transverse phonon absorption in c direction (Kinder, 1972a).

with V^{3+}, with Sn–I–Sn as generator and granular Al–I–Al as detector (Kinder, 1972a). The signal derivative di_S/di_G is plotted as a function of the generator voltage directly expressed in terms of the phonon frequency, according to $\Omega = eV - 2\Delta_G$. At frequencies below the onset of the relaxation phonon signal at $\Omega = 2\Delta_D$, only recombination phonons contribute to the signal. The absorption corresponding to the splitting of the V^{3+} ground-state by spin–orbit coupling is found at 248 GHz, in agreement with microwave and infrared measurements. Time-resolved measurements show the absorption peak for all three phonon polarizations. Kinder (1973a) derived from his measurements numerical values for the interaction strength. For the longitudinal polarization (Fig. 29b) the selection rules are violated, since phonons of this polarization propagating in the *c* direction in Al_2O_3 should not interact with the V^{3+} transitions, in contrast to the experimental findings. Figure 29b, in addition, shows oscillations of the signal amplitude at the beginning of the relaxation signal contribution. These oscillations indicate standing wave resonances in the detector film, which have been found to increase in amplitude (Kinder, 1972b) with thinner detector films. Frequency resolution being only limited by the sharpness of the generator gap, the experimental linewidth can be chosen by the modulation amplitude. Typical values range from 1 to 3% of $2\Delta_G$, corresponding to a pulse power of about 50 μW superimposed on the dc generator bias current (voltage). The relative signal increase at $\Omega = 2\Delta_D$ in Fig. 29b,c resulting from the onset of relaxation phonons is a direct measure of the ratio of relaxation to recombination phonon emission for longitudinal and transverse polarization. Evidently there are no significant changes in this ratio, and on the basis of the discussion in Section V,A we obtain $\bar{D}_t \approx 0.5\bar{D}_l$ for the effective deformation potentials.

With generator and detector on the same crystal surface back scattering or resonance fluorescence of phonons can also be observed. This technique has been used for the detection of the resonance fluorescence of V^{3+} in Al_2O_3, as shown in Fig. 30. By variation of the generator voltage a strong

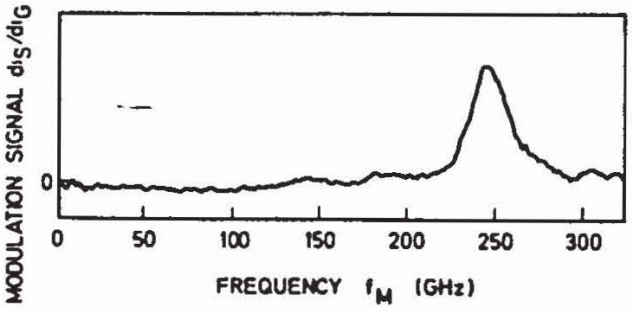

FIG. 30. Phonon back scattering by resonance fluorescence in $Al_2O_3:V^{3+}$. Sn–I–Sn generator and Al–I–Al detector evaporated on the same surface of the substrate crystal. The peak at 248 GHz demonstrates reemission of resonant phonons (Kinder, 1973a).

signal contribution at 248 GHz resulting from phonon resonance fluorescence is found (Kinder, 1973a). Phonon back scattering appears to be a very sensitive means for the detection of crystal impurities (Kinder, 1973b) including isotopes.

Further results obtained with relaxation phonon or Bremsstrahlung spectroscopy are the observation of so far unknown resonance scattering frequencies at 190, 220, 340, and 400 GHz in Verneuille Al_2O_3 crystals, presumably caused by lattice defects (Kinder, 1972c). The 340- and 400-GHz resonances were observed by using the method of high-energy relaxation phonon escape (Welte *et al.*, 1972a,b). Measurements using Pb : Bi generators (Dietsche and Kinder, 1974; see also Kinder, 1973b) with relaxation phonons in the range $\Omega < 2\Delta_G$ verified these results.

Detailed experimental investigations of the OH^- tunneling transitions in NaCl and KBr were performed by Windheim and Kinder, 1974, 1975a) using relaxation phonon spectroscopy in combination with uniaxial stress tuning of the absorption levels. The OH concentration in the experiments was estimated to be of the order of 0.01–0.1 ppm, indicating the high sensitivity of the phonon absorption method. The results indicate 90° tunneling of the OH^- in an octahedral field with a tunneling parameter of $\Delta = 0.138$ meV and a stress splitting parameter $= 6.09 \times 10^{-24}$ cm^3. Similar absorption experiments were reported for $KCl : Li^+$ (Windheim and Kinder, 1975b,c).

C. Phonon Spectroscopy with High-Energy Relaxation Phonons of $\Omega > 2\Delta_G$

As discussed in Section V,D, primary relaxation phonons with energy Ω exceeding the gap energy $2\Delta_G$ are emitted from Al–I–Al junctions with little reabsorption within the generator. The maximum phonon energy is limited in principle by the maximum lattice frequency or by the "Kohn effect," i.e., the momentum conservation limiting condition $k_{ph} = 2q_F$ between phonon and electron momentum. Relaxation phonon spectroscopy thus also becomes possible for frequencies above $2\Delta_G$ using the same modulation techniques as discussed in Section VI,B. At frequencies about one order of magnitude higher than the gap frequency, this modulation technique has to be extended to the second derivative di_S^2/di_G^2 as illustrated in Fig. 31a,b. Figure 31a shows the normal conductor relaxation spectrum for low temperatures. This spectrum is also a good approximation for the superconductor spectrum at high phonon frequencies, i.e., $eV \gg \Delta_G$ (cf. Fig. 25). The first derivative of this spectrum with respect to the generator voltage, i.e., $dN(\Omega, V)/dV$, shows an Ω^2 dependence with a sharp edge at the maximum frequency. Only the second derivative d^2N/dV^2 reveals a singularity at the

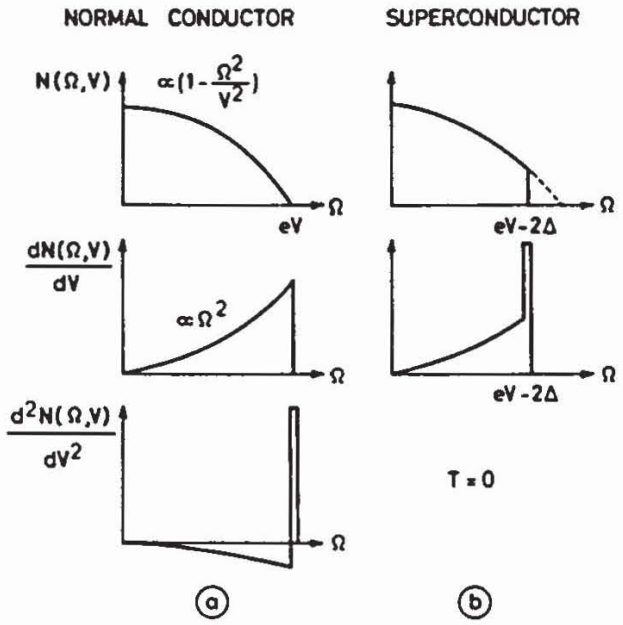

FIG. 31. Modulation of the relaxation spectrum and resulting effective phonon bands. (a) Normal conductor spectrum as approximation for very high-energy relaxation phenomena in superconductors. The first derivative with respect to the generator voltage results in a steplike spectral cutoff. The second derivative corresponds to a small bandwidth phonon line. (b) Normal conductor relaxation spectrum with a cutoff at $eV - 2\Delta_G$ as an approximation for low-energy relaxation phonon emission in superconductors. The first derivative with respect to the generator voltage results in a small bandwidth phonon line (cf. Fig. 23) (Forkel, 1974a).

maximum frequency or the small bandwidth phonon peak suitable for spectroscopy. Since the generator is operated in the almost linear portion of the I–V characteristic, the derivatives dN/dV and d^2N/dV^2 correspond to di_S/di_G and d^2i_S/di_G^2, respectively. The second derivative is obtained from the second harmonic of the detector signal at sinusoidal generator modulation (cf. Section III,A,2).

In Fig. 31b the normal conductor spectrum has been used with a frequency cutoff at the maximum relaxation phonon energy as approximation for the superconductor spectrum at $T = 0$ and under the condition of a small modulation amplitude $\delta eV \ll 2\Delta_G$. Under these conditions the first derivative dN/dV or di_S/di_G already shows the small bandwidth phonon peak as necessary for phonon spectroscopy. As a general rule, the first derivative technique is appropriate for phonon energies up to about $6\Delta_G$. For higher energies and finite temperature or modulation width the second derivative method has proved to be advantageous. Figure 32, as an example for the first derivative technique, shows absorption lines in Verneuille Al_2O_3 at $eV = 1.42$ meV and $eV = 1.65$ meV with Al junctions as phonon generator (Welte *et al.*, 1972a,b; Kinder, 1972c). With higher relaxation energies, finite temperature, and larger modulation width, the second derivative method has been used by Forkel *et al.* (1973) in order to analyze the phonon

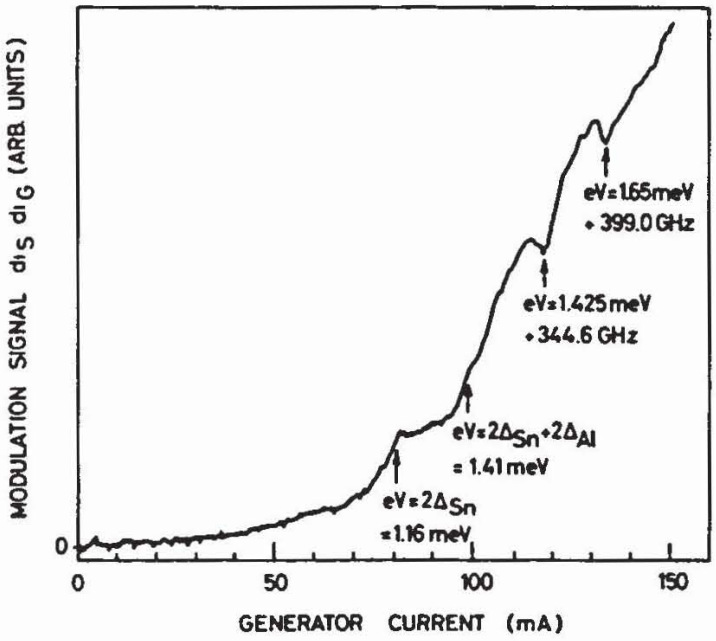

FIG. 32. Resonant absorption in undoped Verneuille Al_2O_3 at 344.6 and 399.0 GHz [Forkel (1973); see also Kinder (1972c) and Welte *et al.* (1972b)]. Substrate, Al_2O_3; generator, Al–I–Al; detector, Sn–I–Sn; $T = 1.03°K$.

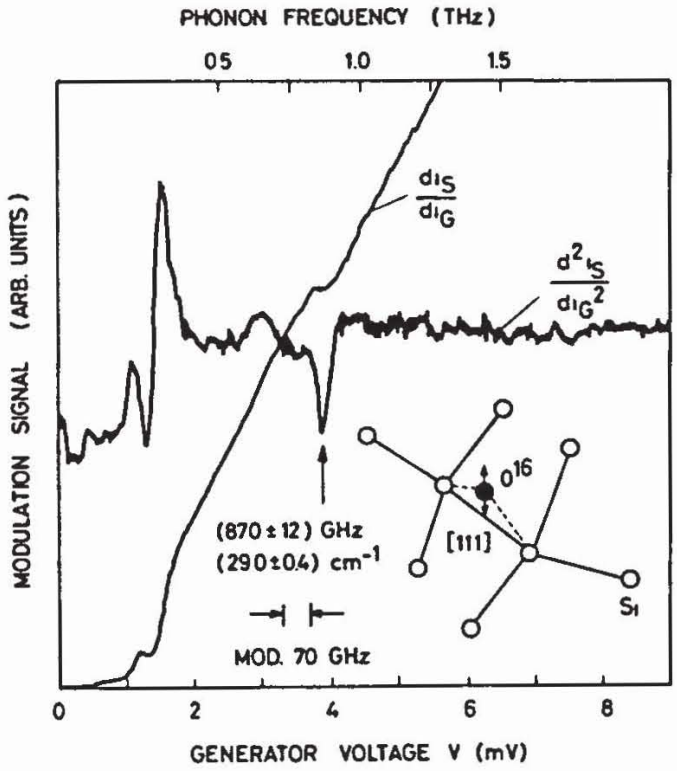

FIG. 33. Phonon absorption at 870 GHz by oxygen impurities in Si. Al–I–Al generator; Sn–I–Sn detector. ^{16}O concentration, 10^{18} cm^{-3}. The second derivative modulation signal amplitudes at the detector are of the order of nanovolts. The modulation width of 70 GHz refers to the second derivative signal (Forkel *et al.*, 1973).

resonance scattering of oxygen impurities in silicon, already known from far infrared absorption (Hayes and Bosomworth, 1969). The first and second derivative of the signal current with Al generator and Sn detector of a sample containing about 10^{18} cm^{-3} oxygen impurities is shown in Fig. 33. The inset shows the lattice position of the oxygen atoms. The oscillation direction is indicated by arrows. In agreement with the far infrared absorption frequency, the position of the phonon absorption line in the second derivative of the signal was found at 870 GHz or 3.59 ± 0.05 meV [2] corresponding to 29.0 ± 0.4 cm^{-1}. This phonon frequency is about 12 times larger than the recombination frequency of the Al generator. In the first derivative signal dependence, the structures at $eV = 2\Delta_D$, $eV = 2\Delta_G + 2\Delta_D$, and $eV = 2\Delta_G + 4\Delta_D$ (by the increase in detector counting rate at $\Omega = 4\Delta_D$) are found as expected (cf. Section V). The oxygen resonance scattering appears as a plateau. The experimental linewidth of 4% can be reduced with smaller modulation voltages. Although relaxation spectroscopy at higher frequencies encounters increasing noise problems the possibility of pulse measurements and time of flight separation of the different phonon modes have also been demonstrated (Forkel, 1975b).

D. Phonon Mean Free Path and Sound Velocity in Thin Normal and Superconducting Metal Layers

Experiments on the phonon mean free path at $\Omega = 2\Delta_{Al} \approx 80$ GHz in evaporated Cu layers and Al films have been performed by Long (1973b). Direct transmission measurements are only possible with thin metal films of the order of 1000 Å thickness, which is comparable to the phonon mean free path at this frequency in normal conductors or superconductors at $\Omega \geq 2\Delta$. The experiments using sandwich structures in the sequence Al generator, insulating SiO film, metal films of different thickness, insulating SiO film, and Al detectors evaporated on top of an Al_2O_3 substrate, resulted in normal conductor mean free path values of $\Lambda = 10{,}000$ Å for Cu and $\Lambda = 5400$ Å for Al. In superconducting Al this number is reduced by a factor of 1.57, resulting from Bobetic's (1964) calculation. Therefore, Long (1973b) finds $\Lambda_w = 3400$ Å for Al at $\Omega = 2\Delta_{Al}$ or a frequency of 80 GHz. These numbers are of the correct order of magnitude as estimated from the free electron theory (Pippard, 1960) or from the extrapolation of ultrasonic absorption data. The mean free path values obtained by Long mainly describe the transverse wave properties, since the generator produces more transverse than longitudinal phonons. A somewhat different mean free path for superconducting Al may be estimated from measurements of the

[2] The absorption maximum is found at the generator voltage of 3.9 mV. This corresponds to a phonon energy of $\Omega = eV - 2\Delta_G = 3.59$ meV with $2\Delta_G = 0.31$ meV.

thickness dependence of the experimental recombination lifetime (Section IV,C). As a linear dependence of τ_{eff} on thickness d is also observed for films of $d < 2000$ Å, a phonon mean free path of $\Lambda_w < 2000$ Å in clean Al films appears more realistic (Long, 1973b; Eisenmenger *et al.*, 1975). In experiments with relaxation phonons using a Sn generator and detection by thin-film granular Al junctions, Kinder (1972b) observed standing-wave phonon interference structures at $\Omega = 2\Delta_D$ corresponding to 150 GHz. From the frequency separation of the interference maxima for longitudinal and transverse pulses the sound velocities in the granular Al films resulted in $c_l = (6.44 \pm 0.3) \times 10^5$ cm-sec^{-1} and $c_t = (3.3 \pm 0.3) \times 10^5$ cm-sec^{-1}. From the agreement of these data with the bulk sound velocities it has been conjectured (Kinder, 1972b) that the energy density of phonon states $F(\omega)$ in granular Al is not affected. Instead, an enhancement of the electron–phonon interaction $\alpha^2(\omega)$ in qualitative agreement with the reduction of the effective recombination lifetime τ_{eff} in granular Al (Kinder, 1972b) may account for the $\alpha^2(\omega)F(\omega)$ change found by Leger and Klein (1969).

The reduction in relative height of the interference maxima by a factor of about 0.25 as the detector film thickness is increased from 620 to 920 Å indicates a mean free phonon path of about 500 Å for longitudinal waves, while the transverse mean free path for granular Al at 150 GHz is estimated to be less than or equal to 300 Å. This mean free path being smaller than for clean Al films is in accord with the reduction of the experimental recombination time τ_{eff} (Kinder, 1972b). For quantitative comparison of the τ_{eff} measurements in granular and clean Al films the phonon escape conditions at the film boundaries must be equal. The clean Al film experiments (Long, 1973a) have been performed in vacuum, while in the granular Al film measurement liquid He contact has been used (Kinder, 1972b).

For Sn films phonon reabsorption mean free path values were estimated with $\Lambda_w \leq 700$ Å (Narayanamurti and Dynes, 1971) from the spectral properties of the 2Δ fluorescence radiation. This agrees with $\tau_{eff}(d)$ measurements, indicating the upper limit $\Lambda_w < 1000$ Å. Further experimental results for Λ_w in the frequency range $\Omega = 2\Delta_G$ are not available. Extrapolation of ultrasonic absorption data to the gap frequency of Pb again results in $\Lambda_w < 1000$ Å (Eisenmenger *et al.*, 1975). One of the major objectives of further work must be the collection of more accurate data on the phonon mean free path in metals at high frequencies.

E. Phonon Mean Free Path in Dielectric Crystals

Phonon propagation at 280 GHz, i.e., $\Omega = 2\Delta_{Sn}$ in Al_2O_3 and Si single crystals, indicates mean free path values of $L \geq 1$ cm. At higher frequencies isotope scattering as directly observed for Ge and KBr in phonon back-

scattering experiments (Kinder, 1973b) with generator and detector on the same crystal surface sets a limit to ballistical phonon propagation. In general, the elastic phonon mean free path is limited by impurities and lattice defects. But even in a perfect isotopically pure crystal the phonon mean free path is limited by inelastic spontaneous or thermally stimulated phonon decay into at least two secondary phonons (Orbach and Vredevoe, 1964; Klemens, 1967). The probability of this three-phonon collision or decay process, depending on the third-order elastic coefficients of the crystal, increases in proportion to Ω^5 in the limit $kT \ll \Omega$. Under isotropic conditions momentum conservation only allows the decay of longitudinal phonons, while transverse phonons have extremely long lifetimes (only in three-phonon processes). A determination of inelastic decay time constants or phonon mean free path values exceeding convenient sample dimensions requires multiple elastic reflections at the sample boundary or a reverberation method (cf. Erlewein *et al.*, 1974). Using different positions of generator (Sn) and detector (Sn) on the crystal surface of pure silicon with sample dimensions of the order of 1 cm under vacuum conditions, reverberation times up to 50 μsec were observed in recent experiments (Böhm, 1975). This corresponds to a mean free path of about 25 cm at 280 GHz for transverse waves, which are the dominant contribution of the generator emission. Changes of the volume to surface ratio of the crystal indicate that the mean free path is limited by inelastic processes, directly or indirectly caused by reflection at the crystal surface. Thus, the bulk mean free path may exceed the value of 25 cm. In these experiments a frequency check by verifying the 4Δ step in the signal derivative (Section III,C) is essential for the distinction between 2Δ-phonons and the contribution of thermalized phonons.

Phonon reverberation experiments and heat conductance measurements exclude significant bulk phonon losses in Si and Al_2O_3 as substrate materials in 280 GHz ($2\Delta_{Sn}$) phonon propagation experiments. This is to be contrasted with absolute measurements of the detector signal amplitude in recombination phonon propagation (Trumpp *et al.*, 1972a,b) resulting in a ratio between observed and calculated signal ranging from 10 to 20% under vacuum conditions. In the calculation of the signal amplitude it is assumed that all [cf. Eq. (3)] recombination phonons are leaving the generator into the substrate and are radiated with a "Lamberts" cosine distribution corrected for phonon focusing. This assumption appears realistic especially on the grounds of the linear thickness dependence of τ_{eff} (cf. Sections IV,C, and VI,F). The detector has been calibrated by direct τ_{eff} pulse decay determination and by measurement of thermal tunneling current (cf. Section IV). The discrepancy between experiment and calculation so far can only be explained by a strongly disturbed surface layer in the crystal, causing additional phonon breakdown.

F. Phonon Transmission and Reflection at Solid–Solid and Solid–Liquid Boundaries

Direct measurements (Trumpp *et al.*, 1972b; Eisenmenger *et al.*, 1975) of the effective recombination lifetime τ_{eff} by phonon pulse excitation especially of Sn detectors on Si showed quantitative agreement with the result of the surface phonon escape model given by Eq. (20). As discussed in Section IV,C, this demonstrates that 2Δ-phonons even under strong trapping conditions either in the generator or detector are completely radiated across the film–substrate interface according to acoustic transmission laws. Phonon transmission rates for normal incidence and also averaged over all angles of incidence are found in Table II. From the agreement of Eq. (20) with experiment and from the very extensive experimental and theoretical work of Weis (1972) on phonon transmission of metal heaters evaporated on insulator substrates, the acoustical model for phonon transmission across solid–solid interfaces can be assumed to be valid up to frequencies in the Terahertz range.

As known from the Kapitza resistance "anomaly" (Challis, 1973), i.e., the phonon transmission into liquid helium, the predictions of the acoustic model are completely wrong for phonon frequencies above about 20 GHz. This was also found in τ_{eff} measurements with Sn junctions in contact with liquid ^{4}He (Trumpp *et al.*, 1972b), indicating a phonon escape rate 3 to 4 times higher than into the crystal substrate and two orders of magnitude exceeding the acoustical rate. Phonon pulse reflection measurements with Sn generator and Al detector (Kinder and Dietsche, 1974) at the Ge–^{4}He boundary indicate that the high phonon escape rate in the frequency range from 130 to 280 GHz shows little frequency dependence, in contrast to expectations based on the singularities in the density of states of the He^{II} dispersion curve at the phonon maximum and the roton minimum. The reflection factors at the solid–liquid interface were separately determined for the different phonon modes in dependence on the thickness of the adsorbed helium film. The bulk limit was reached at about 3 atomic layers with 70% for the longitudinal mode, 45% for the fast transverse mode, and 32% for the slow transverse mode. The measurements provide detailed frequency information and are in agreement with results obtained by heat pulse techniques (see, e.g., Guo and Marris, 1972; Swanenburg and Wolter, 1973). From the discussion of the signal dependence on frequency and thickness of the adsorbed He layer it has been concluded that the high phonon transmission rate at the solid–liquid interface results from strong phonon decay or frequency conversion processes within the first atomic layers of He. Other experiments, such as the observation of the thickness resonance in the films at 80 GHz (Blackford, 1972) and the propagation of 190-GHz phonons in

liquid He at 0.1°K (Dynes and Narayanamurti, 1974), indicate the possibility of enhanced phonon escape without energy change. Therefore, the origin of the Kapitza resistance "anomaly" at frequencies above 50 GHz is still an open question.

G. Phonon Propagation in Liquid ^{4}He

Using identical Al junctions as phonon generators and detectors Dynes and Narayanamurti (1974) found phonon propagation in liquid ^{4}He at 0.1°K under saturation vapor pressure in the frequency range above 190 GHz. This result was obtained by carefully analyzing the differential signal amplitude di_S/di_G as a function of generator voltage. Under these experimental conditions, recombination phonons and the 4Δ structure did not show up. Instead a first signal contribution was observed at relaxation phonon energies exceeding $E_{ph} = eV - 2\Delta_G > 0.7$ meV. Relaxation phonons of this energy exceeding $2\Delta_G$ still have a high escape probability from Al junctions, as described in Section V,D. This is an additional example of the possibility of phonon spectroscopy at energies above $2\Delta_G$. The onset of the relaxation phonon signal clearly indicates that phonons with less energy than 0.7 meV are strongly absorbed in the liquid He. This result is in accordance with predictions of Maris and Massey (1970) and Jäckle and Kehr (1971) that the $\omega(k)$ dispersion curve of liquid He^{II} shows an upward curvature at low energies as concluded from the anomalous high ultrasonic absorption. The onset of phonon transmission at 0.7 meV corresponds to the energy of the inflection point with beginning downward curvature. By increasing the He pressure the onset of the differential phonon signal was demonstrated to shift continuously to lower energies until the entire generator phonon spectrum including recombination phonons was transmitted at the pressure of 24 bar. In this limit the derivative signal corresponds to Fig. 12. At 24 bar the upward curvature of the dispersion curve has completely disappeared and changed to a downward curvature. For this shape of the dispersion relation, phonon decay by three-phonon processes is forbidden since momentum cannot be conserved.

VII. Further Applications and Final Remarks

Phonon spectroscopy with superconducting tunneling junctions is expected in many systems to be superior in sensitivity to far infrared spectroscopy if small amounts of impurities are to be detected. This has already been demonstrated for NaCl:OH^- and KBr:OH^- (Windheim and Kinder, 1975b) and impurities in Ge (Kinder, 1973b). In addition, systems with radiationless transitions, i.e., showing no electric dipole moment, can also be

studied. Finally, superconductors especially at low temperatures are transparent in the phonon energy range $E_{ph} < 2\Delta$ as far as the electron–phonon interaction is concerned.

To a large extent the superconducting tunneling junction as phonon detector with a frequency threshold can be used to obtain information on emitted phonon spectra. In fact, most information on the recombination and relaxation spectra of the tunneling generator has been obtained from this frequency selective detector property (cf. Sections III,C, and V). Direct emission spectroscopy is possible by using a set of detectors with different energy gaps. Detector gap tuning, e.g., by a magnetic field, has turned out also to be possible (cf. Section VI,A). The investigation of radiation from extremely thin heater films, $d < 100$ Å, with tunneling detectors has shown that the phonon spectrum is shifted to higher frequencies (Frick *et al.*, 1975) by the depletion of low-energy phonon states. Tunneling detectors have been further used in work on heat pulse detection (Schulz and Weis, 1970), hot electron–phonon emission in semiconductors (Reupert, 1975), phonon propagation and time of flight spectroscopy in semiconductors (Huet *et al.*, 1972; Huet and Maneval, 1974), and also as fast calibrated thermometers for second sound detection (Buck *et al.*, 1974).

In general, high sensitivity and linearity in a wide temperature range, as compared to superconducting bolometers, the possibility of absolute calibration, the complete control of operation, and the low-frequency threshold, make tunneling detectors a valuable tool in phonon experiments. In spectroscopic applications the tunability of the generators, i.e., of the upper edge of the relaxation spectrum, is advantageous as compared to magnetic or temperature tuning of the recombination phonons.

In principle, the tunneling detector has additional frequency analyzing potentialities, such as probing the energy distribution of quasiparticles excited by different phonon frequencies in a method similar to the one used in relaxation time measurements by Miller and Dayem (1967). Also phonon-assisted tunneling (see, e.g., Kleinman, 1963; Cohen *et al.*, 1970) is expected to show frequency information similar to photon-assisted tunneling (Dayem and Martin, 1962). Corresponding experiments at $\Omega \approx 2\Delta$ so far have not been convincing, possibly as a consequence of the low sensitivity encountered in these processes.

The use of tunneling junctions is restricted to low magnetic fields with the exception of very thin films in a parallel field and also to the generation of small phonon occupation numbers. Saturation experiments, e.g., with ultrasonic waves, are only possible by piezoelectric surface excitation of high-frequency coherent waves (cf. Grill and Weis, 1974), in the THz frequency range. Some of the virtues of tunneling junctions as phonon gener-

ators and detectors are their ease of fabrication and operation over a wide frequency range by simply changing the battery voltage, as well as their high sensitivity as detectors.

ACKNOWLEDGMENTS

I wish to thank A. H. Dayem for close cooperation and extensive discussions, especially in the early stage of this work. For the support of the first experiments and the hospitality extended to me at Bell Telephone Laboratories, Murray Hill, New Jersey, during the summer of 1966 and spring of 1967, I also want to express my gratitude to M. R. Schroeder and S. J. Buchsbaum. I would further like to thank H. Kinder, K. Lassmann, M. Welte, W. Forkel, and H. J. Trumpp for their contributions and fruitful cooperation over the past years. I also gratefully acknowledge helpful discussions with C. J. Adkins, A. R. Long, V. Narayanamurti, K. Renk, and O. Weis.

REFERENCES

Abeles, B., Cohen, R. W., and Cullen, G. W. (1966). *Phys. Rev. Lett.* **17**, 632.
Adkins, C. J. (1973). *Phys. Lett.* **43A**, 537.
Anderson, C. H., and Sabisky, S. (1971). *In* "Physical Acoustics" (W. P. Mason, ed.), Vol. 8. Academic Press, New York.
Bindel, W. (1973). Diplomarbeit. Univ. Stuttgart. Unpublished.
Blackford, B. L. (1972). *Phys. Rev. Lett.* **28**, 414.
Bobetic, V. M. (1964). *Phys. Rev. A* **136**, 1535.
Böhm, K. (1975). Diplomarbeit. Univ. Stuttgart. Unpublished.
Bömmel, H. E., and Dransfeld, K. (1958). *Phys. Rev. Lett.* **1**, 234.
Bömmel, H. E., and Dransfeld, K. (1960). *Phys. Rev.* **117**, 1245.
Buck, J., Lassmann, K., and Eisenmenger, W. (1974). *Phys. Lett. A* **50**, 279.
Burstein, E., Langenberg, D. N., and Taylor, B. N. (1961). *Phys. Rev. Lett.* **6**, 92.
Campbell, C. K., Dynes, R. C., and Walmsley, D. G. (1966). *Can. J. Phys.* **44**, 2601.
Challis, L. J. (1973). *J. Phys. C* **7**, 481.
Clairborne, L. T., and Morse, R. W. (1964). *Phys. Rev. A* **136**, 893.
Cohen, M., Goldstein, Y., and Abeles, A. (1970). *Phys. Rev. B* **3**, 2223.
Dayem, A. H. (1972). *J. Phys. Paris C* **33**, 4–15.
Dayem, A. H., and Martin, R. J. (1962). *Phys. Rev. Lett.* **8**, 246.
Dayem, A. H., and Wiegand, J. J. (1972). *Phys. Rev. B* **5**, 4390
Dayem, A. H., Miller, B. I., and Wiegand, J. J. (1971). *Phys. Rev. B* **3**, 2949.
Dietsche, W., and Kinder, H. (1974). *Verh. Deut. Phys. Ges.* **8**, 810.
Dynes, R. C., and Narayanamurti, V. (1972). *Phys. Rev. B* **6**, 5143.
Dynes, R. C., and Narayanamurti, V. (1973). *Solid State Commun.* **12**, 341.
Dynes, R. C., and Narayanamurti, V. (1974). *Phys. Rev. Lett.* **33**, 1195.
Dynes, R. C., Narayanamurti, V., and Chin, M. (1971). *Phys. Rev. Lett.* **4**, 181.
Eisenmenger, W. (1967a). *In* "Fachberichte," Physikertagung Berlin. Teubner, Stuttgart, p. 88.
Eisenmenger, W. (1967b). Unpublished.
Eisenmenger, W. (1969). *In* "Tunneling Phenomena in Solids" (E. Burstein and S. Lundquist, eds.), p. 371. Plenum, New York.
Eisenmenger, W., and Dayem, A. H. (1967). *Phys. Rev. Lett.* **18**, 125.
Eisenmenger, W., Kinder, H., and Lassmann, K. (1969). Report Deutsche Forschungsgemeinschaft. Unpublished.

Eisenmenger, W., Lassmann, K., Trumpp, H. J., and Krauss, R. (1975). *Proc. Int. Conf. Low Temp. Phys., 14th*, p. 529 and to be publ. in detail.
Erlewein, J., Lassmann, K., and Eisenmenger, W. (1974). *Verh. Deut. Phys. Ges.* **8**, 812.
Forkel, W. (1973). Diplomarbeit, Univ. Stuttgart. Unpublished.
Forkel, W. (1974a). *In* "Microwave Acoustics" (E. R. Dobbs and J. K. Wigmore, eds.), Proc. Int. Congr. Acoustics, 8th, p. 186. Inst. Phys., London.
Forkel, W. (1974b). Private communication.
Forkel, W. (1975a). Private communication.
Forkel, W. (1975b). To be published.
Forkel, W., and Eisenmenger, W. (1976). To be published.
Forkel, W., and Trumpp, H. J. (1975). Private communication.
Forkel, W., Welte, M., and Eisenmenger, W. (1973). *Phys. Rev. Lett.* **31**, 215.
Frick, W., Waldmann, D., and Eisenmenger, W. (1975). *Appl. Phys.* **8**, 163.
Giaever, I. (1969). *In* "Tunneling Phenomena in Solids" (E. Burstein and S. Lundquist, eds.), p. 255. Plenum, New York.
Giaever, I., and Megerle, K. (1961). *Phys. Rev.* **122**, 1101.
Gray, K. E., Long, A. R., and Adkins, C. J. (1969). *Phil. Mag.* **20**, 273.
Grill, W., and Weis, O. (1974). *In* "Microwave Acoustics" (E. R. Dobbs and J. K. Wigmore, eds.), Proc. Int. Congr. Acoustics, 8th, p. 179. Inst. Phys., London.
Guo, C. J., and Maris, H. J. (1972). *Phys. Rev. Lett.* **29**, 855.
Hayes, W., and Bosomworth, D. R. (1969). *Phys. Rev. Lett.* **23**, 851.
Herth, P., and Weis, O. (1970). *Z. Angew. Phys.* **29**, 101.
Huet, D., and Maneval, J. P. (1974). *Phys. Rev. Lett.* **33**, 1154.
Huet, D., Maneval, J. P., and Zylberstejn, A. (1972). *J. Phys. Paris C* **33**, 4–91.
Hunklinger, S., Arnold, W., Stein, S., Nava, R., and Dransfeld, K. (1972). *Phys. Lett. A* **42**, 253.
Jacobsen, E. H. (1974). *In* "Microwave Acoustics" (E. R. Dobbs and J. K. Wigmore, eds.), Proc. Int. Congr. Acoustics, 8th, p. 60. Inst. Phys., London.
Jäckle, J., and Kehr, K. W. (1971). *Phys. Rev. Lett.* **27**, 654.
Kane, E. O. (1969). *In* "Tunneling Phenomena in Solids" (E. Burstein and S. Lundquist, eds.), p. 1. Plenum, New York.
Kinder, H. (1971). *Phys. Lett. A* **36**, 379.
Kinder, H. (1972a). *Phys. Rev. Lett.* **28**, 1564.
Kinder, H. (1972b). *J. Phys. Paris C* **33**, 4–21.
Kinder, H. (1972c). *Int. Conf. Phonon Scattering Solids, Paris.*
Kinder, H. (1973a). *Z. Phys.* **262**, 295.
Kinder, H. (1973b). Physikertag. Deut. Oesterr. Phys. Ges., Plenarvortr., Hamburg, 1973. Physik Verlag, Weinheim.
Kinder, H., and Dietsche, W. (1974). *Phys. Rev. Lett.* **33**, 578.
Kinder, H., Lassmann, K., and Eisenmenger, W. (1970). *Phys. Lett. A* **31**, 475.
Kittel, C. (1967). "Introduction to Solid State Physics," 3rd ed. Wiley, New York.
Kleinman, L. (1963). *Phys. Rev.* **132**, 2484.
Klemens, P. G. (1967). *J. Appl. Phys.* **38**, 4573.
Leger, A., and Klein, J. (1969). *Phys. Lett. A* **28**, 751.
Leibowitz, J. R. (1964a). *Phys. Rev. A* **133**, 84.
Leibowitz, J. R. (1964b). *Phys. Rev. A* **136**, 22.
Little, W. A. (1959). *Can. J. Phys.* **37**, 334.
Long, A. R. (1972). *J. Phys. Paris C* **33**, 4–73.
Long, A. R. (1973a). *J. Phys. F* **3**, 2041.
Long, A. R. (1973b). *J. Phys. F* **3**, 2023.
Long, A. R., and Adkins, C. J. (1973). *Philos. Mag.* **27**, 865.

Maris, H. J., and Massey, W. E. (1970). *Phys. Rev. Lett.* **25**, 220.
Meservey, R., and Schwartz, B. B. (1969). *In* "Superconductivity II" (R. D. Parks, ed.). Dekker, New York.
Miller, B. I., and Dayem, A. H. (1967). *Phys. Rev. Lett.* **18**, 1000.
Morse, R. W. (1959). *Progr. Cryog.* **1**, 221.
Narayanamurti, V., and Dynes, R. C. (1971). *Phys. Rev. Lett.* **27**, 410.
Orbach, R., and Vredevoe, L. A. (1964). *Physics (Long Island City, N.Y.)* **1**, 91.
Parker, W. H., and Williams, W. D. (1972). *Phys. Rev. Lett.* **29**, 924.
Pippard, A. B. (1955). *Philos. Mag.* **46**, 1104.
Pippard, A. B. (1960). *Proc. R. Soc. London, Ser. A* **257**, 165.
Pokrovskii, V. L. (1961). *Zh. Eksp. Teor. Fiz.* **40**, 898 [*Sov. Phys.—JETP* **13**, 628].
Renk, K. F. (1972). *Fest. Koerperprobleme* **12**, 107.
Renk, K. F., and Deisenhofer, J. (1971). *Phys. Rev. Lett.* **26**, 764.
Reupert, W. (1975). Diplomarbeit, Univ. Stuttgart. Unpublished.
Rolcke, R. (1973). Unpublished.
Rothwarf, A., and Taylor, B. N. (1967). *Phys. Rev. Lett.* **19**, 27.
Rothwarf, A., Sai-Halasz, G. A., and Langenberg, D. N. (1974). *Phys. Rev. Lett.* **33**, 212.
Schulz, J. P., and Weis, O. (1970). *Phys. Lett. A* **32**, 381.
Sheahen, T. P. (1966). *Phys. Rev.* **149**, 370.
Shiren, N. S. (1961). *Phys. Rev. Lett.* **6**, 168.
Solymar, L. (1972). "Superconductive Tunneling and Applications," pp. 45, 234. Chapman & Hall, London.
Swanenburg, T. J. B., and Wolter, J. (1973). *Phys. Rev. Lett.* **31**, 693.
Taylor, B., Maris, H. J., and Elbaum, C. (1971). *Phys. Rev. B* **3**, 1462.
Tewordt, L. (1962a). *Phys. Rev.* **127**, 371.
Tewordt, L. (1962b). *Phys. Rev.* **128**, 12.
Trumpp, H. J. (1971). Diplomarbeit, Univ. Stuttgart. Unpublished.
Trumpp, H. J., Epperlein, P., and Lassmann, K. (1972a). *J. Phys. Paris C* **33**, 4–29.
Trumpp, H. J., Lassmann, K., and Eisenmenger, W. (1972b). *Phys. Lett. A* **41**, 431.
von Gutfeld, R. J. (1965). *In* "Physical Acoustics" (W. P. Mason, ed.), Vol. V, p. 233. Academic Press, New York.
von Gutfeld, R. J., and Nethercot, A. H. (1964). *Phys. Rev. Lett.* **12**, 64.
Weis, O. (1969). *Z. Angew. Phys.* **26**, 325.
Weis, O. (1972). *J. Phys. Paris C* **33**, 4–49.
Welte, M. (1973). Private communication.
Welte, M. (1974). *In* "Microwave Acoustics" (E. R. Dobbs and J. K. Wigmore, eds.), Proc. Int. Congr. Acoustics, 8th, p. 183. Inst. Phys., London.
Welte, M., Lassmann, K., and Eisenmenger, W. (1972a). *Verh. Deut. Phys. Ges.* **6**, 699.
Welte, M., Lassmann, K., and Eisenmenger, W. (1972b). *J. Phys. C* **33**, 4–25.
Wilkins, J. W. (1969). *In* "Tunneling Phenomena in Solids" (E. Burstein and S. Lundquist, eds, p. 333. Plenum, New York.
Windheim, R., and Kinder, H. (1974). *Verh. Deut. Phys. Ges.* **8**, 810.
Windheim, R., and Kinder, H. (1975a). *Phys. Lett.* To be published.
Windheim, R., and Kinder, H. (1975b) *Verh. Deut. Phys. Ges.* **5**, 612.
Windheim, R., and Kinder, H. (1975c). *In* "Phonon Scattering in solids" (J. Challis, V. Rampton, and A. Wyatt, eds.), p. 220. Plenum, New York.
Yokota, H., Kushibe, H., and Tsuneto, T. (1966). *Progr. Theor. Phys.* **36**, 237.